Thesis

Motion Cueing Tuning and Evaluation in CH-47 Helicopter Simulation Using the Eigenmode Distortion Method

H. van Donge

Delft University of Technology

TU Delft

Cover image from: Ministerie van Defensie[1]

[1] https://www.defensie.nl/onderwerpen/materieel/vliegtuigen-en-helikopters/boeing-ch-47d-en-ch-47f-chinook-transporthelikopter, accessed on 18 November 2019

Thesis

Motion Cueing Tuning and Evaluation in CH-47 Helicopter Simulation Using the Eigenmode Distortion Method

by

H. van Donge

to obtain the degree of Master of Science
at the Delft University of Technology,
to be defended publicly on Monday 30 March 2020 at 14:00.

Student number:	4230345	
Project duration:	22 November 2018 – 30 March 2020	
Thesis committee:	Professor dr. ir. M. Mulder,	TU Delft, Control & Simulation, chair
	Assistant professor dr. O. A. Sharpanskykh,	TU Delft, Air Transport & Operations, examiner
	Researcher ir. O. Stroosma,	TU Delft, Control & Simulation, supervisor
	Dr. ir. M. Wentink,	Desdemona B.V.

TU Delft

Contents

Acknowledgements

Completing a Master Thesis project is a difficult task and it would not have been possible without the help and support of a number of people, who undoubtedly deserve my gratitude. The first of whom is Olaf Stroosma, as he spend endless hours on guiding, supporting and troubleshooting me and my work. I could not have wished for a better supervisor. Olaf was always quick to respond, I never got a 'no time' on any question. It is safe to say that Olaf got me interested in the field of flight simulators with his enthusiastic lectures and the course of Real-time Distributed Flight and Space Simulation. It was also through this course that I got to know Desdemona.

Also invaluable to my thesis work, is Ivan Miletović, who pointed out an essential piece of literature to explain the transient amplification effects. This effect had kept Olaf and me busy for just too many weeks, until Ivan clarified the mystery. I am thankful for the time and effort he was willing to put into this work.

Just as essential for this result are the friends at Desdemona B.V., who first of all taught me how to create the best espresso's and cappuccino's. Next to that they were of great value in creating the model of the Chinook and its SCAS.

I would like to thank Max Mulder who gave me the opportunity to perform a thesis outside the Delft University of Technology and brought me in contact with Desdemona B.V. as graduation company.

Finally I thank my beloved wife and friend, as well as my family, for their infinite support.

H. van Donge

Soesterberg, 14 January 2020

1

Paper

Motion Cueing Tuning and Evaluation for CH-47 Helicopter Simulation Using the Eigenmode Distortion Method

H. van Donge

18 March 2020

Abstract

In a moving base simulator, the eigenmodes of the simulated vehicle are perceived as distorted due to the added dynamics of the motion filter. The Eigenmode Distortion (EMD) method evaluates flight simulator motion cueing fidelity based on the perceived distortion of relevant eigenvectors of specific vehicle dynamics. This method was previously applied to models of the AH-64 Apache and the Cessna Citation II.

The goal of this study is to investigate the use of EMD in structured tuning of a motion cueing algorithm (the classical washout algorithm (CWA)) for CH-47 simulation, and to identify whether the resulting filter is rated better, according to the motion fidelity rating (MFR), than manually tuned filters. To this end, the EMD filter is compared, in an experiment, to a manually tuned filter, which is currently in use at Desdemona for CH-47 simulations. The CH-47 EMD filter is also compared to an EMD motion filter, tuned for the AH-64 Apache in a previous experiment, in order to test whether a single EMD filter can or cannot be used for different vehicles. In this experiment, three pilots participated, with experience in flying the CH-47 helicopter.

The results of this experiment show a preference for the vehicle-specific, EMD-based approach, based on which it can be said that EMD is preferred, by the participating pilots, over current, manual tuning methods.

Symbols

Notation	Description	Unit
M	Non-dimensional moment derivative in body pitch axis	[–]
X, Z	Non-dimensional force derivatives in body x- and z-direction	[–]
$\square_0$	subscript indicating trim value	[–]
$\square_{\theta_{0C}}$	derivative w.r.t. collective input	[–]
$\square_{\theta_{1S}}$	derivative w.r.t. longitudinal cyclic	[–]
$\square_{cg}$	subscript indicating centre of gravity	[–]
$\square_s$	subscript indicating simulator related quantity	[–]
$\square_u, \square_w, \square_q$	derivative w.r.t. vehicle states u,w,q	[–]
$\square_v$	subscript indicating vehicle related quantity	[–]
λ	eigenvalue	[–]
ω_b, ω_n	filter break frequency, eigenfrequency	[rad/s]
θ	pitch angle	[rad]
θ_{0C}	collective pitch angle	[rad]
θ_{1C}	lateral cyclic pitch angle	[rad]
θ_{1S}	longitudinal cyclic pitch angle	[rad]
fx	specific force along body x-axis	[m/s^2]
fz	specific force along body z-axis	[m/s^2]
g	gravitational acceleration, 9.81	[m/s^2]
q	rotational rate in body frame around y-axis	[rad/s]
u,w	velocity in body frame along x- and z-direction	[m/s]
kt	knots, nautical miles per hour	[M/h]

1 Introduction

Over the years multiple attempts have been made to perform objective motion cueing evaluation[1–4] and one of the latest developments in this area is the objective motion cueing test (OMCT).[4, 5] The OMCT is now included in the International Civil Aviation Organization (ICAO) standard for simulator qualification.[6] The OMCT evaluates the combination of motion cueing algorithm (MCA) and motion drive system of the simulator, based on the system response to an array of input frequencies. However, it does not account for task- and vehicle-related properties.

Dalmeijer et al. found that tailoring the OMCT test signals to a specific task and vehicle model, resulted in noticeable differences in identified motion cueing characteristics.[7, 8] To expose the MCA-induced distortion of motion cues, a new method called Eigenmode Distortion (EMD) was developed.[8] In short, EMD evaluates the MCA based on the difference between the system's perceived eigenmodes before and after cueing (see Figure 1).

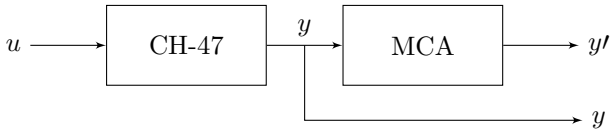

Figure 1: Comparison of output behaviour before and after cueing

Evaluation of the EMD method has been conducted previously with a model of the AH-64 Apache[8] and the Cessna Citation II[9]. This study aims to investigate the use of EMD in structured tuning of a motion cueing filter for CH-47 Chinook simulation, by tuning an MCA using EMD for the CH-47 Chinook, validating the resulting MCA in a pilot-in-the-loop experiment, and comparing it to the MCA tuned in a previous experiment for the AH-64 Apache.[8]

First, it is studied whether structured tuning, using EMD, results in a more preferred MCA for the CH-47, according to its (test) pilots. This is evaluated in an experiment, where EMD-based tuning is compared to the MCA currently in use at Desdemona B.V. for CH-47 simulation. Preference is measured using the motion fidelity rating (MFR) and pair-wise comparisons.

The OMCT has prescribed fidelity regions that encompass "good" filter settings, which are simulator-specific, but not vehicle-specific. This differentiates EMD from the OMCT, as EMD assumes that both simulator- and vehicle-specific cueing is necessary. Therefore, in the experiment it is also tested whether a filter can be used for a different vehicle of the same class, i.e., helicopter, by coupling the CH-47 model to an MCA designed for an AH-64. This is again measured using MFRs and pair-wise comparisons.

During the MCA design, the effectiveness of the method is compared to conventional tuning methods, regarding on-line simulator time requirements for testing, implementation difficulty of EMD compared to OMCT and knowledge prerequisites.

It is expected that an EMD-based MCA is preferred over conventionally tuned MCAs, and that an aircraft-specific MCA cannot be generalised to other aircraft if the dynamic characteristics of the vehicles do not match. This is expected, because the eigenmodes are distorted differently, if the initial eigenmodes are different.

This paper is structured as follows: Section 2 introduces the proposed EMD methodology. In Section 3 the experiment is explained and the results are discussed in Section 4. A discussion of the results follows in Section 5 and a conclusion in Section 6.

2 Eigenmode Distortion Methodology

The current state-of-the-art method for motion cueing fidelity evaluation, the OMCT, analyses the frequency response of the MCA to a set of sinusoidal input signals to all six input channels: three angular rates and three specific forces.[6]

Where the current OMCT falls short is that its input signals do not realistically represent motions experienced during simulations of different aircraft types.[8] Also, the response to each signal is studied in isolation, while the motions of the aircraft, and consequently the cues sent to the MCA, are linked through the vehicle dynamics.[8]

EMD aims to address these shortcomings, by analysing the distortion of the vehicle's eigenmodes due to the MCA.[8] Distortion in this context means the difference between the system's eigenmodes before and after cueing (Figure 1).

To analyse the eigenmode distortion, a linear vehicle model has to be available or derived, which is discussed in Subsection 2.1. This model is subsequently linked to a linearised model of the MCA (see Subsection 2.2). In linear dynamic systems the combination of eigenvalues and eigenvectors describe the dynamic behaviour of the system. By comparing the shape of the eigenvectors (orientation and size of its components) after cueing with the vehicle's eigenvectors before cueing (see Figure 1), EMD predicts the simulator motion fidelity. This is further explained in Subsection 2.3.

Note that EMD analysis yields the distortion of the perturbed linear model, therefore the analysis is only valid close to the linearisation point. Away from this operating point the eigenmodes can change, which means that the MCA can have different distortion effects on the motion cues. More about the linearisation is discussed in Subsection 2.1.

2.1 Linearised Aircraft Model

Desdemona B.V., partner in this project, operates a CH-47 Chinook simulation model for pilot training, which is also used for this project. This model was linearised at 20 kt, to be used in the experiment, discussed in Section 3. The matrices of the vehicle's model state-space system are shown in Equation 1. Note that the C- and D-matrices are expanded, in order to also output the derivative of states u, w and q. Also, the simplification is made that the specific body forces are equal to the derivative of the velocities: $fx_v = \dot{u}$ and $fz_v = \dot{w}$. The state, input and output vector definitions are shown in Equation 2. This model is based on the implementation of Miletović[10]. The linearised model only describes longitudinal motion, as will further be discussed in Section 3.

The Desdemona CH-47 model includes an accurate, non-linear model of the stability and control augmentation system (SCAS). More information about this system is available at the United States Army Warfighting Center[11]. This system is also linearised, thereby introducing a relatively large number of additional states and eigenmodes.

Addition of the SCAS increases the complexity and number of states of the model considerably, mainly due to the filters and actuators present in the SCAS, such as the differential airspeed hold (actuator) (DASH) and integrated lower control actuator (ILCA). The non-linear SCAS incorporates logic which changes the behaviour of the SCAS considerably, depending on the state of the aircraft and input of the pilot. For the linearisation of the SCAS, some assumptions are made, which are shown below.

- no ground contact
- airspeed below 40 kt
- no failures, gyroscopes are valid
- pitch angle stays between $-11.5°$ and $23.5°$
- ideal servos: no delay, no limits (except for the DASH, its dynamics are linearised)
- no intermediate centering device release (CDR), magnetic brake (mag brake) or beep trim used
- longitudinal stick deflection (with 1 inch aft bias) between 2.2 inch aft and 1.75 inch forward
- longitudinal stick rate smaller than 0.142 inch/s (DASH control velocity limit)
- roll attitude stays between $-2.29°$ and $2.29°$ (± 0.04 rad)

$$
A = \begin{bmatrix} X_u & X_w - q_0 & -g\cos(\theta_0) & X_q - w_0 \\ Z_u + q_0 & Z_w & -g\sin(\theta_0) & Z_q + u_0 \\ 0 & 0 & 0 & 1 \\ M_u & M_w & 0 & M_q \end{bmatrix}
$$

$$
B = \begin{bmatrix} X_{\theta_{0C}} & X_{\theta_{1S}} \\ Z_{\theta_{0C}} & Z_{\theta_{1S}} \\ 0 & 0 \\ M_{\theta_{0C}} & M_{\theta_{1S}} \end{bmatrix}
$$

$$
C = \begin{bmatrix} 1 & 0 & 0 & 0 \\ 0 & 1 & 0 & 0 \\ 0 & 0 & 1 & 0 \\ 0 & 0 & 0 & 1 \\ X_u & X_w - q_0 & -g\cos(\theta_0) & X_q - w_0 \\ Z_u + q_0 & Z_w & -g\sin(\theta_0) & Z_q + u_0 \\ M_u & M_w & 0 & M_q \end{bmatrix} \tag{1}
$$

$$
D = \begin{bmatrix} 0 & 0 \\ 0 & 0 \\ 0 & 0 \\ 0 & 0 \\ X_{\theta_{0C}} & X_{\theta_{1S}} \\ Z_{\theta_{0C}} & Z_{\theta_{1S}} \\ M_{\theta_{0C}} & M_{\theta_{1S}} \end{bmatrix}
$$

$$
\vec{u} = \begin{bmatrix} \theta_{0C} \\ \theta_{1S} \end{bmatrix}, \quad \vec{x} = \begin{bmatrix} u \\ w \\ \theta \\ q \end{bmatrix}, \quad \vec{y} = \begin{bmatrix} u \\ w \\ \theta \\ q \\ fx_v \\ fz_v \\ \dot{q_v} \end{bmatrix} \tag{2}
$$

2.2 Motion Cueing Algorithm

For this study a common MCA implementation is used: the classical washout algorithm (CWA)[8, 9, 12]. It is readily available and straightforward to implement, linearise, analyse and tune. The implementation used in this particular study is adopted from Stoev et al.[9] The structure is illustrated in Figure 2, which shows how the algorithm incorporates a second-order high-pass filter on pitch-rate, a third-order high-pass filter on specific forces and a second-order low-pass filter for tilt-coordination. Its parameter values are changed as part of the experiment, which is discussed in Section 3. The input and output vector definitions of the CWA are defined as:

$$
\vec{u} = \begin{bmatrix} \dot{q_v} \\ fx_v \\ fz_v \end{bmatrix}, \quad \vec{y} = \begin{bmatrix} \dot{q_s} \\ fx_s \\ fz_s \end{bmatrix} \tag{3}
$$

2.3 Eigenvector Distortion Analysis

Analysis of the eigenmodes requires knowledge of which eigenvectors should be analysed. Previous studies have used mode participation factor (MPF) analysis to determine the relative importance of eigenmodes.[8, 9] However, due to the multitude of states, some of which are unobservable, this method is difficult to use in this particular set-up. In combination with state-reconstruction, MPF analysis might be possible, however, this is not tested. Based on MPF analysis results in previous studies[8, 9] and simulator expert experience, the assumption was made that the fastest longitudinal eigenmode (with the highest eigenfrequency) was the most important mode in a low speed longitudinal

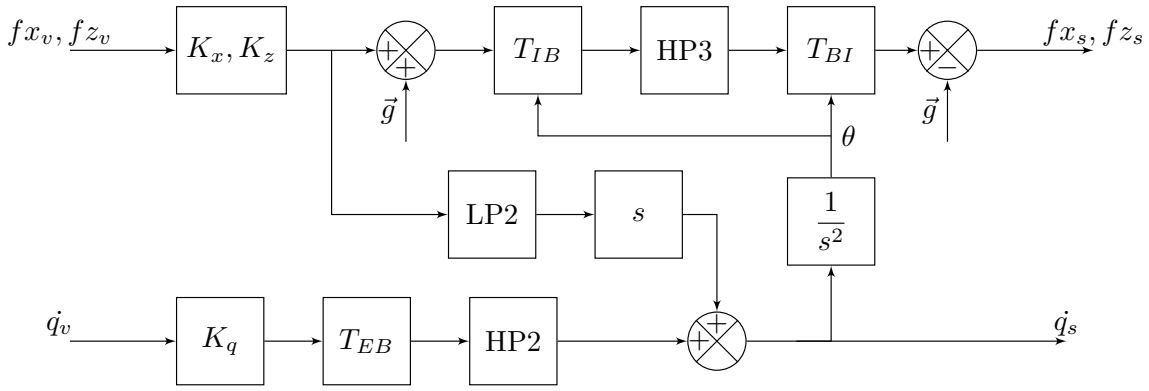

Figure 2: CWA Structure

reposition task. The eigenvalues of the simulated system (helicopter with augmentation) are shown in Table 2. Due to the multitude of modes, it is difficult to name the modes. The first mode mostly consists of heave, but also exhibits some surge and pitch; this could be named a short period. The second mode is almost entirely heave, so this can be called periodic heave subsidence, or heave damping. The third mode is unstable and aperiodic, but very slow; an unstable aperiodic phugoid. The last mode is from the SCAS, specifically the DASH.

Table 2: Real and imaginary parts of the eigenvalues of the CH-47 Chinook with augmentation

σ	$j\omega$
-2.5950	± 1.8123
-0.4544	± 0.9740
0.0069	
-0.0427	
-0.2019	
-0.5317	
-0.5263	

Table 3: Motion cueing settings for main condition

	EMD CH-47 (C)
K_x	0.4
ω_{n_x}	1.2
ω_{b_x}	0.6
$\omega_{n_{lp_x}}$	0.5
ζ_x	1.0
K_z	0.5
ω_{n_z}	1.0
ω_{b_z}	0.8
ζ_z	0.9
K_q	0.8
ω_{n_q}	0.5
K_p	0.7
ω_{n_p}	2.0

As the MCA is a linear feed-forward connection (see Figure 1), the linearised dynamics of the motion cueing do not change the complex eigenvalues of the vehicle, however, the shape of the eigenvectors is changed. This is shown in Figure 3, where it can be seen how the eigenvectors are affected by a CWA, which is specifically tuned for the CH-47 using EMD.

EMD evaluates motion cueing fidelity, based on the level of preservation of the relevant vehicle eigenmode(s).[8] This is determined based on the relative size and phase of the eigenvectors. As seen from the perspective of EMD, the goal is to minimise the change in eigenvectors due to cueing. Ideally, the eigenvectors after cueing coincide with those before cueing. However, this is generally not possible, because filtering is applied, due to limitations in motion space of the simulator. Simulator motion space limitations are not included in EMD analysis, which means that iterative tuning can be necessary, depending on the task and pilot control behaviour.

Since a clear-cut tuning strategy using EMD is currently not defined, a motion filter tuning strategy is needed. The strategy used, generally aimed at a combination of low gain and low break frequency, instead of a high gain and high break frequency. This was done to avoid the transient amplification area of influence as much as possible (as will be discussed in Subsection 2.4). In situations where

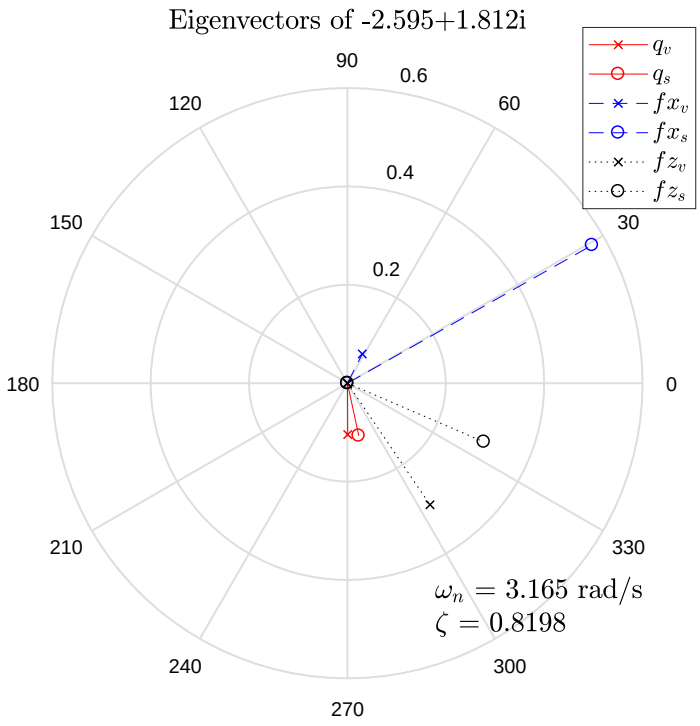

Figure 3: Eigenvector distortion in case of EMD CH-47 (C)

EMD is applied to different vehicles, the transient amplification effect can maybe be utilised to get a higher effective gain, without having a high filter gain.

2.4 Eigenmode Distortion Interpretation

The EMD method calculates the magnitude and phase distortions that an MCA imposes on the vehicle's perceived states, as illustrated in Figure 3. It is not always straightforward to interpret these distortions and relate them to the parameters of the MCA, or to the results of other motion cueing evaluation techniques, such as the OMCT. For example, a large difference can be observed between the gain K_z in Table 3 and the effective heave gain (the ratio of the length of the eigenvectors, $G_z = |fz_s|/|fz_v|$) from Figure 3 and Table 6. Normally, one would expect that $G_z = K_z$, or, due to steady-state high-pass filter characteristics, $G_z \leq K_z$. However, in this example $K_z = 0.5$ and $G_z = 1.01$, meaning that $G_z > K_z$. This is caused by a phenomenon called *transient amplification*, which is rooted in the difference between the Laplace domain and the Fourier domain.

The Fourier domain is used in many motion cueing evaluation techniques, including the Sinacori-Schroeder criterion and the OMCT.[2, 3, 6] In case of the OMCT, the analysis happens at 12 different un-damped frequencies, which are described by Equation 4. The response of a channel is plotted on a Bode diagram. Generally, this can be viewed as the Fourier transform of a particular channel of the MCA.

$$\omega = 10^{k/5-1} \text{ rad/s for } k = \{0, \ldots, 11\} \tag{4}$$

When the transfer function, that describes a certain motion cueing channel, is viewed in the Laplace domain, however, an interesting effect appears. The frequency domain is only that part of the Laplace domain where $s = j\omega$, whereas in general the Laplace variable is $s = \sigma + j\omega$. In time domain this is analogous to adding damping to the input sinusoids, similar to how the eigenmodes are damped sinusoids, which introduces transients into the system. This effect is explained with an example, using

the heave cueing filter. The transfer function, describing this filter (see Equation 5), is a third-order low-pass filter, with its parameters as described in Table 3.

$$H_{fz}(s) = 0.5\,\frac{s^3}{s^3 + 2.6s^2 + 2.44s + 0.8} \tag{5}$$

In Figure 4a the magnitude of the transfer function is shown in Laplace domain, instead of in Fourier domain (or frequency domain). The magnitude plot in the frequency domain is shown as the red line in Figure 4b, making it clearly visible that this represents only a small portion of the Laplace domain. The bold white band in Figure 4b and Figure 4d shows where the gain of $H(s)$ is equal to 1. The blue band in Figure 4b also appears in Figure 4c and Figure 4d, showing how the amplification changes, when the damping of the input signal, in the case of EMD the vehicle's eigenmode, changes.

Most aircraft motions are not purely periodic, so evaluating the motion cueing system based on the steady-state response, means that the MCA is valued, based on something that is at most partially relevant. Therefore the transient response of the MCA must be part of the evaluation, like it is done with EMD. The differences between the steady-state response and the transient response can be large. In this example G_z is more than twice as large as K_z. The difference with OMCT is even larger, which evaluates the magnitude distortion at $\omega = \omega_n$ as 0.46. Figure 4c shows that the effective magnitude gain of this eigenmode exactly crosses the intersection between $H(\omega_n)$ and $real(\lambda)$. This indicates that the observed amplification in EMD is fully described by this transient amplification and not by any other effects of the MCA. In this figure, the OMCT gain is the value of the blue line at $\sigma = 0$. Figure 4d shows the same magnitude plot, but the coordinate system is changed to ω_n-ζ. This way of plotting makes it easier to see the effect of the MCA on a different eigenmode, and can therefore be more relevant for use in filter tuning.

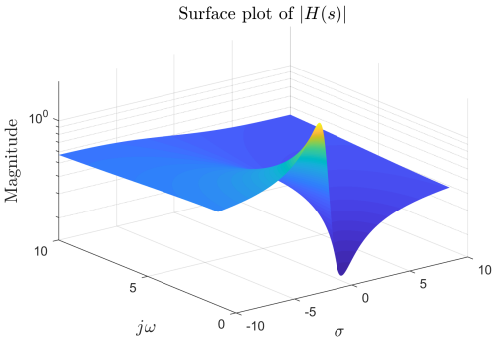

(a) Magnitude plot in three dimensions

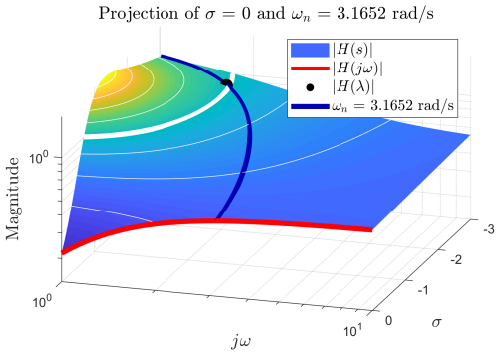

(b) Magnitude plot with projection of Bode plot and profile of eigenfrequency

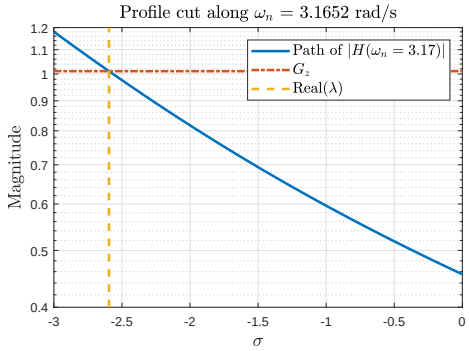

(c) Projection of $H(\omega_n)$ on σ-axis, together with the intersection of the real part of the eigenvalue and the apparent relative gain of the eigenvector (G_z)

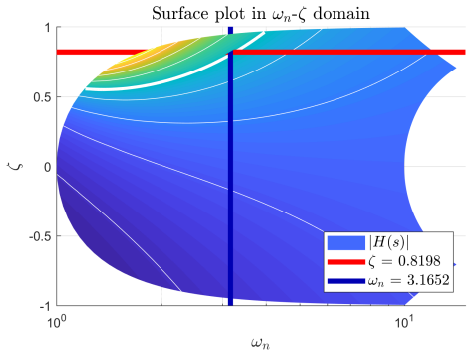

(d) Surface plot in different coordinate system

Figure 4: Bode magnitude plot in 3D for fz_v to fz_s, applied to $\lambda = -2.5950 + 1.8123i$

3 Method

In order to meet the objectives of this study, an experiment was designed to compare a vehicle-specific, EMD-based tuning set, with manually tuned settings, and with an EMD-tuned MCA for a different vehicle. The experiment was performed in the Desdemona simulator.

Four different motion configurations of the MCA were used, which are abbreviated according to Table 4. The first condition (V) is a vibration-only configuration, which consists of vertical vibrations at the frequency of the rotors. The vibration-only condition is included to have a baseline to compare the other conditions against. The other three conditions also include vibrations, in addition to MCA configurations as presented in Table 5. The eigenvector distortion diagrams belonging to those conditions are shown in Figure 3 and Figure 5, and the corresponding gain and phase distortion values are listed in Table 6. Note that the MCA tuning set of Condition A is borrowed from the short period motion condition of Miletović et al.[8]

Table 4: Condition corresponding to each number

abbreviation	condition
V	**V**ibrations only
C	EMD CH-47 **C**hinook
A	EMD AH-64 **A**pache
D	**D**esdemona default

Table 5: Motion cueing settings for the different conditions

	EMD CH-47 (C)	EMD AH-64 (A)	Desdemona (D)
K_x	0.4	0.3	0.7
ω_{n_x}	1.2	1.25	n/a
ω_{b_x}	0.6	n/a	n/a
$\omega_{n_{lpx}}$	0.5	n/a	0.5
ζ_x	1.0	1.0	n/a
K_z	0.5	0.8	1.0
ω_{n_z}	1.0	1.2	n/a
ω_{b_z}	0.8	n/a	2.0
ζ_z	0.9	1.0	n/a
K_q	0.8	1.0	0.7
ω_{n_q}	0.5	0.2	0.5
K_p	0.7	0.7	0.7
ω_{n_p}	2.0	2.0	1.0

The second condition (C, first column of Table 5) is the condition designed using EMD for this specific vehicle and eigenmode. The tuning strategy used for this configuration, is described in Subsection 2.3. The third condition (A, EMD AH-64) is the cueing set as used for the AH-64 Apache experiment of Miletović et al.[8], which is expected to clarify the sensitivity of an EMD based tuning set to differences in a vehicle model. The last condition (D) is used to compare EMD based motion cueing with the motion cueing that is currently in use for this vehicle at Desdemona. This can also help the company to improve on their cueing solution.

The roll channel settings were intended to remain identical for all motion conditions, however, the fourth condition unintentionally had a slightly different cut-off frequency. This might have affected the results of the experiment, as there were two comments on increased roll cueing in Condition D, despite the pilots being briefed to focus on longitudinal motion only.

The eigenvector distortion of these conditions is shown in Figure 3, Figure 5 and in Table 6. First, it is noteworthy that all three conditions have pitch-rate cues with relatively low magnitude and phase distortion. Compared to Condition C (Figure 3), Condition A (Figure 5a) has less phase

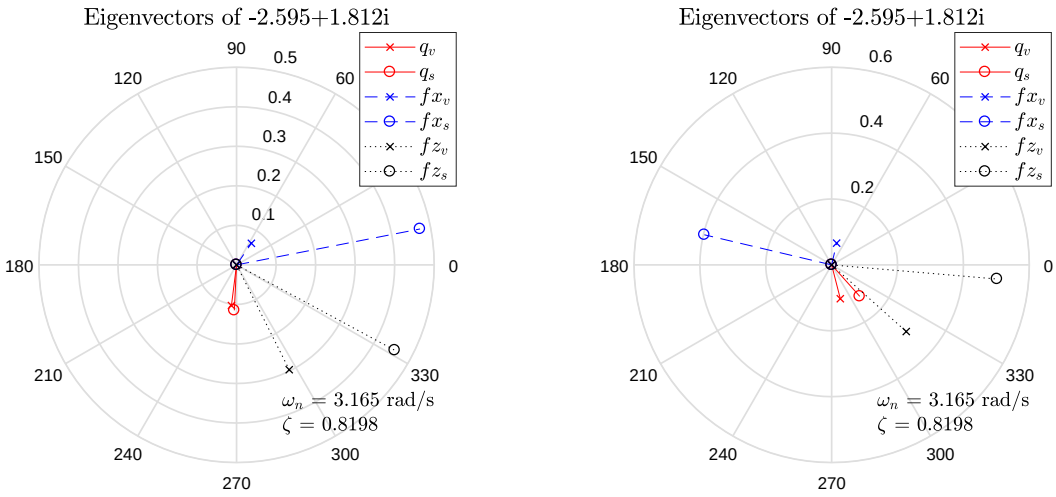

(a) Eigenvector distortion in case of EMD AH-64 (A)

(b) Eigenvector distortion with Desdemona default settings (D)

Figure 5: Eigenvector distortion of the last two motion conditions

Table 6: Magnitude and phase distortion of the eigenvectors for all three conditions

	EMD CH-47 (C)		EMD AH-64 (A)		Desdemona (D)	
	gain (−)	phase (°)	gain (−)	phase (°)	gain (−)	phase (°)
q	1.05	11.9	1.11	4.4	1.21	27.4
f_x	8.57	−33.6	7.14	−44.4	5.86	89.6
f_z	1.01	32.6	1.53	35.0	1.66	36.9

distortion in pitch (4.4° vs 11.9°), but slightly more magnitude distortion (1.11 vs 1.05). Condition D (Figure 5b) has both more phase and more magnitude distortion (27.4° & 1.21 respectively), compared to Condition C. When comparing the heave axis (f_z), all conditions have similar phase distortion, but the magnitude distortion for Condition C is comparatively small (1.01). In order to achieve this, the filter damping ratio was slightly decreased.

Regarding the surge axis (f_x), a different design choice has been made in the cases of Condition C and Condition A compared to Condition D. The Chinook is a heavy-lift helicopter, without direct forward propulsion, resulting in mostly coordinated flight and little specific forces along the body x- and y-axes. This, combined with the layout and characteristics of the Desdemona simulator[13], lead to Desdemona B.V. ignoring surge cueing. In the experiment, which will be discussed later on, the largest portion of flight was coordinated. Also during initial testing, very small surge cues were noticed to input and output the MCA, which puts less emphasis on this axis in the design of Condition C.

Note that all EMD gains are larger than 1. This means that all filters, despite the low filter gains, amplify the studied eigenmode to a magnitude higher than what will be felt in the real helicopter.

3.1 Participants

For this experiment three participants were available with varying experience levels, and all are familiar with flying the CH-47. The number of flight hours, on the CH-47 only, are listed below for each participant.

Subject 1 Novice CH-47 pilot - 300 flight hours
Subject 2 Experienced CH-47 test pilot - 5000 flight hours
Subject 3 Experienced helicopter test pilot - 30 flight hours

3.2 Simulator Setup

The experiment was performed in the Desdemona simulator, operated by Desdemona B.V., in Soesterberg, The Netherlands. More about this simulator is described in [13]. The simulated vehicle is a non-linear, analytical CH-47 model, based on the Delft Rotorcraft Simulation (Draftsim) model[10]. This is the same model as where the linear model, described in Subsection 2.1, is derived from. The non-linear model is augmented with a SCAS, modelled according to [11]. The experiment task is performed on a taxiway of a virtual model of Aviano Air Base (ICAO: LIPA) in north-eastern Italy.

Visuals The pilot is provided a virtual reality (VR) head-mounted display, showing the area of Aviano Air Base and the interior of the helicopter, including instruments. A background of the Alps and some airport hangars, buildings and trees, increase the visual cues available (Figure 6).

Sound Rotor and engine sound is played in the background, mostly to enhance immersion and to mask the sound of the simulator actuators. The pilot is also wearing a headset for communications with the control room.

Controls Replicas of CH-47 controls are used in combination with accurate control loading systems.

3.3 Experiment Task

Pilots were asked to fly a prescribed task, derived from the aeronautical design standard (ADS)-33E[14] Acceleration and Deceleration mission task element (MTE). Cargo helicopters are not required to perform this task within the mentioned performance standards, however, it was chosen as a basis, because this kind of manoeuvre is regularly executed during (training) missions. The task was adapted to be attainable by the CH-47 with limited aggressive control inputs. The maximum speed requirement was decreased to 30 kt and the length of the track was extended to 400 m. The time requirement was dropped altogether, as it was difficult to complete the task in the set time-frame with a loaded CH-47, and therefore it was not a realistic practice scenario. The track is shown in Figure 6. On each side of the centreline two rows of pylons were placed at 10 ft and 20 ft. The start and end lines were marked by a double row of pylons and a 5 by 5 meter hover plate (as can be seen in the centre of Figure 6). The midway point was also indicated by a double row of cones. The task was flown without wind or turbulence.

The pilots were asked to start in a stabilised hover, then accelerate to approximately 30 kt, and subsequently stop the helicopter above the target position in a stable hover. Then they were asked to do a hovering turn and do the same manoeuvre in the opposite direction. They were asked to land the helicopter after each run (once up and down the track), fill in the MFR and report back both the rating and their preference between this run and the previous. The objective was to perform the MTE within desired performance boundaries, but the boundaries were treated more like guidelines.

Desired performance was defined as:

- Maintain heading within $\pm 10^\circ$,
- Maintain steady airspeed ± 5 kt,
- Maintain lateral track within ± 10 ft,
- Maintain height below 50 ft,
- End in a hover with pilot seat above the target.

The reason these performance targets were given was to give the pilots a task, which is representative for realistic training flight, but limit it to longitudinal motion only. Also the state of the aircraft had to stay close to the linearised operating point, as the motion filters were specifically tuned for this trim point. The pilots were given some freedom in how they perform the task, to make the task more comparable to training scenarios.

3.3.1 Familiarisation Phase

Each pilot got sufficient time to familiarise with the flight model, controls and control loading, visuals and task. Familiarisation started on the ground. Then the pilot was asked to hold the vehicle in a

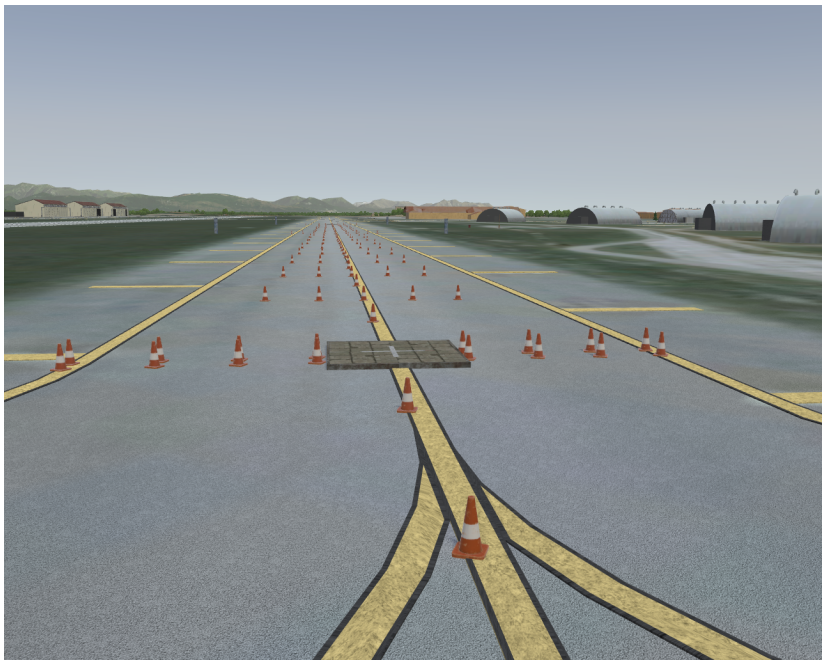

Figure 6: Simulation graphic showing the course that the pilots were asked to fly

Table 7: Condition of each run for each pilot. For the meaning of abbreviations see Table 4

run:	1	2	3	4	5	6	7	8	9	10	11	12	13
participant 1	V	A	C	D	C	A	V	C	V	D	A	D	V
participant 2	A	D	V	C	D	A	V	D	C	V	A	C	A
participant 3	V	C	D	A	D	V	D	C	A	C	V	A	V

hover, do a standard take-off run, fly a left-handed circuit, approach, land and fly more if desired. Subsequently he was asked to move the helicopter to the start point of the experiment and fly the track up, down and land again. This phase was flown in the vibrations-only condition, V. After this task, the pilot was asked to express any comments on the flight model and/or controls, to help the pilot differentiate between possible deficiencies in the flight model and/or flight controls, and the motion system, during the evaluation phase.

3.3.2 Evaluation Phase

Following familiarisation, the evaluation phase was started with the experiment task, as described earlier. The order in which the motion conditions appeared is shown in Table 7. In the design of this matrix, particular attention was paid to the number of times each pair appears. A pair was defined as the combination of a run and the previous run. For example (see Table 7), Participant 1 starts with Condition V, then Condition A (which together was a pair with Condition V), then Condition C (which was a pair with the previous condition, Condition A), then Condition D (which forms a pair with condition C), and so on. Each pair appears in both orders (e.g., C-A and A-C) for each participant. This method of testing means that thirteen runs were required per participant, and therefore one condition appears four times. Therefore, the first run of each participant was ignored in the MFR results, resulting in three runs for each condition.

3.4 Dependent Measures

The two most important dependent measures are the median of the MFR and the pilot's preferred motion configuration from each pair (the pair-wise comparison method is explained in Subsubsection 3.3.2). The MFR, as provided to the pilots on a knee-board, is shown in Figure 7[15]. Additionally, inputs from the pilot, outputs from the flight model, body velocities and latitude, longitude and altitude were also logged, but not used for analysis.

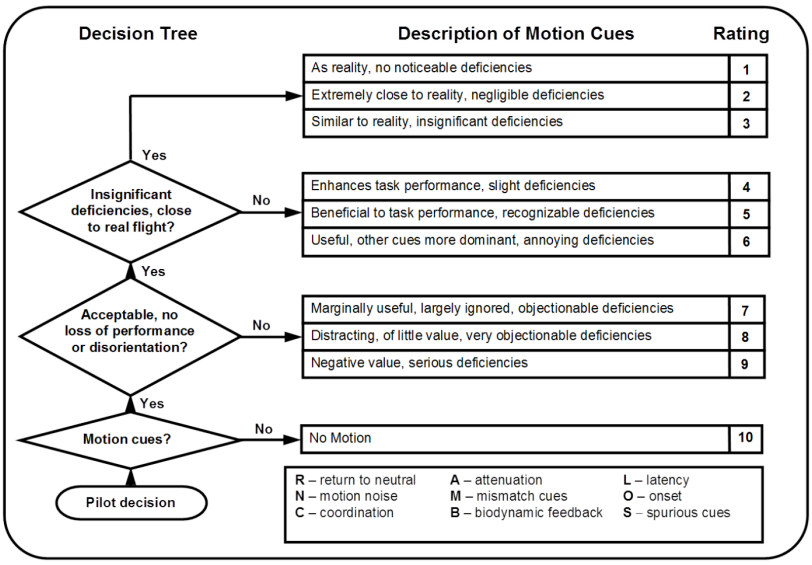

Figure 7: Motion Fidelity Rating scale[15]

3.5 Hypotheses

It was expected that, on average, Condition C was preferred over Condition V, as the latter condition exhibited only vibrations. For this reason, it was also expected that Condition V received high (hence, worse) scores on the MFR, compared to condition C. When comparing Condition C to Condition A, it was expected that Condition C was pair-wise preferred and also rated lower (better) on the MFR scale.

Condition D is currently in use for CH-47 training, which suggests that it should be a good tuning set. However, it was still expected that Condition C was preferred over Condition D, both regarding the pair-wise comparisons and the MFR. In short, it was predicted that Condition C was to be preferred over all other conditions.

3.6 Data Analysis

The preference score is calculated by adding 1 to the score for every instance a condition is preferred over the previous condition, and adding 1 to the previous condition, if the current motion condition was not preferred. Each condition appears three times for each subject (ignoring the first run), so a perfect score for a condition would be 6, the worst is 0.

To analyse the pair-wise preferences, a Matlab implementation[1] of the Bradley-Terry model[16] is used, with a Newton-Raphson optimisation method. This is a probability model that predicts the outcome of pair-wise comparisons, and returns the probability that condition i is preferred over j (see Equation 6).

$$Pr\left(i > j\right) = \frac{p_i}{p_i + p_j} \tag{6}$$

[1] `http://personal.psu.edu/drh20/code/btmatlab/`, accessed on 16 December 2019

4 Results

The results of the experiment are discussed, starting with the MFR each pilot provided after each run, see Figure 8. In this figure, there are four sets (representing the four conditions) of three or four bars (representing the three or four runs) for each of the three participants. The height of a bar shows the choice a participant has made in that run, and the horizontal thin red lines denote the rating at which a different choice is made in the decision tree of the MFR scale (compare to Figure 7). The bold black lines show the median score of each condition. Some conditions have four bars instead of three. Of those sets the first bar corresponds with the first run of a participant. Those first runs are ignored in calculation of the median, to avoid the number of occurrences influencing the score. This figure should be read as follows: e.g. Participant 1 (the top plot), scored Condition V with a 6 on the MFR scale, after the first occurrence of that condition. After the second occurrence, he rated the same condition with a 5. Then, after the third and fourth occurrences of Condition V, the condition was rated with a 4 both times.

From Figure 8, the first observation is that Participant 2, in the last occurrence of Condition C (marked in yellow in Figure 8), gave a score much worse than in the two preceding runs. During this run, however, the simulation accidentally froze for a few seconds. This might have caused detrimental effects on perception, due to which the score was negatively affected. Therefore it was decided to disregard the results of this run. In hindsight this run should have been repeated.

Secondly, Participants 2 and 3 showed signs of degrading happiness/appreciation towards the end of the experiment, both in verbal comments, as in the ratings given. This can be seen in Figure 8, as all last runs of each condition are rated at least as bad as the preceding occurrence. The experiment took approximately one hour per participant, and Participant 3 agreed to take a break halfway through the experiment. Participant 2 mainly mentioned the rising temperature inside the simulator cabin as uncomfortable.

And lastly, Participant 1 gave very similar results for all conditions. This might, for example, be caused by inexperience, or by using very subtle control inputs. It is therefore suggested to push pilots more, e.g., to complete the task in less time, such that the system dynamics are excited more.

Results of the other dependent measure, motion preference, are shown in Figure 9. This figure shows that the pilots were not very consistent in their choices. Especially Participant 1 was somewhat contradicting, seemingly having a slight preference for Condition A. Participant 2 disfavoured Condition V and had a modest preference for Conditions C and D. Note that this score is corrected for the disturbed simulation as discussed above, ignoring the preference score of that run and the subsequent one. Participant 3 disliked Conditions A and D, but preferred Conditions V and C equally, contrasting with other pilots. As Condition C has overall less pronounced motion, it seemed that this participant preferred less motion over the more reactive conditions. Figure 9 also shows the average score, which indicates a preference for Condition C.

The Bradley-Terry model, discussed in Subsection 3.6, estimates the probability of preference of the four conditions, as shown in Table 8. The standard error is calculated according to [17]. The results indicate that, for example, in a direct comparison between Condition C and the next-best condition, Condition D, the chance is $0.460/(0.167+0.460) = 73\%$ that Condition C wins. The other values are all very similar, which makes it difficult to form a ranking between the other conditions. The results from Table 8 support the same conclusions as the MFR scores indicated above.

Table 8: Probability scores according to the Bradley-Terry model for all conditions, including standard error

condition	probability	standard error
p_V	0.140	0.064
p_C	0.460	0.133
p_A	0.153	0.073
p_D	0.167	0.073

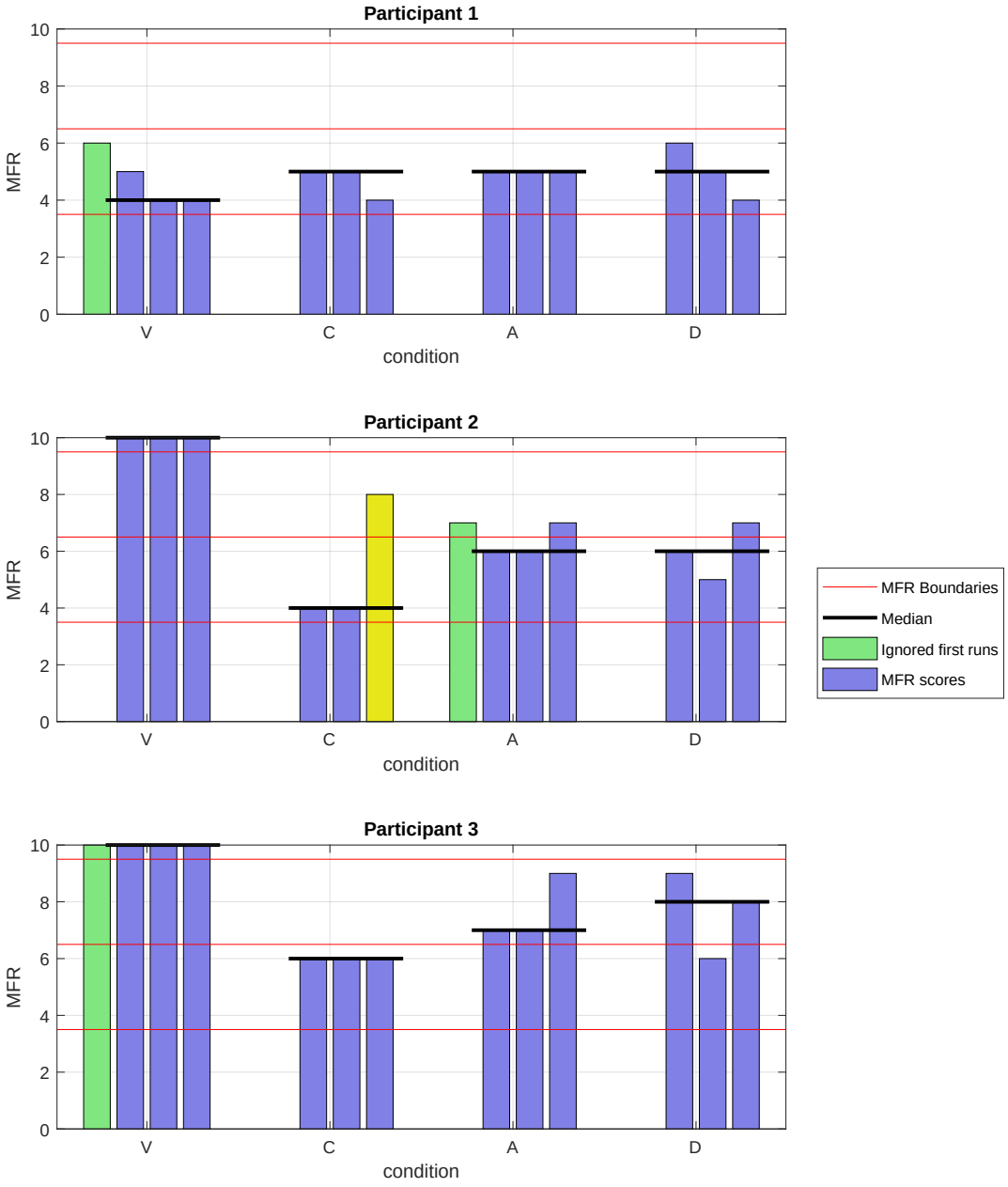

Figure 8: MFR of each run for every subject. Note the outlier of Participant 2, Condition C, run 3

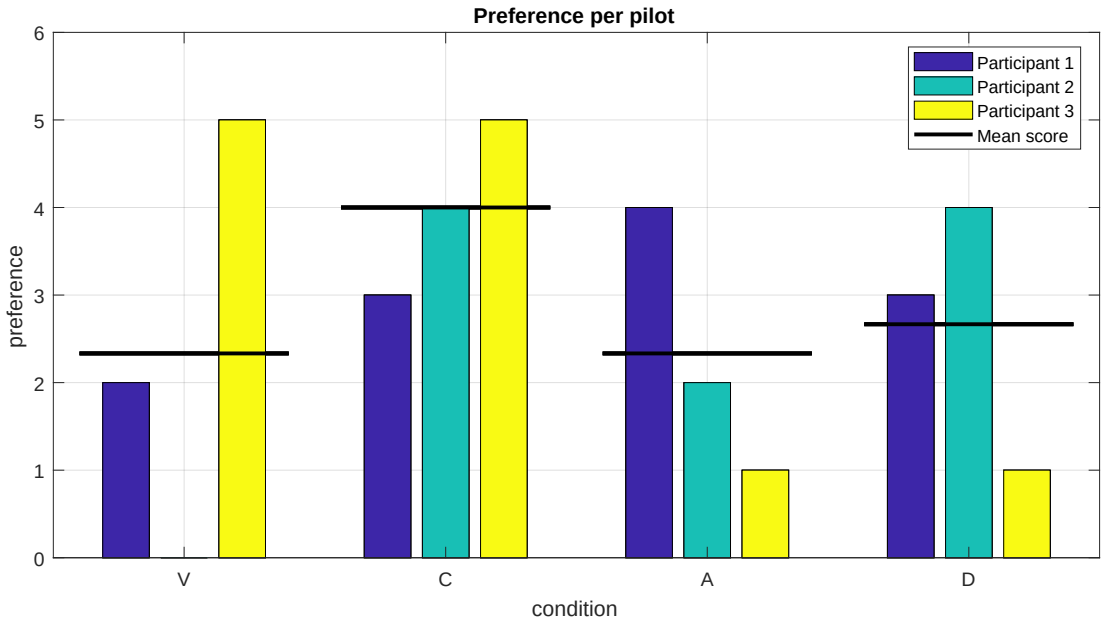

Figure 9: Pair-wise preference of each subject and mean score of each condition

5 Discussion

Following the results, in this section the implications of those results are discussed. To start off, the experiment was performed with only three participants, each of them having flown thirteen runs. This means that the data are too limited to do statistical testing, and the results are merely indications of what a larger population might prefer.

The first measure, MFR, shows that Participants 2 and 3 rated Condition V consistently with a 10 (no motion). This condition included vibrations to avoid the direct choice for "no motion" in Figure 7, but apparently that did not work as expected. These participants rated Condition C higher than all other conditions. Participant 1 seems to rate Condition V better than Condition C, however, that is not reflected in the pair-wise comparison, which in turn indicated that this participant preferred Condition V the least.

The median MFR rating of Condition A indicates that the motion cueing of the AH-64 has deficiencies, ranging from *recognizable* to *objectionable*. Compared to Condition C, this would indicate that an MCA, optimised for a certain vehicle, can sometimes be used for another vehicle, but degraded fidelity can be expected. This indicates that no single filter is perfect for a simulator, regardless of the simulated vehicle, contrasting with the OMCT.

Condition D received a considerably spread rating from all participants. In Table 3, it can be seen that Condition D operates with relatively high gains and high break frequencies, compared to Conditions C and A. This makes the filter active in the higher frequency range, but also makes it more exposed to transient amplification in the area around the break frequency. This could indicate that this tuning set highly depends on the way the task is executed. Some pilots commented on the high responsiveness of this condition. According to the median MFR scores, Condition C is rated better than Condition D. This indicates that structured tuning using EMD, results in a better tuned CWA than a manually tuned filter. This is also reflected in the pair-wise comparisons.

From Figure 9 it seems that Participant 3 prefers Condition V distinctly more than the other participants do. This raised the question if this subject did fly the same task and the same model. After reviewing the flight data logs it was observed that Participant 3 had a different average collective input, compared to Participants 1 and 2 (see Figure 10). This was presumably caused by a different aircraft mass being used during the experiment runs of Participants 1 and 2, who flew a model mass of 17.5 t. Using a different mass than the model was linearised for (15 t) could yield the model inac-

curate. To investigate the impact of this error, the model was adapted for the different mass and the new modes were calculated. Most eigenvalues shifted by less then 1%, including the mode considered for this experiment. Also the shape of the mode was mostly unaffected, and thereby the influence of this inadvertency was considered minimal. The cause of why Participant 3 preferred Condition V more than Participants 1 and 2 did, was not discovered.

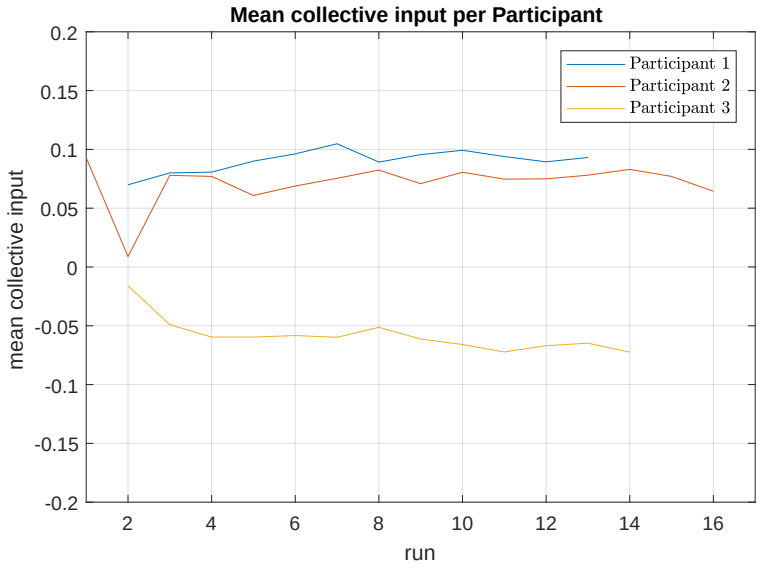

Figure 10: Mean collective input per participant. Input ranges between -1 and 1

One purpose of the experiment was to investigate if structured tuning, using EMD, results in a more preferred MCA for the CH-47, compared to the motion configuration currently in use at Desdemona B.V. By comparing Conditions C and D, both measures (MFR and pair-wise comparisons) show a clear advantage of using EMD in this scenario.

In the experiment it was also tested whether a single filter can be used for different vehicles, by coupling the CH-47 model to an MCA designed for the AH-64. This was again measured using MFRs and pair-wise comparisons. By comparing the results of both measures of Conditions C and A, it follows that Condition C is preferred over Condition A. As discussed above, the absolute MFR ratings indicate that Condition A is still useful in CH-47 simulation, but relative to Condition C it is valued worse. This indicates that a vehicle does require a unique MCA solution for "optimal" fidelity, except when the relevant eigenmodes coincide. This corresponds with the hypothesis, and supports the principles of EMD.

In Section 3 it was assumed that surge cueing is less relevant for this type of helicopter. This seems to have been a valid assumption, as the condition with the worst magnitude distortion in f_x, Condition C, was preferred, both according to the MFR and the pair-wise comparisons.

During the MCA design, the effectiveness of the EMD method was compared to conventional tuning methods, regarding on-line simulator time requirements, implementation difficulty of EMD compared to OMCT and knowledge prerequisites. This was not directly part of the experiment, and only observations about tuning with the EMD method can be shared. First of all, for this method to work, a few components have to be available. A model of the vehicle, linearised at the most important operating point, has to be available. This can be a single operating point, or multiple can be combined for use of gain scheduling (and possibly break-frequency scheduling). Furthermore a linear model of the MCA should be available. Generally the CWA is well documented and easy to use for this purpose, but a more complicated MCA can take more effort to linearise.

Subsequently the eigenmodes of the complete system must be calculated. This is not too difficult with the use of a control systems library, available in many programming languages. Then the most important eigenmode, the one which will be used to optimise the MCA for, has to be found. A general starting point is the fastest mode which falls within the human perception and control frequency range.

A better approximation is to fly the intended task and calculate the largest MPF for the task.[8, 18] This indicates which modes the pilot "activates" when controlling the vehicle. However, the system has to be observable to be able to derive the MPFs.[8, 18, 19] In case of this CH-47, mainly due to its complex SCAS, the system was not fully observable, hence the MPFs could not be calculated. All in all this method is not straightforward and also not always possible, and more research could help to clarify which eigenmode is most important for tuning and vehicle control.

In order to develop a tuning recipe, possibly a connection can be made to pilot perception models, such that the loop can be closed. Over the years, much effort has been put into the development of pilot perception models, of which many are reviewed in Xu et al.[20] Linking the combination of linear vehicle model and linear MCA, with a linear pilot perception model, can maybe clarify which modes are important for vehicle control, how important a mode is, and to what degree false cues are noticeable. A first step would be to scale the eigenvectors shown in this study, with respect to the sensory thresholds at the studied eigenfrequency.[21] Further research is required to explore the feasibility and usefulness of such expansions. A different solution is to use EMD as expansion on OMCT, where OMCT is used in the basis and EMD is used in particular areas of the domain to check the distortion of the most important mode, or to use both methods in an iterative procedure.

Tuning the MCA with the EMD method was perceived easy, but not necessarily well-defined. Once the eigenvector diagrams are created, it is straightforward to examine how the MCA affects the studied eigenmode. However, as there are multiple ways to reduce the magnification or phase distortion of an eigenvector (change the gain or vary the break frequency of the filter), it is not a straightforward recipe to optimise the MCA. It depends on the available motion space that the simulator has, on the task that needs to be performed and on how aggressively the task is carried out. Further study is needed to come up with a tuning recipe that optimises for both the used motion space and the eigenmode shape.

6 Conclusions

In this paper, the use of Eigenmode Distortion (EMD) in structured tuning of a motion cueing filter, was investigated. The method was applied to a model of the CH-47 Chinook and evaluated in a pilot-in-the-loop experiment. It is shown that EMD-based filter settings are preferred over current tuning settings. Future work is necessary to find a method to prioritize the vehicle's different eigenmodes, and to develop a recipe for effective motion cueing tuning. Expansion of this method with a pilot perception model can help to achieve this goal. Also, it is shown that a tuning set designed for a specific task, vehicle and simulator could be used for a different vehicle, but decreased fidelity can be expected. Implementation of EMD itself is attainable, but the method can be improved by adding alternatives for mode participation factor (MPF)-based eigenmode selection.

References

[1] S. K. Advani, R. J. A. W. Hosman and M. Potter, 'Objective Motion Fidelity Qualification in Flight Training Simulators', in AIAA Modeling and Simulation Technologies Conference and Exhibit (Aug. 2007), 10.2514/6.2007-6802.

[2] J. A. Schroeder, *Helicopter Flight Simulation Motion Platform Requirements*, tech. rep. NASA-TP-1999-208766 (National Aeronautics and Space Administration, Ames Research Center, Moffett Field, CA, USA, July 1999).

[3] J. B. Sinacori, *The Determination of Some Requirements for a Helicopter Research Simulation Facility*, tech. rep. NASA-CR-152066 (Systems Technology Inc., Mountain View, CA, USA, Sept. 1977).

[4] R. J. A. W. Hosman, S. K. Advani and J. Takats, 'Status of the ICAO Objective Motion Cueing Test', in Autumn Flight Simulation Conference: Flight Simulation Research - New Frontiers (Royal Aeronautical Society, Nov. 2012).

[5] R. J. A. W. Hosman and S. K. Advani, 'Design and Evaluation of the Objective Motion Cueing Test and Criterion', The Aeronautical Journal **120**, 873–891 (2016), 10.1017/aer.2016.35.

[6] Anonymous, *Manual of Criteria for the Qualification of Flight Simulation Training Devices - Volume 1 - Aeroplanes*, 3rd ed., ICAO Doc 9625 (2009).

[7] W. Dalmeijer, I. Miletović, O. Stroosma and M. D. Pavel, 'Extending the Objective Motion Cueing Test to Measure Rotorcraft Simulator Motion Characteristics', in 73rd AHS International Annual Forum (May 2017), pp. 1876–1891.

[8] I. Miletović, M. D. Pavel, O. Stroosma, D. M. Pool, M. M. van Paassen, M. Wentink and M. Mulder, 'Eigenmode Distortion as a Novel Criterion for Motion Cueing Fidelity in Rotorcraft Flight Simulation', in 44th European Rotorcraft Forum (Sept. 2018).

[9] S. Stoev, O. Stroosma, M. M. van Paassen, I. Miletović and M. Mulder, 'Eigenmode Distortion Analysis for Motion Cueing Evaluation in Fixed-Wing Aircraft Simulators', in AIAA Scitech 2019 Forum (Jan. 2019), 10.2514/6.2019-0179.

[10] I. Miletović, 'Motion Cueing Fidelity in Rotorcraft Flight Simulation, A New Perspective Using Modal Analysis', PhD dissertation (TU Delft, 2020) Chap. Appendix A.

[11] United States Army Warfighting Center, *CH-47D Advanced Flight Control System (AFCS)*, 011-2105-6 (Fort Rucker, AL, USA, Oct. 2006).

[12] L. D. Reid and M. A. Nahon, *Flight Simulation Motion-Base Drive Algorithms. Part 1: Developing and Testing the Equations*, tech. rep. UTIAS 296 (University of Toronto, Institute for Aerospace Studies, Dec. 1985).

[13] A. R. Valente Pais, M. Wentink, M. M. van Paassen and M. Mulder, 'Comparison of Three Motion Cueing Algorithms for Curve Driving in an Urban Environment', Teleoperators and Virtual Environments **18**, 200–221 (2009), 10.1162/pres.18.3.200.

[14] Anonymous, *Aeronautical Design Standard, Performance Specification, Handling Qualities Requirements for Military Rotorcraft, ADS-33E-PRF*, U.S. Army Aviation and Missile Command, Mar. 2000.

[15] S. J. Hodge, P. Perfect, G. D. Padfield and M. D. White, 'Optimising the Vestibular Cues Available from a Short Stroke Hexapod Motion Platform', in 67th AHS International Annual Forum (2011).

[16] R. A. Bradley and M. E. Terry, 'Rank Analysis of Incomplete Block Designs: I. The Method of Paired Comparisons', Biometrika **39**, 324–345 (1952), 10.2307/2334029.

[17] F. Wickelmaier and C. Schmid, 'A Matlab Function to Estimate Choice Model Parameters from Paired-comparison Data', Behavior Research Methods, Instruments, and Computers **36**, 29–40 (2004), 10.3758/bf03195547.

[18] G. D. Padfield, *Helicopter Flight Dynamics*, 2nd ed. (Wiley India Pvt Ltd, 2011).

[19] J.-S. Hwang, H. Kim and B.-H. Cho, 'Modal Parameters Estimation of Building Structures from Vibration Test Data Using Observability Measurement', Shock and Vibration, 1–13 (2015), 10.1155/2015/627852.

[20] S. Xu, W. Tan, A. V. Efremov, L. Sun and X. Qu, 'Review of Control Models for Human Pilot Behavior', Annual Reviews in Control **44**, 274–291 (2017), 10.1016/j.arcontrol.2017.09.009.

[21] E. Groen, M. Wentink, A. R. Valente Pais, M. Mulder and M. M. van Paassen, 'Motion Perception Thresholds in Flight Simulation', in AIAA Modeling and Simulation Technologies Conference and Exhibit (Aug. 2006), 10.2514/6.2006-6254.

A

MPF Explanation

In the past Miletović et al. and Stoev et al. have used mode participation factors (MPFs) to determine the relative importance of eigenmodes for a certain manoeuvre. The procedure of MPFs did not work for the CH-47 Chinook in this study, and this appendix tries to explain why. The following text is heavily based on the paper of Miletović et al.[1].

The dynamic response of linear systems can be fully described in terms of modal coordinates. In effect, the value of the linear (vehicle) system state, excited by external inputs, at any given time, can be written in terms of the system's eigenvalues and eigenvectors.

$$\vec{x}\,(t) = \sum_{i=1}^{n} \left(v_i^{\mathsf{T}} \vec{x}_0 w_i\right) e^{\lambda_i t} + \sum_{i=1}^{n} \int_0^t \left(v_i^{\mathsf{T}} B \vec{u}\,(\tau)\, w_i\right) e^{\lambda_i (t-\tau)} d\tau \tag{A.1}$$

In this equation, $\vec{v_i}^{\mathsf{T}}$ and $\vec{w}_i$ are the left and right eigenvectors, respectively, corresponding to the i-th eigenvalue of the system λ_i.

$$\vec{v_i}^{\mathsf{T}} A = \vec{v_i}^{\mathsf{T}} \lambda_i \tag{A.2}$$

$$A\vec{w}_i = \lambda_i \vec{w}_i \tag{A.3}$$

The eigenvectors form the basis of the modal coordinate transformation. In this transformation, a vector $\vec{r}(t)$ is defined for each state $\vec{x}(t)$ such that:

$$\vec{x}(t) = W\vec{r}(t) \tag{A.4}$$

$$\vec{r}(t) = W^{-1}\vec{x}(t) \tag{A.5}$$

with $W^{-1} = V^{\mathsf{T}}$, where V is the matrix of left eigenvectors and W the matrix of right eigenvectors.

$$MPF_i = \int_0^T |r_i(t)| dt \quad \text{for } i \in (1, n) \tag{A.6}$$

Integrating $|r_i(t)|$ over the time of the manoeuvre T yields a single scalar value for each mode. However, if just $|r_i(t)|$ is plotted over time it gives an indication of how each mode is participating at each time-step. The absolute value is taken because generally $\vec{r}(t)$ is complex-valued.

So to see how $|r_i(t)|$ evolves over time, only $V^\mathsf{T}\vec{x}(t)$ is needed. Since a linear model of the system is known, V is known. The linear model has 3 outputs and 9 states. The 3 recorded states are q, f_x and f_z, but the eigenvectors have 9 states. The states are unknown, but the system outputs are known: $y(t) = Cx(t)+Du(t)$. Assuming that $D = 0$, the state can be reconstructed using $x(t) = C^{-1}y(t)$, assuming that C is invertible. The MPF can now be calculated using $|r(t)| = |W^{-1}C^{-1}y(t)| = |V^\mathsf{T}C^{-1}y(t)|$.

The eigenvectors can be converted to the output space using the relation $V' = CV$. The MPFs can also be calculated using $|r(t)| = |(V')^\mathsf{T}y(t)|$. Combining the above two calculations, it follows that $V^\mathsf{T}C^{-1} = (CV)^\mathsf{T}$ must hold. Matrix multiplication rules say that $(CV)^\mathsf{T} = V^\mathsf{T}C^\mathsf{T}$, which, combined with the previous relation, results in $V^\mathsf{T}C^{-1} = V^\mathsf{T}C^\mathsf{T}$. Since C, in this case, is not square, this relation cannot hold, and therefore the MPFs cannot be calculated.

This is also reflected in the observability of the system. Due to the presence of the stability & control augmentation system (SCAS) in the Chinook model, there are unobservable states. Observability of a system is achieved when the rank of the observability matrix is equal to the number of states. The observability matrix OB is calculated as follows:

$$OB = \begin{bmatrix} C \\ CA \\ CA^2 \\ \vdots \\ CA^{n-1} \end{bmatrix} \tag{A.7}$$

where A and C are the system dynamics and state output matrices respectively. Due to the wide range of values in this matrix (9 orders of magnitude between smallest and largest value, see Figure A.1) calculating the rank can be difficult. If the tolerance is set at 1×10^{-3} or higher the rank is 8, smaller than the number of states. Possibly due to this fact the MPFs do not make sense. For completeness the results of above calculations are shown in Figure A.2. There is no sign of a phugoid, pitch subsidence, heave subsidence or any distinct mode: all values seem to rise and fall in relative equal measures.

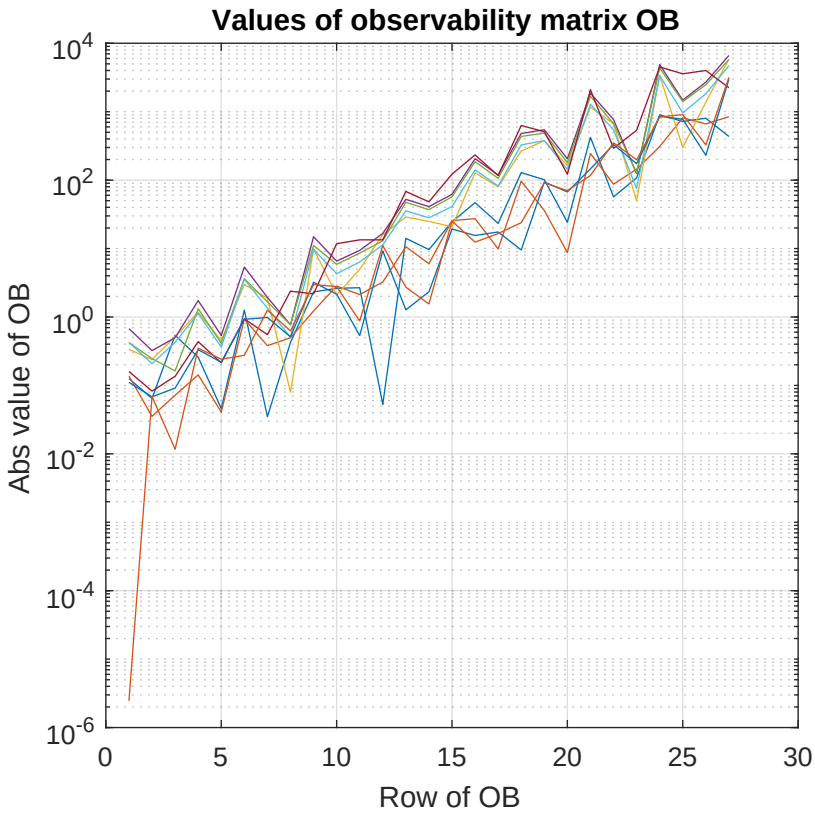

Figure A.1: Absolute values of the observability matrix

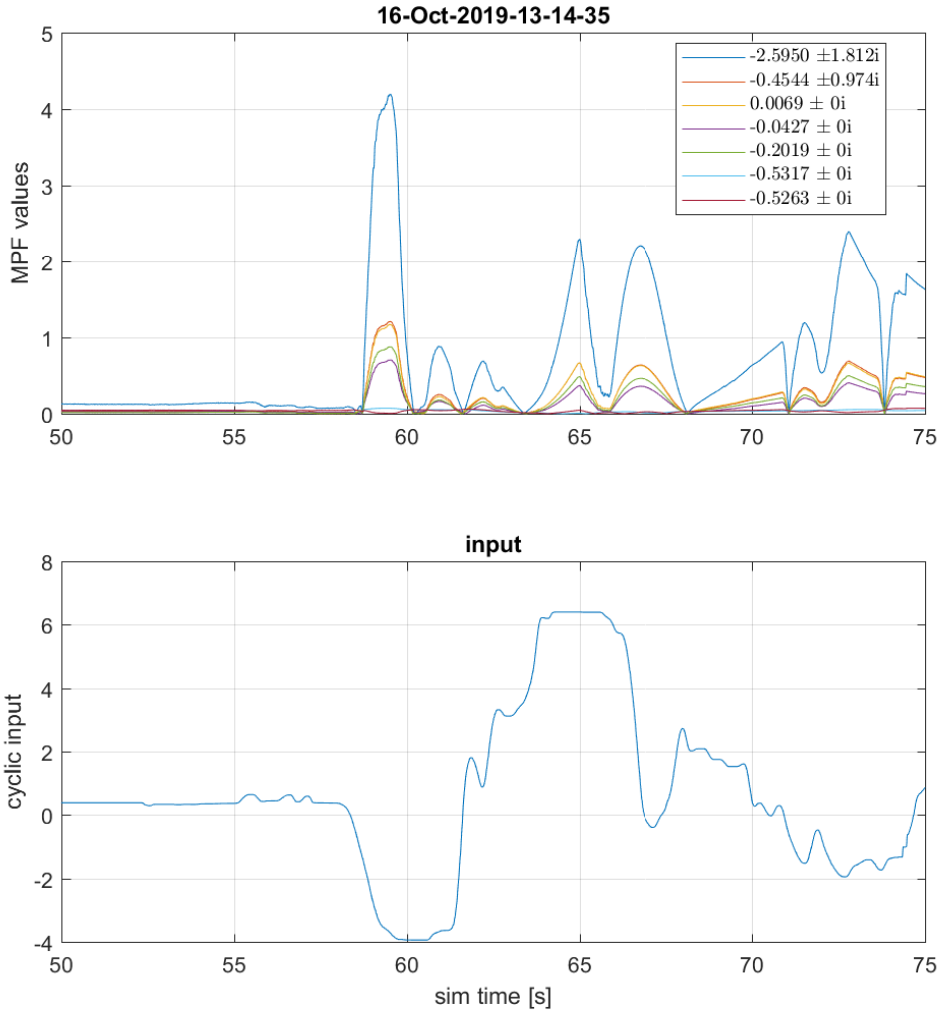

Figure A.2: Partical time trace of the MPFs calculated as above

B

Effect of Weight Difference

By mistake participant 1 and 2 have flown with a different helicopter mass than the model was linearised with. This difference was found by analysing the collective input data, which showed that the mean collective input of participant 3 was noticeably different from the average of participants 1 and 2. The model was linearised for a mass of 15 t, whereas the vehicle flown by participants 1 and 2 was 17.5 t; participant 3 did fly the correct mass. By adapting the model for this difference it was possible to calculate the effect on the eigenmodes. It was found that most eigenvalues shifted only slightly.

Table B.1: Eigenvalues of the CH-47 Chinook with a mass of 15 t and 17.5 t

15 t		17.5 t	
σ	$j\omega$	σ	$j\omega$
−2.5950	±1.8123	−2.5946	±1.8135
−0.4544	±0.9740	−0.4544	±0.9710
0.0069		0.0089	
−0.0427		−0.0420	
−0.2019		−0.1995	
−0.5317		−0.4649	
−0.5263		−0.5263	

The distortion of the eigenmodes did change as well, as is shown in Table B.2. The only noticeable difference is in fx, where both the gain and phase distortion slightly increases. Since it is assumed that the Chinook flies mostly coordinated, this vector does not actually contribute much to the feeling, and therefore it is argued that the effect of this discrepancy is negligible. One effect that can be expected is that it takes more effort to excite the systems' modes, as the helicopter needs more force to respond when it is heavier. Therefore maybe the pilots which flew the heavier model did not feel as much as the third participant did. This cannot be checked however, as the MPFs could not be reconstructed.

Table B.2: Magnitude and phase distortion of the eigenvectors for all three conditions

	EMD CH-47 (C)		EMD AH-64 (A)		Desdemona (D)	
	gain (−)	phase (°)	gain (−)	phase (°)	gain (−)	phase (°)
			15 t			
q	1.05	11.9	1.11	4.4	1.21	27.4
f_x	8.57	−33.6	7.14	−44.4	5.86	89.6
f_z	1.01	32.6	1.53	35.0	1.66	36.9
			17.5 t			
q	1.05	11.9	1.11	4.4	1.21	27.4
f_x	9.95	−34.0	8.31	−44.7	6.82	90.0
f_z	1.01	32.6	1.53	35.0	1.66	36.9

Bibliography

[1] I. Miletović, M. Pavel, O. Stroosma, et al., "Eigenmode Distortion as a Novel Criterion for Motion Cueing Fidelity in Rotorcraft Flight Simulation", in 44th European Rotorcraft Forum: Delft, The Netherlands (Sept. 2018).

[2] S. Stoev, O. Stroosma, M. M. van Paassen, I. Miletovic, and M. Mulder, "Eigenmode Distortion Analysis for Motion Cueing Evaluation in Fixed-Wing Aircraft Simulators", in AIAA Scitech 2019 Forum (Jan. 2019), 10.2514/6.2019-0179.

C

Experiment Briefing

Briefing that was provided to the pilots before the experiment. Translated to English.

Experiment Briefing

To investigate the applicability of the EMD method to the CH47 Chinook

Thank you for your contribution to this scientific endeavour! You will be (voluntarily) participating in a motion evaluation experiment in the Desdemona simulator in Soesterberg. In this experiment a new method of motion design and evaluation will be evaluated using a horizontal manoeuvre task. This briefing will introduce you to the experiment and to what is expected of you as participant.

In addition, while very unlikely for the current experiment, it is possible that some participants may develop nausea (simulator sickness) during the simulator tests. In case you experience the first symptoms of simulator sickness (feeling very warm, sweating profusely, stomach awareness), please inform the experiment conductor, such that appropriate measures can be taken.

Experiment Goal

The goal of this experiment is to investigate the applicability of the Eigenmode Distortion (EMD) method to the CH-47 Chinook. EMD is a new method developed to better predict and design motion conditions. For this experiment a few motion conditions are designed, and the experiment aims to confirm or deny the applicability of this method. The results of the experiment can be used to improve simulator motion design.

Experiment Task

The task you are asked to carry out is a scaled-down version of the ADS-33 Acceleration and Deceleration Mission Task Element (MTE). The goal is to start in a stabilised hover, then accelerate to approximately 20 knots, and subsequently end over the target in a stable hover. Then do a hovering turn and do the same manoeuvre in the opposite direction. Your objective will be to perform the MTE as accurately as possible. Desired performance is:

- Maintain steady airspeed at 30 knots ±5 knots
- Maintain heading within ±10 degrees
- Maintain lateral track within 10 ft
- Maintain height below 50 ft
- End in a hover with pilot seat above the target

This task will be repeated several times, while for each run the motion settings will be changed. You are asked to fill in the Motion Fidelity Rating (MFR) scale after each run. Please focus on longitudinal motion (heave, pitch and surge) only. You are also asked to choose between the previous motion setting and the current one; or in other words: is this better or worse than the previous motion condition? Good motion is motion that you would expect in this manoeuvre in the real helicopter. If you would rate the motion differently when at speed compared to hover, please say so.

Familiarisation Phase

Before the experiment starts you have the chance to familiarise with the task, flight model and the controls. After this familiarisation you are asked to express any comments on the flight model and/or controls, to avoid possible deficiencies in the flight model interfering with evaluation of the motion system settings.

Experiment Procedures

During the experiment you will perform the same manoeuvre several times with different motion conditions. The different conditions will be presented to you in a random order. The researcher will keep track of your performance and ratings, and will announce when the experiment has been completed.

Each run consists of two longitudinal repositions in opposite directions. Short breaks can be taken between runs, a longer break will be taken halfway the experiment. The experiment will last approximately 1 hour.

For each tracking run, the subsequent procedure will be followed:

1. The researcher applies the settings for the next run.
2. The researcher checks whether the participant is ready to go.
3. The researcher initiates the run after a countdown (3-2-1-go).
4. The participant performs the MTE.
5. The researcher stops the simulator.
6. The participant gives the score of the MFR and choses between this and the previous motion setting after the completed run.

Contact information researcher:	Contact information research supervisor
Henk van Donge	Ir. Olaf Stroosma
h.vandonge@student.tudelft.nl	o.stroosma@tudelft.nl
+31 6 25128395	+31 (0)15 27 85344

Thank you for participating!

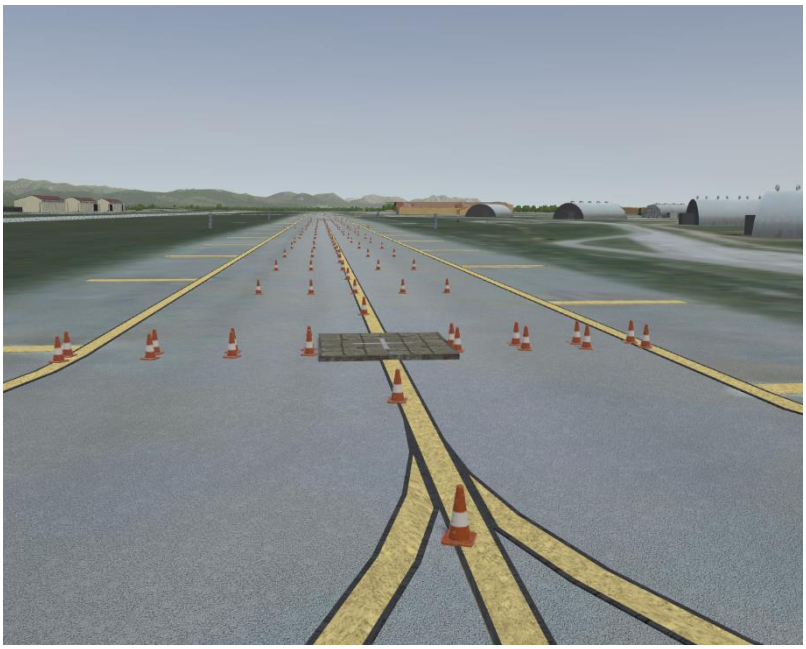

D

Experiment Logs

Logs of the results of the experiment. Translated to English.

Participant: 1

Name:

Date: 06-11-2019

run	condition	time of ending	MFRS rating	compared to previous	comments
1	1	15:13	6		
2	3	15:24	5	better	Feels more direct
3	2	15:28	5	worse	
4	4	15:32	6	worse	Feels like unstable roll
5	2	15:36	5	better	
6	3	15:41	5	better	
7	1	15:45	5	worse	
8	2	15:50	4	better	
9	1	15:55	4	better	
10	4	16:00	5	worse	
11	3	16:04	5	worse	
12	4	16:08	4	better	
13	1	16:13	4	worse	

Participant: 2

Name:

Date: 06-11-2019

run	condition	time of ending	MFRS rating	compared to previous	comments
1	3	16:49	7		Too much surge
2	4	16:53	6	better	More roll
3	1	16:56	10	worse	
4	2	17:00	4	better	
5	4	17:03	5	worse	
6	3	17:07	6	worse	
7	1	17:10	10	worse	
8	4	17:13	7	better	Realistic pitch cues
9	2	17:17	4	better	Pleasant
10	1	17:20	10	worse	
11	3	17:23	6	better	Weak cues
12	2	17:33	8	worse	Hot in the cabin (system crash)
13	3	17:37	7	better	Little difference

Participant: 3

Name:

Date: 07-11-2019

run	condition	time of ending	MFRS rating	compared to previous	comments
1	1	14:03	10		
2	2	14:08	6	better	Mostly heave
3	4	14:12	9	worse	
4	3	14:16	7	better	
5	4	14:20	6	better	
6	1	14:24	10	better	
7	4	14:29	8	worse	(break)
8	2	14:49	6	better	
9	3	14:54	7	worse	High gain
10	2	14:58	6	better	
11	1	15:01	10	better	
12	3	15:06	9	worse	Unpleasant
13	1	15:10	10	better	

E

Preliminary Thesis

This part is already graded, it is only included for your reference.

Preliminary Thesis

To investigate the applicability of the EMD method to the CH-47 Chinook

by

H. van Donge

to obtain the degree of Master of Science
at the Delft University of Technology.

Student number:	4230345	
Project duration:	22 November 2018 – 4 February 2020	
Thesis committee:	Prof. dr. ir. M. Mulder,	TU Delft, Control & Simulation section chair
	Ir. O. Stroosma,	TU Delft, supervisor
	Ir. I. Miletovic,	TU Delft, Ph.D.
	Dr. ir. M. Wentink,	Desdemona B.V.

TU Delft

Preface

This report shows the preliminary steps taken to conclude my master's thesis at the division of Control and Simulation of the faculty of Aerospace Engineering at the Delft University of Technology in Delft, The Netherlands. This thesis project was started on 22 November 2018.

First of all I would like to thank my supervisor, Ir. O. Stroosma, for all his effort and support in guiding me through this project. Prof. dr. ir. M. Mulder for providing me with very helpful feedback and a connection to industry. Next I also would like to thank all the people from Desdemona and Multisim for their help, support and motivation, as well as teaching me how to make the best coffee.

H. van Donge
Delft, December 2019

List of Figures

List of Tables

Abbreviations

Notation	Description
AFCS	automatic flight control system
CDR	centering device release
CPT	control position transducer
CWA	classical washout algorithm
DASH	differential airspeed hold (actuator)
DERP	design eye reference point
DoF	degree of freedom
EMD	Eigenmode Distortion
FADEC	full authority digital engine control system
FRF	frequency response function
FSTD	flight simulator training device
GND	ground
HSI	horizontal situation indicator
ILCA	integrated lower control actuator
IMU	inertial measurement unit
LCT	longitudinal cyclic trim actuator
LTP	local tangent plane
mag brake	magnetic brake
MCA	motion cueing algorithm
MFR	motion fidelity rating
MPF	mode participation factor
MTE	mission task element
NED	north, east, down
OMCT	objective motion cueing test
RMS	root mean square
RNLAF	Royal Netherlands Air Force
SCAS	stability & control augmentation system
SRS	SIMONA Research Simulator
SS	state-space
TU Delft	Delft University of Technology
VMS	vertical motion simulator

Symbols

Notation	Description	Unit
V_∞	freestream airspeed	[m/s]
Ω	rotor rotational speed	[rad/s]
α	angle of attack	[rad]
β	sideslip angle	[rad]
χ	heading angle	[rad]
γ	flight path angle	[rad]
μ	bank angle	[rad]
ϕ	roll angle	[rad]
ψ	yaw angle	[rad]
ρ	air density	[kg/m^3]
θ	pitch angle	[rad]
θ_0	collective pitch angle	[rad]
θ_{1C}	lateral cyclic pitch angle	[rad]
θ_{1S}	longitudinal cyclic pitch angle	[rad]
$_s$	Subscript indicating simulator related quantity	[-]
$_v$	Subscript indicating vehicle related quantity	[-]
p	rotational rate in body frame around x-axis	[rad/s]
q	rotational rate in body frame around y-axis	[rad/s]
r	rotational rate in body frame around z-axis	[rad/s]
u	velocity in body frame along x-direction	[m/s]
v	velocity in body frame along y-direction	[m/s]
w	velocity in body frame along z-direction	[m/s]
CG	centre of gravity	[-]
kn	knots, nautical miles per hour	[M/h]

Contents

1 Introduction

This report describes a preliminary steps taken in a study to investigate the broader applicability of a novel method, called Eigenmode Distortion (EMD). This method aims to improve the objectivity of motion cueing assessment. As subject for the study a CH-47 Chinook transport helicopter is chosen, which is further detailed in Chapter 2. The motion cueing side is described in Chapter 3. In Chapter 4 the results of the preliminary analysis are shown, whereas in Chapter 5 more details about the frequency domain are discussed based on the results of Chapter 4. Finally the results are discussed in Chapter 6.

This chapter will first introduce the background of the problem that is to be solved, then the problem itself is described, as well as which questions will be answered in order to solve the problem.

1.1. Background

Simulators are widely used for training of a large variety of tasks. Flight simulators, specifically designed to replicate some aircraft's characteristics, are generally used to train pilots, but also for design and development of aircraft and to study flight characteristics and handling qualities. Most training flight simulators are equipped with visual systems to increase the immersion. Trainees benefit in multiple ways from motion cues during flight simulator training sessions. Motion can help to avoid motion sickness by reducing the mismatch between visual and vestibular cues. Motion can also help the trainee to transfer his knowledge gained in the simulator to the real aircraft. Lastly it can help improving control performance in the simulator.

For these benefits to have effect it is important that the motion the pilot feels approaches what they would feel in the real aircraft. There is however one main problem: a simulator is usually located inside a (fixed) building, or in more technical terms: its motion space is limited. If it wouldn't be, it is a real aircraft and not a simulator. Limited motion means that it cannot equal the aircraft motion completely. So the question is: when does the motion of the simulator match that of the vehicle enough? This is also known as motion fidelity. As can be imagined, there is a trade-off between fidelity and costs. As motion fidelity is directly related to the available motion space, "better" motion requires a larger simulator, which will also be more expensive. To transform the calculated motion to the limited motion space a motion cueing algorithm (MCA) is used. The MCA can be tuned, which changes its fidelity, thus having an effect on how pilots feel the aircraft. An algorithm which is widely used for this is the classical washout algorithm (CWA), which will be introduced in Section 3.2.

The next question then is to classify what is high fidelity and what is low fidelity. This is not a trivial question to answer. Since it is all about how the pilot experiences motion, a certain setup can easily be experienced differently by another pilot, which inherently means there is a lot of subjectivity involved. Sinacori proposed a method to measure the distortion of the motion in frequency domain. It relies on measuring the response of the simulator to a sinusoidal input of 1 rad/s. Subsequently the magnitude and phase change of specific forces and rotational rates at that frequency were calculated, which gives an indication of how well the motion system represents the simulated motion.

The method developed by Sinacori is an analysis tool, but it can in turn also be used to improve the

tuning of the MCA. However, an optimal solution in this metric is limited to a single frequency. Industry saw the need for an enhanced method which analysed a broader domain. Therefore the objective motion cueing test (OMCT) was developed, which measured the same parameters as Sinacori did, but across twelve different frequencies ranging from 0.10 rad/s up to 15.85 rad/s. It also measures cross-coupling and false-cues. This method is a big improvement, however it still has some shortcomings. These shortcomings mainly come from the fact that OMCT assumes linearity and disconnection between the vehicle simulation and the motion system. The OMCT with its attributes will further be explored in subsection 3.3.1.

Most vehicles are not linear and the motion is coupled with the vehicle dynamics. The new EMD method attempts to remove these assumptions to obtain a more accurate prediction of motion fidelity. This method is however not thoroughly tested and evaluated, which is where this research will focus on.

1.2. Problem statement

EMD focusses mainly on the coupling of vehicle and simulator dynamics, but its applicability is not fully understood yet. This new method will undergo some evaluation together with an evaluation of the whole motion cueing tuning and evaluation domain. The research aim and questions are defined below.

Research aim

"To investigate the applicability of the EMD method to the CH-47 Chinook by designing an MCA by means of the EMD method and validating it in pilot-in-the-loop experiments, and comparing it to other types of aircraft."

Research questions

1. Will an EMD-based MCA be better compared to conventionally tuned MCAs for this type of aircraft?
   (a) How does one compare several MCAs?
2. Will EMD-based tuning be a better method than conventional tuning methods?
   (a) How does one compare and test different tuning methods?
3. How sensitive is the EMD-based tuning method to different aircraft types?
   (a) Will the eigenmodes resulting from this EMD-based MCA be different compared to other types of aircraft?
   (b) Which of the eigenmodes appear in both aircraft?
   (c) Which eigenmodes are important?
   (d) How can one compare eigenmodes and when do they differ enough?

2

Model of CH-47 Chinook

In this chapter the model of the aircraft at hand, the Boeing CH-47D Chinook, is discussed (Section 2.1), as well as its stability & control augmentation system (SCAS) (Section 2.2). Note that in the implementation of the model the longitudinal cyclic trim actuators (LCTs) are part of the analytical model, but they are treated as part of the SCAS.

In Figure 2.1 the structure of the model can be seen. This chapter covers the first two blocks, while the MCA is discussed in Chapter 3.

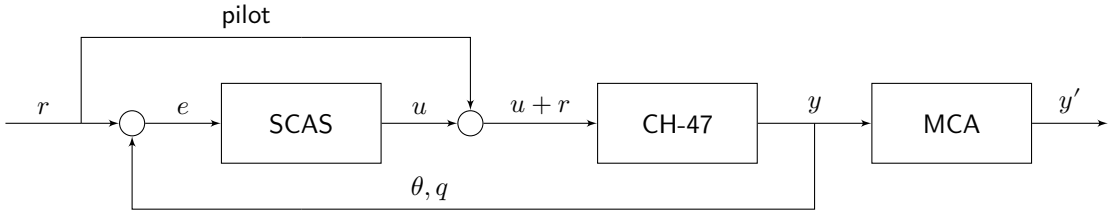

Figure 2.1: Combined Model Structure in longitudinal motion

2.1. Vehicle model

The Delft University of Technology (TU Delft) and Desdemona B.V. have jointly developed a modular flight dynamics model aimed at helicopter flight dynamics analysis, handling qualities evaluation and real-time flight simulation. This model is successfully applied to the AH-64 Apache attack helicopter as well as the AS-532 Cougar multi-purpose helicopter and is currently in use at Desdemona B.V. A side goal of this project was to apply the same model to the CH-47 Chinook transport helicopter and develop a model to be used for training for Desdemona B.V. In the next sections the structure and development of the model will be explained.

2.1.1. Analytical model

The flight dynamics model of the aircraft used in this research is heavily based on Miletović et al. [2]. The model as described in [2] is applied on the AH-64 Apache, but this model is easily adapted for the CH-47 Chinook. The main mathematical differences are the absence of the tail-rotor and the presence of a second counter-rotating main rotor system. The model consists of several separate parts which are subsequently linked. Those components are the rotor systems and the fuselage. As this model is aimed at basic manoeuvring flight and intended to run in real-time, some assumptions are made to simplify the model. The most important assumptions are:

- Rigid rotor blades. All flexibility is located at the flapping hinge.
- Consequently the main rotor blades' lead-lag and torsional dynamics are entirely neglected.
- The rotational speed of the rotors is assumed to be constant. Generally this is a valid assumption

through the use of full authority digital engine control systems (FADECs), except for rare cases such as auto-rotation.

- Blade aerodynamics are assumed to be linear, thus neglecting dynamic and stall effects.
- Terms in the various rotor equations to be developed that are $\ll \mu^2$, where μ is the rotor advance ratio, are neglected. According to Padfield, this incurs an error of less than 10% in the rotor's (flapping) response.
- The interaction between rotors is neglected.

This helicopter model will move in a widely used reference frame, namely the local tangent plane (LTP) frame. This reference frame neglects earth's curvature and relativistic effects. Such simplifications will introduce some errors, but they will not be noticeable given the speed and altitude range of this helicopter. The LTP-frame used is a north, east, down (NED) frame, denoted as $\{E\}_e$, defining the orientation of the x-axis pointing north, positive y is east, and z is pointing down towards the earth's centre. The value of z is therefore the negative of altitude.

Whereas $\{E\}_e$ is especially useful in navigational tasks, it is less so for simulator applications, where the movements of the body are more important than the location of it in the world. Therefore another reference frame is defined, which is attached to the body of the aircraft: $\{E\}_b$. It's x-, y- and z-axis are aligned with the front, side and bottom respectively, while the origin is located in the vehicles' centre of gravity (CG).

The transformation between the two reference frames is done by the transformation matrix T_{be}, shown in Equation 2.1. The order of rotation is important, so rotate first around yaw angle (ψ), then pitch angle (θ) and lastly roll angle (ϕ) angle.

$$
\begin{aligned}
\{E\}_b &= T_{be}\{E\}_e \\
\{E\}_b &= \begin{bmatrix} 1 & 0 & 0 \\ 0 & \cos(\phi) & \sin(\phi) \\ 0 & -\sin(\phi) & \cos(\phi) \end{bmatrix} \begin{bmatrix} \cos(\theta) & 0 & -\sin(\theta) \\ 0 & 1 & 0 \\ \sin(\theta) & 0 & \cos(\theta) \end{bmatrix} \begin{bmatrix} \cos(\psi) & \sin(\psi) & 0 \\ -\sin(\psi) & \cos(\psi) & 0 \\ 0 & 0 & 1 \end{bmatrix} \{E\}_e \\
T_{be} &= \begin{bmatrix} \cos(\psi)\cos(\theta) & \sin(\psi)\cos(\theta) & -\sin(\theta) \\ \sin(\phi)\sin(\theta)\cos(\psi) - \sin(\psi)\cos(\phi) & \cos(\phi)\cos(\psi) + \sin(\phi)\sin(\psi)\sin(\theta) & \sin(\phi)\cos(\theta) \\ \sin(\phi)\sin(\psi) + \sin(\theta)\cos(\phi)\cos(\psi) & -\sin(\phi)\cos(\psi) + \sin(\psi)\sin(\theta)\cos(\phi) & \cos(\phi)\cos(\theta) \end{bmatrix}
\end{aligned}
\tag{2.1}
$$

For this transformation it holds that $T_{eb} = {T_{be}}^{\mathsf{T}}$.

The last relevant main reference frame is the wind or aerodynamic reference frame $\{E\}_a$. It is also attached to the CG of the aircraft and the z-axis remains in the body xz-plane (generally plane of symmetry), but the x-axis is aligned with the current speed vector. The angle of attack (α) is defined as the angle between the x-axes of the aerodynamic frame and the body frame:

$$\alpha = \arcsin\left(\frac{w}{|\vec{V}|}\right)$$

and sideslip angle (β) as

$$\beta = \arcsin\left(\frac{v}{|\vec{V}|}\right)$$

The model has only six rigid-body degrees of freedom (DoF): three translational and three rotational. As stated before, the flapping mode was included in the model, but it's dynamic effects have been incorporated in the linearised model and therefore removing a DoF from the model. The model treats the forces of the subsystems as quasi-steady forces and moments acting in the c.g. Further details about the contribution of each subsystem can be found in [2]. Resulting from this model is a system of equations which describe the motion of the helicopter, both the response to (pilot) inputs as well as the response to an initial condition.

This system of equations is also known as the equations of motion. In general this system can be described as follows:

$$\begin{aligned} \dot{\vec{x}} &= \mathbf{F}(\vec{x}, \vec{u}) \\ \vec{y} &= \mathbf{G}(\vec{x}, \vec{u}) \end{aligned} \tag{2.2}$$

The input, state and output vectors are defined as follows: Equation 2.3. The input vector contains the controls of the pilot, namely collective, longitudinal and lateral cyclic and pedals. Although the CH-47 Chinook does not have a tail rotor, differential lateral cyclic does achieve the same goal, which is why the notation for standard helicopter configurations is retained. The state vector includes the position $\vec{r}$ (x, y, z) and attitude $\vec{\Phi}$ (ϕ, θ, ψ) in the inertial frame, and translational $\vec{V}$ (u, v, w) and rotational $\vec{\omega}$ (p, q, r) velocities in body frame. The output vector can contain any variable which is a function of $\vec{x}$ and $\vec{u}$.

$$\begin{aligned} \vec{u} &= \begin{bmatrix} \theta_0 & \theta_{1_s} & \theta_{1_c} & \theta_{0_{tr}} \end{bmatrix}^\mathsf{T} \\ \vec{x} &= \begin{bmatrix} \vec{r}^\mathsf{T} & \vec{V}^\mathsf{T} & \vec{\Phi}^\mathsf{T} & \vec{\omega}^\mathsf{T} \end{bmatrix}^\mathsf{T} \\ \vec{y} &= \mathbf{G}(\vec{x}, \vec{u}) \end{aligned} \tag{2.3}$$

Also it is useful to understand that some of the states, namely velocity $\vec{V}$ and rotational rate $\vec{\omega}$, are the time-derivatives of other states: position $\vec{r}$ and attitude $\vec{\Phi}$ respectively. However, since the reference frame in which they are defined is not the same, a conversion has to be made. Hence, following basic kinematics, $\dot{\vec{r}} = T_{eb}\vec{V}$ and $\dot{\vec{\Phi}}$ is shown in Equation 2.4.

$$\dot{\vec{\Phi}} = \begin{bmatrix} 1 & \sin(\phi)\tan(\theta) & \cos(\phi)\tan(\theta) \\ 0 & \cos(\phi) & -\sin(\phi) \\ 0 & \dfrac{\sin(\phi)}{\cos(\theta)} & \dfrac{\cos(\phi)}{\cos(\theta)} \end{bmatrix} \vec{\omega} \tag{2.4}$$

The derivatives of velocity and rotations are a function of aircraft characteristics, pilot inputs and the state of the aircraft. The definitions are given in Equation 2.5 and Equation 2.6, in which $\vec{F}_{c.g.}$ is the total resulting force acting at the CG, and similarly $\vec{M}_{cg}$ is the total moment at the same point. The moment of inertia tensor J is defined as shown in Equation 2.7, bearing in mind however that most aircraft and helicopters (including the CH-47 Chinook) are symmetric in the body xz-plane, I_{xy} and I_{yz} are zero.

$$\dot{\vec{V}} = \frac{\vec{F}_{cg}(\vec{x}, \vec{u})}{m} + T_{be}\vec{G} - \vec{\omega} \times \vec{V} \tag{2.5}$$

$$\dot{\vec{\omega}} = J^{-1}\left(\vec{M}_{cg}(\vec{x}, \vec{u}) - \vec{\omega} \times J\omega\right) \tag{2.6}$$

$$J = \begin{bmatrix} I_{xx} & -I_{xy} & -I_{xz} \\ -I_{xy} & I_{yy} & -I_{yz} \\ -I_{xz} & -I_{yz} & I_{zz} \end{bmatrix} \tag{2.7}$$

2.1.2. Linearisation

To perform eigenmode analysis, the system has to be linearised. However, before linearisation is performed, the model is split in two separate models: one for longitudinal and one for lateral motion. Since this report will only cover longitudinal modes, the lateral model is neglected. Motion in the longitudinal plane is limited to heave, surge and pitch, therefore reducing the model from six DoF to three DoF. This has as effect that all components of forces, moments, rotations and translations which are not in that plane are neglected. Hence,

Equation 2.5 and Equation 2.6 reduce to Equation 2.8. The corresponding kinematic equations simplify to Equation 2.9.

$$\begin{aligned} \dot{u} &= \frac{F_{cg}^{x}}{m} - g\sin(\theta) - qw \\ \dot{w} &= \frac{F_{cg}^{z}}{m} + g\cos(\theta) + qu \\ \dot{q} &= \frac{M_{cg}^{y}}{I_{yy}} \end{aligned} \tag{2.8}$$

$$\begin{aligned} \dot{x} &= u\cos(\theta) + w\sin(\theta) \\ \dot{z} &= -u\sin(\theta) + w\cos(\theta) \\ \dot{\theta} &= q \end{aligned} \tag{2.9}$$

Most variables in the above equations are a result of the simulation itself, values which where calculated in the previous time-step or defined by an initial condition. This does not hold for forces and moments acting on the vehicle, they have to be calculated based on the characteristics of the vehicle. During linearisation, these components are assumed to be a linear combination of the states of the vehicle, control inputs and constant parameters. The constants are called stability derivatives (in case of values which depend on the state of the aircraft) and control derivatives (for values depending on the control input). In reality the value of these "constants" are not constant, but around an operating point they can be assumed to be constant. This means that the validity of the linear model will decay the further away from the operating point it is analysed.

Generally an operating point is chosen to have no resulting rotational and translational accelerations. Such a point is also called a trim point. A trim algorithm is used to calculate the initial condition of the state and input vector[4]. As it is expected that the CH-47 has quite different behaviour at different airspeeds, several trim conditions are chosen for this research. More characteristics of the Chinook can be found in [5–7].

This helicopter type has several key operating states of the stability & control augmentation system (SCAS), which changes the behaviour significantly. Also the longitudinal cyclic trim actuators (LCTs) are assumed to have a significant effect on the flight dynamics. The LCTs are actuators which change the entire installation angle of the main rotor shafts in order to reduce stress, drag and vibrations at higher speeds. More information about operation of LCT can be found in [8]. The trim conditions are chosen to be in the most linear part of the flight-envelope. The LCT starts adjusting from about 40 kn, up to 120 kn. Besides the LCT, the SCAS also has a major switching point at 40 kn. To avoid non-linearities around the switch-on-switch-off points, the linearisation is performed at 0, 20, 80 and 160 kn.

The resulting linear model fits the general structure shown in Equation 2.10, in which $\vec{x}$ is the state vector, $\vec{y}$ the output vector and $\vec{u}$ the input vector.

$$\begin{aligned} \dot{\vec{x}} &= A\vec{x} + B\vec{u} \\ \vec{y} &= C\vec{x} + D\vec{u} \end{aligned} \tag{2.10}$$

2.1.3. Parameters and final LTI

In the previous subsections the state, input and output vectors are defined, as well as the structure of the model. In this subsection the matrices are filled. Equation 2.11 shows the matrices to be substituted in the state-space system of Equation 2.10. The state, input and output vector definitions are shown in Equation 2.12.

$$A = \begin{bmatrix} Xu & Xw-q & -g\cos(\theta) & Xq-w \\ Zu+q & Zw & -g\sin(\theta) & Zq+u \\ 0 & 0 & 0 & 1 \\ Mu & Mw & 0 & Mq \end{bmatrix} \quad B = \begin{bmatrix} Xu0 & Xus \\ Zu0 & Zus \\ 0 & 0 \\ Mu0 & Mus \end{bmatrix}$$
$$C = \begin{bmatrix} 1 & 0 & 0 & 0 \\ 0 & 1 & 0 & 0 \\ 0 & 0 & 1 & 0 \\ 0 & 0 & 0 & 1 \end{bmatrix} \quad D = \begin{bmatrix} 0 & 0 \\ 0 & 0 \\ 0 & 0 \\ 0 & 0 \end{bmatrix} \tag{2.11}$$

$$\vec{x} = \vec{y} = \begin{bmatrix} u \\ w \\ \theta \\ q \end{bmatrix}, \quad \vec{u} = \begin{bmatrix} \theta_0 \\ \theta_{1S} \end{bmatrix} \tag{2.12}$$

The exact values of the model can be found in Appendix B. The stability and control derivatives are given in Table B.1 and Table B.2 respectively.

2.2. AFCS

A big portion of the helicopters flight characteristics, besides due to the double rotor design, are induced by the SCAS. As part of the assignment the SCAS had to be modelled as well, based on documentation[8]. This section describes the functioning and structuring of the automatic flight control system (AFCS), the process of designing the modelled version, the assumptions made in the design as well as linearisation, and finally the linearisation itself. For positioning this section in the broader picture, please refer to Figure 2.1.

The functions of the AFCS are numerous[8]:

1. Stability about all axes
2. Bank angle hold
3. Heading hold
4. Airspeed hold
5. Pitch attitude hold
6. Positive stick gradient
7. Altitude hold
8. AFCS trim
9. Heading select
10. Longitudinal Cyclic Trim (LCT)

The system is dual, meaning in normal operation both AFCS-units provide half of the control and authority for the system to operate, but when only one system is switched on it provides the total output. After linearisation only the stability and control augmentation and positive stick gradient remain intact.

2.2.1. Structure

The total system is composed of several components, as can be seen in Figure 2.2. Summarising it comes down to displays and controls for the pilots, sensors, actuators and computers.

Regarding the actuators, there are basically two types of actuators: the fast integrated lower control actuators (ILCAs) and the slower differential airspeed hold (actuator) (DASH). Whereas the DASH introduces control actions for Airspeed hold, Pitch attitude hold and Positive stick gradient[8], the functionality of the ILCA includes the following[8]:

1. Stability
2. Bank angle hold

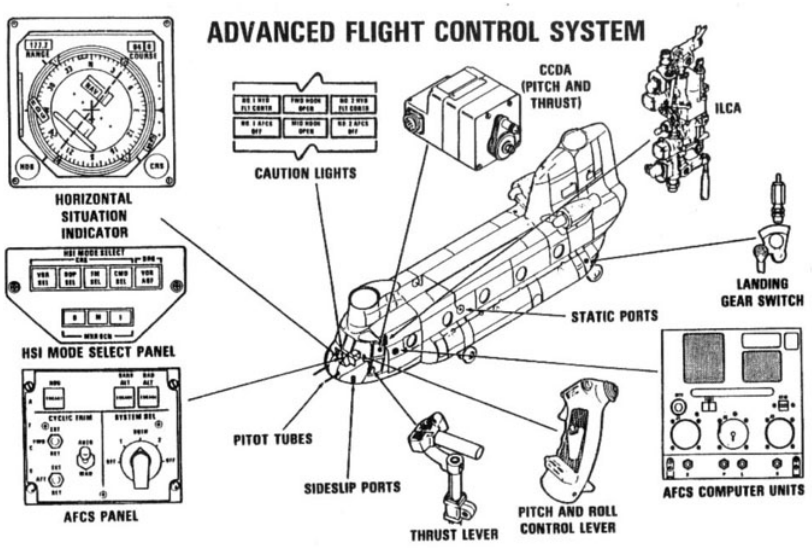

Figure 2.2: Context overview of components of the AFCS system[8]

3. Bank angle trim
4. Heading hold
5. Heading select
6. Coordinated turns

The sensors of the system include the control position transducers (CPTs), which sends the cyclic and pedal control positions to the AFCS, and the landing gear proximity switches, which most relevant functions are to reduce the AFCS pitch stabilisation signal by 50% and move the LCTs to the ground (GND) position. Then there are also the pitot tubes, which gives the system information about the speed of the aircraft; three static ports, giving information about the barometric altitude, and the sideslip ports sensing the lateral pressure difference when moving sideways.

Also important for the system to function are the gyroscopes. There are several of them, providing information about different motions. First there is the yaw-rate gyroscope, which provides a rate-of-motion signal to compensate the yaw-rate. And secondly there are the vertical gyroscopes, which sense pitch and roll attitude and rate signals. Lastly there is the directional gyroscope which provides information about the heading to the horizontal situation indicator (HSI). It is different to the yaw-rate gyroscope in that it is coupled with the compass, and it measures an angle instead of an angular rate.[8]

The pilots have several ways to interact with the AFCS. That includes the HSI, the centering device release (CDR), the AFCS mode control panel, and of course using the normal flight controls. The Dutch CH-47D Chinooks have flight director steering, but this system is not modelled because it is rarely used in the training scenarios for which the model is developed.

The research will cover only longitudinal motion, but since the AFCS will also be used in operational training situations, all three axis are modelled and therefore also treated here. Now the pitch, roll and yaw axis operation will be treated.

2.2.2. Pitch

In pitch axis, the two relevant actuators are the pitch ILCA and the DASH. The structure can be seen in Figure 2.3. The ILCA is used for stability augmentation in the inner loop, where it supports the pilot to make the flight more comfortable and safe and less exhausting. The pitch rate signal is derived from the vertical gyroscope. This signal is filtered and subsequently compensated for the yaw-rate. Then it is passed through another low-pass filter, together with a feed-forward signal which is cancelled when both GND-switches are on. This total signal is the main pitch damping signal which is send to the ILCA.

Secondly there is a signal, taken from the CPTs, which is modified, band-pass filtered and added to the pitch ILCA channel with the purpose of control augmentation. The same signal is passed through a set of low-pass filters, instead of a band-pass filter, and send to the DASH.

Other signals that constitute the DASH signal are the pitch angle, also low-pass filtered, and the airspeed. The airspeed is first limited at 40 kn minimum, then passes via a gust-filter into the DASH servo.

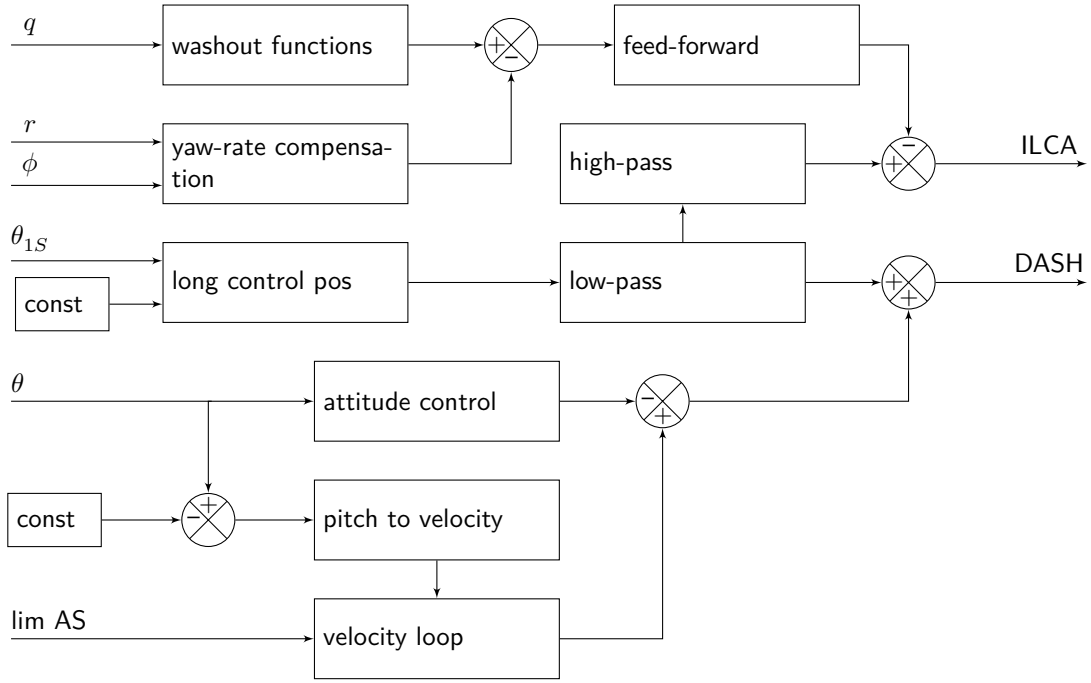

Figure 2.3: Structure of AFCS in longitudinal axis

2.2.3. Roll

Analogous to the design in pitch, the roll rate signal is first filtered with a notch filter and a low-pass filter before it is passed to the roll ILCA. Another component of the roll-rate damping signal is dependent on the state of a switch, which in turn depends on the stick inputs, roll-rate, the fact if the cyclic magnetic brake is depressed and some other, for this research less relevant, states. Similarly the lateral cyclic input is band-pass filtered and sent to the roll ILCA as control augmentation.

Thirdly there is a signal which maintains a certain roll angle. This angle is controlled by a synchroniser which enables when the lateral cyclic stick input is out-of-detent. In this way the roll attitude will automatically be held if the pilot lets go of the stick. The roll angle can also be controlled by a trim switch, which incrementally changes the reference roll angle.

Lastly the CPT signal in the lateral axis is checked if it is out-of-detent. This discrete signal is used in above control logics. It synchronises if the cyclic magnetic brake (mag brake) is depressed.

2.2.4. Yaw

The yaw channel is very similar to the roll control channel design, in the sense that is has angle hold (heading hold), rate damping (yaw damper), control augmentation and out-of-detent detection. Additionally, in the yaw channel there is a signal which compensates for the roll rate, as well as a signal which automatically reduces the lateral pressure difference, thus reducing sideslip angle and therefore increasing efficiency and reducing pilot fatigue.

2.2.5. Assumptions

Just like with the aerodynamic model of the helicopter the AFCS has to be linearised to be useful for eigenmode analysis. For this to be possible some assumptions had to be made. This includes the states of all switches. The state of certain switches, and therefore the behaviour of the AFCS, changes with the state the aircraft is in, of which the airspeed is the most noticeable one. Therefore the assumptions are different for

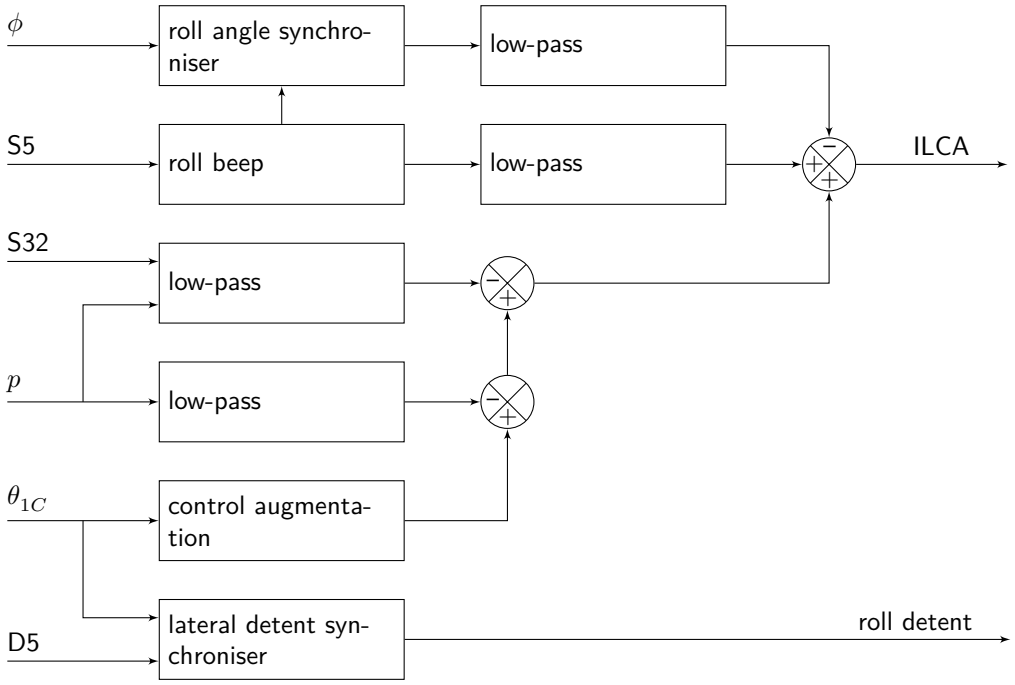

Figure 2.4: Structure of AFCS in roll axis

different airspeeds, and the linearisation, including its structure, is different for different airspeeds. Below the assumptions at hover conditions are given. Some of the assumptions, most notably the stick rate, will likely be violated during the experiments. This will make the linear model less accurate, but that is unavoidable for linearisation.

- no ground contact
- speed close to 20 kn
- no failures, gyroscopes are valid (D3)
- pitch angle stays between -11.50 and $23.50°$
- perfect servos: no delay, no limits (except for the DASH, which dynamics are linearised)
- no intermediate CDR, mag brake or beep trim used
- longitudinal stick deflection (with 1 inch aft bias) between 2.20 inch aft and 1.75 inch forward.
- longitudinal stick rate smaller than 0.14 inch/s (VDASH Dash longitudinal control velocity limit)
- roll attitude stays between -0.04 and 0.04 rad ($\pm 2.29°$)

2.2.6. Linearisation

Now the conditions and states of AFCS and its switches are determined, the actual linearisation can be discussed.

Most blocks of Figure 2.3 are composed of several switches, rate limits, saturation limits and transfer functions. So to linearise this, each block has to be linearised. To accomplish this, each channel, from each input to each output, is separately linearised. This is done by separating each channel as much as possible, after which the assumptions mentioned above are applied, removing most non-linearities. The remaining transfer functions and gains are easily converted to state-space systems. In some cases an equivalent transfer function is constructed, in order to reduce the order of the transfer function. This equivalent transfer function is closely matched in the frequency domain to the original signal behaviour using the Bode diagrams of the transfer functions.

It is also worth noting that later the input of the AFCS is added to the pilot inputs. In the model there is

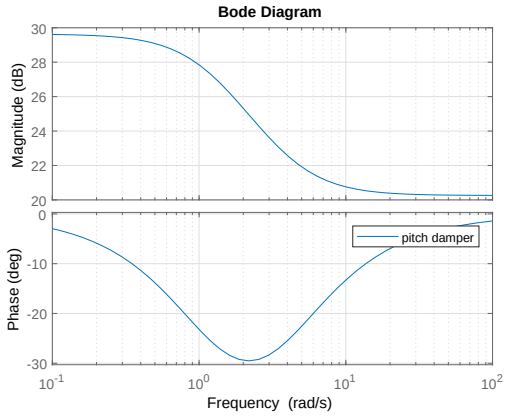

(a) Pitch-rate damping channel

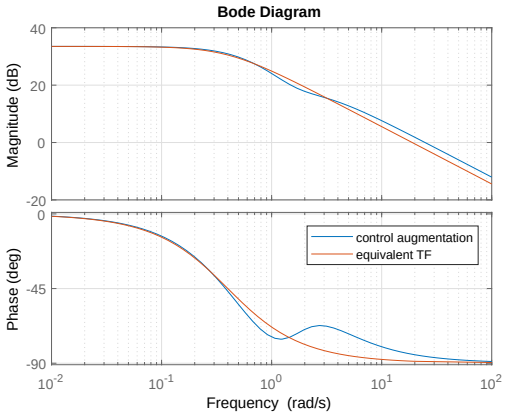

(b) Control augmentation channel

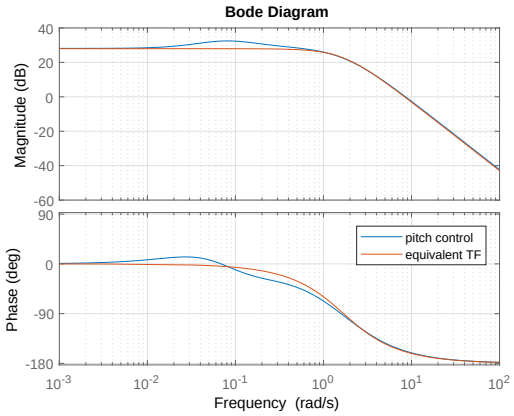

(c) Pitch attitude control channel

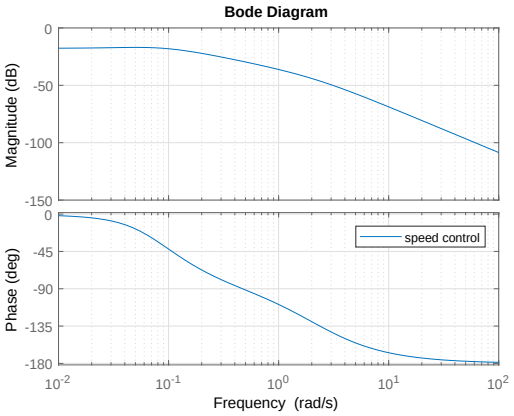

(d) Velocity hold channel

Figure 2.5: The bode diagrams showing the characteristics of all channels in the longitudinal control axis

no distinction between the DASH and LCT, after the output is generated both signals are added together and added to the pilot control inputs. So the longitudinal AFCS can be reduced to a combination of three inputs to one output. The original AFCS also has two constant offsets in the signal, which is treated as a constant input in this linear model. In Figure 2.5 the bode diagrams of the signals are shown. Note that in Figure 2.5b and Figure 2.5c two lines are shown: one for the "true" modelled channel response, and one for the reduced order model. Initially the reduced order version was used, but later it was decided that the full model was used combined with pole-zero cancelling. The constant inputs in Figure 2.3 are also modelled, but some pass through high-pass filters which reduce the signal to zero.

The matrices of the corresponding state-space representation of the system are shown in Equation B.3. Note that only the minimal realisation[1] of the system is shown, due to the size of the full matrices.

2.3. Combined model

Now both the linear, time-invariant models are known, they can be combined into a single model (see Figure 2.1 again). The first step is to connect the AFCS with the pilot control inputs in parallel. This is done with the `parallel` command in Matlab. The bypass (as the pilot control inputs 'bypasses' the AFCS) is modelled as a unity gain matrix. Then the output of both the pilot and the AFCS are connected in open loop series to the CH-47 model. Subsequently the feedback loop is created by again a unity feedback matrix, and the `feedback` command. The full procedure is shown in Figure B.1.

The combined non-linear model should be a good model. However, just claiming that it is a good model does not convince anyone about the validity. Therefore the model was tested and subsequently used in an

[1] `https://nl.mathworks.com/help/control/ref/minreal.html`, accessed on 4 July 2019

operational training environment, by active Royal Netherlands Air Force (RNLAF) pilots, instructors and flight test engineers. During the first tests a few minor issues with the settings of the control hardware were found, but after some tweaking the set-up was deemed to be ready for testing in a training environment. During the training session approximately nine pilots flew the model in the Desdemona simulator over a period of several days, but no complaints emerged, and even some pilots mentioned the correctness of the model compared to the original.

Most model evaluations also include objective evaluations. It was difficult to validate the model in that fashion as the CH-47 Chinook is mostly a military helicopter and its data is not widely available. Some tests were performed with limited accuracy. This included the step-response in pitch and roll motion and some acceleration and deceleration tests. The conclusion of those tests was that the model had similar characteristics as found in references.

3

Motion Cueing

Whereas the previous chapter discussed the model of the CH-47 Chinook and its AFCS, this chapter explains the motion cueing part of the study. Firstly some history of motion cueing in general will be shown, focussing on the most related literature along the way. Subsequently the problem which EMD tries to solve will be reviewed.

3.1. Historical relevance

As Adams et al.[9] wrote, control performance in simulator environments can be increased with the aid of motion cues. The motion cues can be as essential as visual cues for manual control of a system. For this reason it is important to see how motion cueing evaluation evolved.

3.1.1. Experimental work on motion perception

The lack of detailed knowledge of motion perception inspired the start of the experimental work on motion perception[10]. A 3-DoF simulator was used in this experiment, which enabled 5-DoF motion simulation, due to low-frequency body tilt. The first goal of the research was to find out if this simulator was appropriate to determine the human perception thresholds. If the results were positive, further research on pilot perception and motion simulation could be started. Also, pilot modelling was analysed in this project. It was assumed that the pilot has a mental model of the system that he is interacting with. This model is the result of a learning process. Based on these considerations some experiments were performed to investigate the influence of information processing on motion perception.

Two different experiments were designed. The first to determine the thresholds for cupula and otolith deflections, the second to demonstrate the effect of mental load on the processing of vestibular information.

Results show that the threshold increases with frequency. It is also shown that mental load increases the threshold values. There was some spread in the results due to differences in judgement; some subjects were more inclined to guess than others. This effect was tried to diminish by training, but it was still present. The subjects were able to tell "movement" way before they could identify the mode or frequency. Experiment 1 seems to confirm the "internal model" of the system, which enables the operator to feel motion, which he expects to feel, way before unexpected motion is noticed.

Motion perception thresholds are used in MCAs in the tilt-coordination channel, where the tilt-rate is limited just below the perception threshold, such that the pilot feels the effect of tilting, but not the rotation itself.

3.1.2. Improving motion cues

The lack of realistic motion cues in a number of flight conditions was a constant problem experienced by airlines. In 1985 a study was performed, aimed at investigating the possibility of applying improved software algorithms to commercial flight simulators in order to solve these problems[11]. The goal was to maximise the motion cueing effect, while maintaining motion limits by the maximum displacement, velocity

and acceleration of the system motion hardware.

During the first phase of this project three different MCAs were studied: the *classical washout algorithm* currently widely used, an *optimal algorithm* and an *adaptive algorithm*. These algorithms are not universally applicable, but they have to be tuned for a specific motion-base system, as well as the mission task and the vehicle. For example a large simulator motion base which is used for simulation of a Boeing 747 can be much more generous with the filtering, compared to a smaller simulator used to simulate tight manoeuvring in a fighter jet.

Generally a 3rd order washout filter is used for translational motion, and a 2nd order washout for rotational motion which need te be tuned. During the evaluation of motion-base drive algorithms the need arose to develop motion sensation models[11, 12]. It is suggested to only consider CWA in the current study, since other motion cueing options are not widely used in industry, despite being around for over thirty years. Also, from this report it can be concluded that no substantial benefits appear in using adaptive methods[11]. And lastly, the non-linear nature of optimised algorithms are difficult to combine with EMD, because the adaptation due to these methods cause eigenvector movement, resulting in obscured parameter measurements.

3.1.3. First efforts in motion cue requirement definitions

Later Sinacori performed a study to find requirements for the motion and visual subsystems of flight simulators, more specifically helicopter simulators, through which to determine the expected costs of a full-flight simulator.

The proposed methodology for motion calculation is called *washout filtering*, which attenuates the low frequency movements, but tries to keep the mid and high frequencies. This is done to keep the motion feeling of the real aircraft in high frequencies, without having the simulator leaving its motion base or the room it is operating in. Sinacori proposed a series of second order washout filters ([1] Figure 2, page 5-7) with parameters defined in Table 1, page 8, including tilt-coordination[1]. In an experiment, in which an aircraft model was flown by a pilot, the 6-DoFrates, velocities and positions were analysed, which form the basis of the tuning parameters mentioned in the document[1]. This motion cueing system is still almost universally used and forms the core on which most motion algorithms are based. This type of motion filtering is further analysed in Section 3.2.

3.2. Classical washout filter

In this section more attention is given to the classical washout algorithm (CWA). The name itself already gives some clues. The term *classical* is used because it was the first practical algorithm applied to motion-base drive systems. Then, it is called a *filter* because the method filters the signals which it gets from the vehicle model calculations. Generally the fine movements are passed through, while the larger, slower movements are attenuated by the filter. Then lastly the term *washout* refers to the fact that an input of a constant acceleration will result in an initial acceleration, but then the simulators acceleration is smoothly reduced and it is returned to the initial position.

The complete CWA consists of three different channels: the specific force channel, the rotational rates channel and the tilt-coordination channel. The complete diagram of this filter is shown in Section B.4, Figure B.3. This model is reduced for longitudinal motion only, as shown in Figure 3.1, where the three different channels are clearly visible.

As can be seen from the figure, each channel starts with a gain, which scales the entire motion. After that, the channels differ from each other. In the translational channel first the gravity vector is added, and subsequently it is transformed to inertial specific forces. Then the signal is filtered by a third-order high-pass filter. The filter needs to be of 3rd order to return the simulator to neutral after a step input on acceleration. This is proven with the Final Value Theorem, Equation 3.1. The fraction $1/s$ is the Laplace transform of a step input, and $1/s^2$ integrates twice to go from simulator acceleration to position. In translational motion a step input on acceleration is common, for example during a take-off run or during a looping. However, a step on rotational acceleration is rarely encountered[14]. Therefore in the rotational channel only a 2nd order high-pass filter is used. Lastly there is tilt-coordination, which simulates long-time accelerations by tilting the simulator cabin, therefore using the rotated gravity vector as imitation. This tilting is low-pass filtered, and there is a "soft" hard limit, usually $3\,^\circ/\mathrm{s}$, on the rotational speed in this channel, to stay below

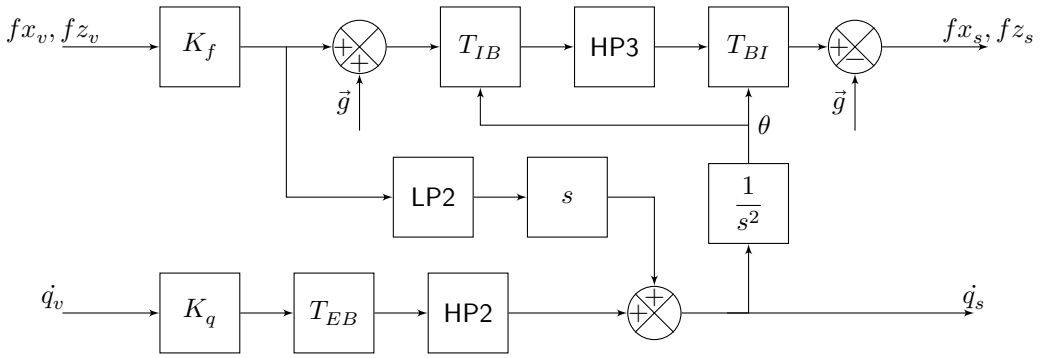

Figure 3.1: Structure of CWA in longitudinal axis, from [13]

the perception threshold of the participant. The limit is not truly hard as otherwise bumps can be felt when the limits are encountered. In this description some details are skipped, but more information can be found in [11, 13, 14].

$$\lim_{t\to\infty} x(t) = \lim_{s\to 0} sX(s) = \lim_{s\to 0} s\left(H_{HP3}(s)\frac{1}{s}\right)\frac{1}{s^2} = \lim_{s\to 0}\frac{1}{s^2}\left(\frac{ks^2}{s^2+2\zeta\omega_n s+\omega_n^2}\frac{s}{s+\omega_b}\right) = 0 \tag{3.1}$$

3.3. Objective motion evaluation

If one looks back at the research questions in Chapter 1, the main subject of research is the comparison between tuning methods and between tuning algorithms. In the next section literature concerning the evaluation and differences of cueing algorithms is reviewed in order to answer the first research question.

3.3.1. OMCT

In the previous section the historical context of motion cueing is given. In the quest of finding an objective motion evaluation and comparison tool, Sinacori is already mentioned for his requirement definitions for helicopter simulation. He also proposed a method of quantifying motion fidelity, which was based on the measurement of the gain and phase distortion at a frequency of 1 Hz[1]. This primary concept is used since then, albeit in different variations. The boundaries and requirements are refined by Schroeder[15].

In 2006 Advani and Hosman proposed the beginnings of what would later be knows as the OMCT in search for a more objective motion evaluation method. In 2007 Advani et al. performed test evaluations on four research simulators[17]. The criterion matched expectations, as it classified motion systems, which are considered to be well-tuned, within limits. One simulator which was neither optimally tuned nor accepted by pilots, did fall outside the boundaries. This solidified the proposed method as a valuable tool to evaluate motion.

The OMCT is included in ICAO Doc 9625[18], Revision 3, Part II, Attachment F. As implemented, this method is similar to the method first described by Sinacori and later by Schroeder, but instead of measuring the gain and phase distortion at a single frequency, it evaluates the distortion at twelve prescribed frequencies. The frequencies follow from Equation 3.2, the test signals are shown in Table B.4 and Table B.5. In Figure 3.2 it is shown how the gain and phase are compared. The gain is the ratio between the amplitude of the output and the input signals. The phase is defined as the time shift as fraction of the period. The time shift can be positive or negative (lag or lead), and is generally written in terms of radians. A ratio of 1 means that the output signal lags one full period behind the input signal, which is written as 360° or 2π rad.

According to the OMCT direct motions should have a high gain and low phase, but for the parasitic motion the gain should be low. Direct motions are the diagonal elements of Table 3.1, the false cues are the off-diagonal motion tests. The results (gain and phase difference) can either be shown in a Bode plot or a Nichols plot.

$$\omega = 10^{k/5-1} \text{ rad/s for } k = \{0, \ldots, 11\} \tag{3.2}$$

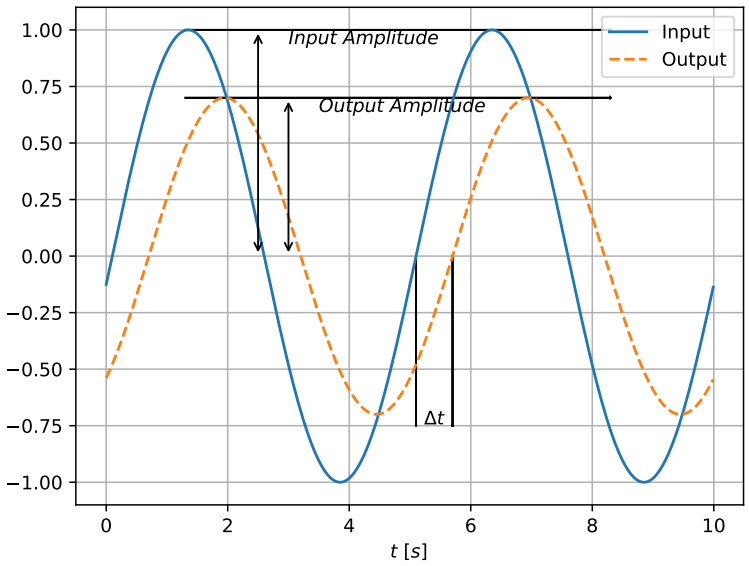

Figure 3.2: Gain and phase difference between input and output signals. Adapted from [18].

Table 3.1: Matrix with OMCT test sequences, adapted from [18]

	Pitch	Roll	Yaw	Surge	Sway	Heave
Pitch	1			2		
Roll		3			4	
Yaw			5			
Surge	7			6		
Sway		9			8	
Heave						10

This method is a thorough evaluation and documentation tool. It gives good insight in all of the relevant characteristics of both the motion hardware and the software side. Evaluation of the method has revealed a few key points[19]. Hosman et al. wrote: "The unanimous impression is that the results of the test are highly valuable and meaningful. The OMCT provides a better insight into the behaviour of the Motion Cueing System." Also, he noted that the differences in OMCT results indicated significant differences between flight simulator training devices (FSTDs).

Based on these and more observations, some improvements were recommended. Firstly, the test results contained outliers, of which the background have to be understood. Secondly, to enable significant contributions to the simulator industry, the test needs to be combined with a criterion, which is most likely a combination of phase and gain boundaries. Thirdly, the test takes approximately three hours to complete, which is a notable amount. Hosman et al. mentioned the possibility of combining certain test signals, for example multiple frequencies, or unrelated channels. A problem that can occur due to these solutions is that the limits of the actuators are reached faster than in case were the different frequencies were tested individually. Lastly, the test results are not necessarily clear for national aviation authority inspectors and simulator motion evaluators. Basic frequency domain analysis and control engineering will become highly valuable, if not required, skills.

As one of the conclusions, Hosman et al. claimed that "When accepted, the big advantage of the OMCT is that the acceptance of simulator motion depends no longer only on the subjective judgement of an individual inspector." According to Stroosma et al. the purpose of the OMCT is to supplement subjective evaluation with an objective measure. It also enables comparison between different simulators and MCAs[14].

Stroosma et al. evaluated the OMCT on the SIMONA Research Simulator (SRS) in 2013. A detailed description is given about the actual implementation of OMCT in combination with the CWA, based on [11].

This implementation of the CWA will also be used in the research this report is concerned with. Stroosma et al. noted that "The number of periods in the measurement phase (...) is a compromise between the need to dampen out transients, having a sufficient number of periods for analysis and minimizing the time needed to do the measurement."[14] Depending on the simulator design, injecting the OMCT signals in the MCA can be easy. Retrieving the measurement data however is often more difficult. Since the OMCT reference point (which is 35 cm below the design eye reference point (DERP)) generally does not coincide with the measurements datum, some transformations have to be performed to translate motion of the inertial measurement unit (IMU) to OMCT motion. This also holds if actuator deflections are used as data source instead of the IMU.

Some of the observations mentioned by Stroosma et al. are included below. Firstly, it is pointed out that an off-line simulation of the MCA in combination with the OMCT reference signals compares well to the on-line simulation and measurements. This indicates that the motion system hardware is well-known and the MCA respects the hardware limits. But it can be seen as a drawback, as the aircraft's motion characteristics may have been disconnected from the test signals. For example, the coupling between yaw and sway at the pilot position in larger aircraft can be significant, but is untouched by the OMCT. Lastly, also Stroosma et al. mentioned the lack of criteria.

In conclusion, the OMCT cannot paint the complete motion cueing picture, as it disassembles the signals in different axes which would otherwise be coupled, but it does provide a more elaborate metric than previous methods, like Sinacori and Schroeder. In a research environment it supplements the documentation of a cueing solution, in order to make comparisons between cueing solutions and between different simulators easier.

In an effort to come up with fidelity criteria, Zaal et al. performed research on the vertical motion simulator (VMS) with a relatively large pool of pilots. The results were based on both objective and subjective parameters. Pilots had to grade the motion set-up, based on two questions. Also the deviation from the optimal/desired parameters, such as descent rate at touch-down and speed are considered as objective measures. In conclusion the research found that a larger motion space leads to better performance and better pilot acceptance. However there is no clear-cut optimum in the trade-off between high-gain-but-low-phase-distortion versus low-gain-but-high-phase-distortion. A set-up with too large gain distortion however is not well perceived. Based on these results and previous research, Zaal et al. proposed some initial, relatively wide, fidelity boundaries. Further research is required to refine the boundaries.

In the fourth edition of the *Manual of Criteria for the Qualification of Flight Simulation Training Devices - Volume 1 - Aeroplanes* criteria are included in the the "Frequency-Domain Motion Cueing System Performance Test" chapter, which are mostly based on research from Hosman and Advani[21]. Finally there were relevant fidelity criteria included in the OMCT, albeit without significant scientific support. The boundaries are based on the frequency domain analyses of ten accepted simulators. The outliers are removed from the dataset, and the criteria are set such that the left-over roughly fits in the boundaries. The OMCT is a true step forward in objective flight simulator motion cueing evaluation, but the goal has not yet been achieved. It is also still not clear how to optimise the MCA to achieve a good OMCT rating. There are several optimisation algorithms proposed[22, 23], but it remains a challenge to define an objective, transparent cost function[2], as currently it is mostly based on engineering judgement. And secondly, the methods based on OMCT and related frequency-domain analyses consider the motion system as an isolated system. However, it is linked with the vehicle model and the mission, which can change the behaviour of the combined system significantly, as will be explained in subsection 3.3.2.

3.3.2. EMD

As mentioned a shortcoming of the OMCT is the fact that it neglects the interactions between the task, vehicle dynamics and motion cueing. A recent study showed that adapting the OMCT test signals to incorporate vehicle characteristics and task properties generate considerable differences in the frequency response[2, 24]. To "expose this intricate three-way interaction between 1) task, 2) vehicle dynamics and 3) motion cueing"[2], Eigenmode Distortion (EMD) was developed. The basic working principle is to expose the distortion of the eigenmodes of the vehicle by the MCA. Each eigenmode is represented by its eigenvectors, and the movement of the eigenvectors in the complex plane will tell us how the mode is 'warped' by the MCA.

The interaction between vehicle dynamics and task will be monitored using mode participation factors (MPFs)[3]. The MPF is a measure of how much each mode of the system is excited at a point in time, in a relative scale. In other words, how much each mode participates in the motion, as fraction of the total motion. The definition is given in Equation 3.3. In this equation $\vec{r}\,(t)$ is a vector which contains the values of each mode's participation at time t and W^{-1} is equal to V^{T}, which in turn is defined as the matrix consisting of the left eigenvectors of the system. The last element is $\vec{x}\,(t)$, the state of the system at time t. As Miletović et al. states, "Comparison of the magnitudes of individual MPFs thus yields the relative importance of each mode. This knowledge can be valuable as an objective guide in the design and configuration of MCAs."[25]

$$\vec{r}\,(t) = W^{-1}\vec{x}\,(t) \tag{3.3}$$

The relation between vehicle dynamics and motion cueing dynamics is studied with the use of eigenvector diagrams (see Figure 4.1a)[2]. It is used as preliminary analysis in Chapter 4, which can also be viewed as example. The eigenvectors plots show the change of vector magnitude and direction when motion cueing is applied to the calculated vehicle motion. The absolute magnitude or direction of a single vector is not relevant, but the relative magnitude does reflect the relative importance of a movement in a single mode.

When due to cueing the direction and/or magnitude of a vector changes a lot, it is hypothesised that the pilot will feel a lot of distortion. A changed vector direction will indicate lead or lag, whereas an increased or decreased vector length will imply a change in the amount of motion.

4

Preliminary Analysis

In this chapter the first steps taken to answer the research questions will be shared. This involves primarily the eigenmode analysis of the CH-47 Chinook, and in Section 4.2 the comparison with a different helicopter, namely the AH-64 Apache, will be made.

4.1. Eigenmode analysis

The different blocks of the system, as shown in Figure 2.1, are connected and the eigenvalues and -vectors are extracted (code shown in Figure B.1). First the eigenmodes of the helicopter without any augmentation are analysed. The analysis is done from the linearised form, in longitudinal motion only and at four different airspeeds, as written in subsection 2.1.2. Currently only the analysis at 20 kn is shown.

The eigenvalues of the linearised model of the helicopter (without augmentation) are shown in Table 4.2. It is noteworthy that there is a major unstable eigenmode. From analysis of the reconstructed eigenvectors it is shown that biggest contribution to that mode is the longitudinal speed.

Subsequently the AFCS is separately analysed, and the results are again shown in Table 4.2. It is a little surprising that the AFCS has a periodic mode. This mode is caused by the speed hold mode, which has a second order nature. After that the AFCS is connected in open-loop fashion to the flight model of the helicopter. The eigenvalues do not change due to this connection, so the eigenvalues of this system are just the combination of the previous ones (Table 4.2).

Lastly the feedback channel is added, which does actually change the eigenmodes, as can be seen in Table 4.2. Of the previous eigenvalues only -0.5263 remains unchanged. Also the highly unstable eigenvalue is reduced to 0.0069, which corresponds to a time constant of $\tau = -1.45 \times 10^2$ s. The biggest contribution of this eigenvalue is in F_x, which does correspond with what was found before. Considering this is a linearised model, and the DASH is very non-linear in nature, this eigenvalue will most likely be spurious. The eigenvalues are graphically shown in Figure 4.2.

Now the eigenmodes of the combined system are known, a preliminary analysis can be performed of how the MCA will modify them. The MCA used in this analysis is the classical washout algorithm (CWA). Of course the characteristics of this MCA depend on the settings used. For the first analysis the same settings are used as Stoev et al. used in their research[13]. These settings are shown in Table 4.1. The eigenvalues of this system itself, are shown in Table 4.3. The next step is to pass the model of the Chinook through the MCA and see how it distorts the motion. Since the MCA is coupled in series to the model, the eigenvalues do not change. Hence, the complete eigenvalues are just the combination of the previous ones.

Now the eigenvalues are known, the next step is to analyse how the eigenvectors corresponding to those eigenvalues look like, and how they change due to the interaction with the MCA. The eigenvectors of before and after cueing are shown in Figure 4.1. The undefined eigenvectors could be part of the AFCS.

From the analysis of the figures of the eigenvectors in Figure 4.1, it can be seen that there is a large difference between both the size as well as the phase of the eigenvectors. This raises the question if this is correct,

because after all the MCA is meant to replicate the motion of the vehicle. The biggest concern is the fact that, based on what is best visible in Figure 4.1a, the MCA amplifies both fx and fz, although the linear gain of the MCA is not larger than 1. In the process of elucidating this unclarity, three different cases where considered. More on the problem-solving process can be found in Section B.5. The last option turned out to answer the question satisfactory, which is that the shown behaviour is actually correct but not fully understood yet. The concept is explained in Chapter 5.

Table 4.1: Settings of the CWA used

K_x	ω_{n_x}	ω_{b_x}	$\omega_{n_{lp_x}}$	ζ_x	K_z	ω_{n_z}	ω_{b_z}	ζ_z	K_q	ω_{n_q}	ζ_q
0.7	0.8	0	2.5	1	0.5	2.5	0.2	1	0.7	0.8	1

Table 4.2: Eigenvalues of the CH-47 Chinook with and without augmentation

Re	Im
CH-47 without augmentation	
0.2975	
−0.2658	±0.3105
−1.2375	
AFCS	
−2.1786	
−1.2739	
−0.0743	±0.0296
−0.5263	
Open-loop	
−2.1786	
−1.2739	
−1.2375	
0.2975	
−0.5263	
−0.2658	±0.3105
−0.0743	±0.0296
Closed-loop	
−2.5950	±1.8123
−0.4544	±0.9740
0.0069	
−0.0427	
−0.2019	
−0.5317	
−0.5263	

Table 4.3: Eigenvalues of the CWA with settings as described in Table 4.1

CWA	
Re	Im
−0.8 (4×)	
−0.2	
−2.5 (4×)	

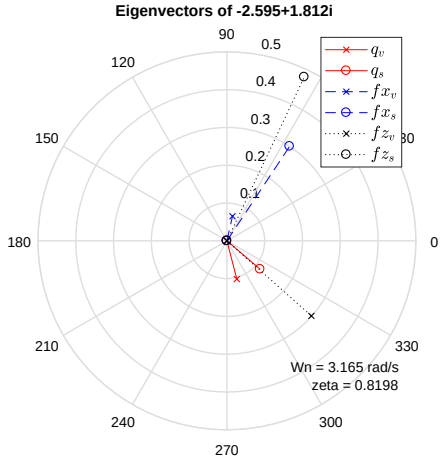

(a) Eigenvectors of the short-period motion

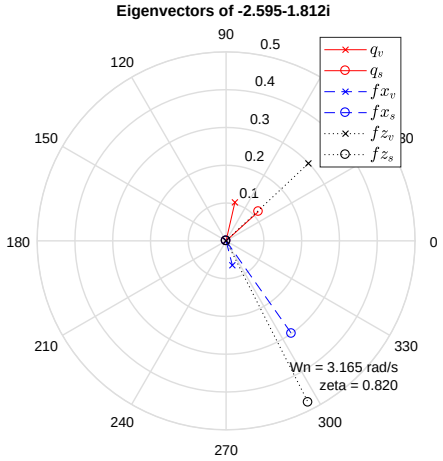

(b) Eigenvectors of the short-period motion

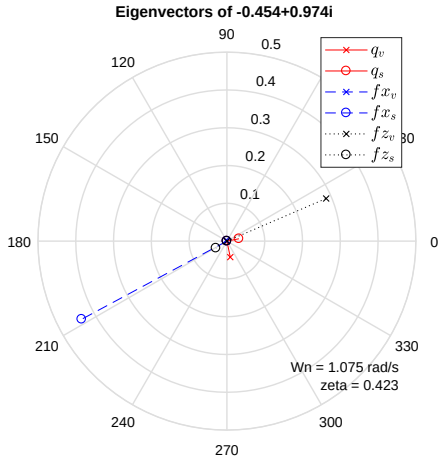

(c) Eigenvectors of the heave motion

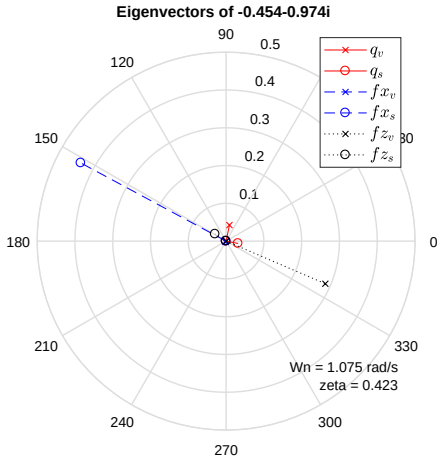

(d) Eigenvectors of the heave motion

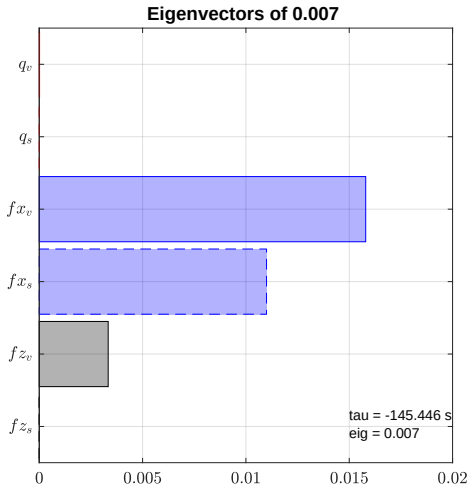

(e) Eigenvectors of the unstable aperiodic pitch

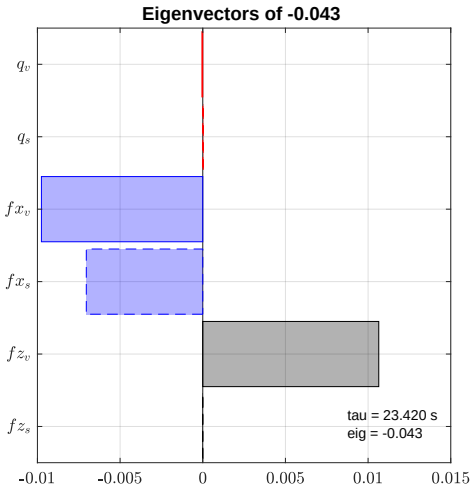

(f) Eigenvectors of aperiodic pitch motion

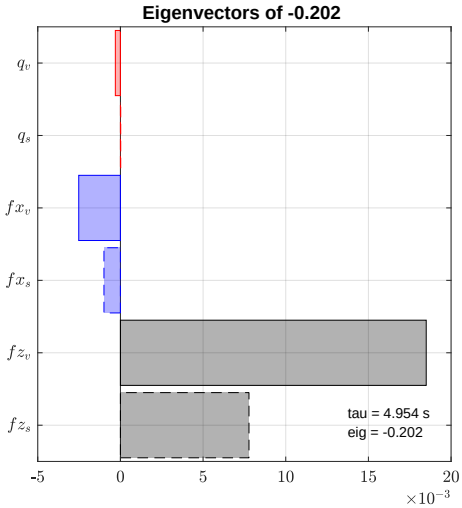

(g) Undefined eigenvectors

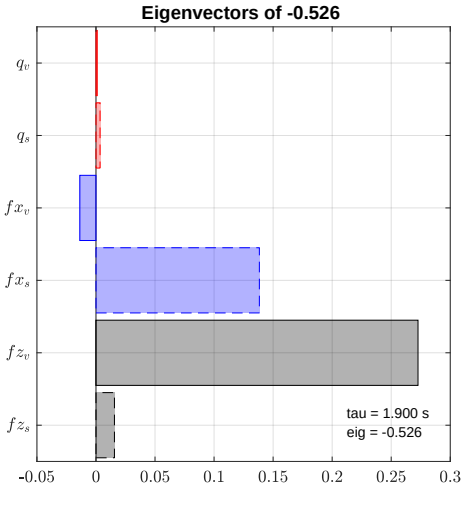

(h) Undefined eigenvectors

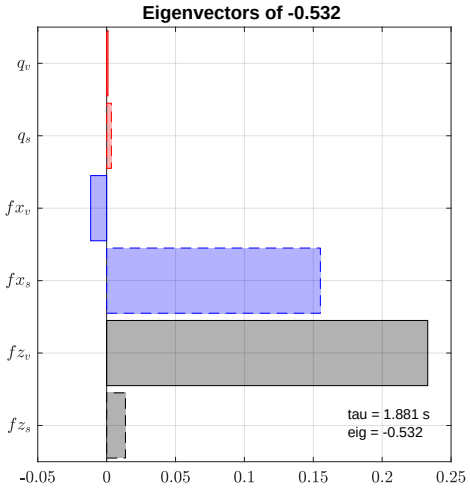

(i) Undefined eigenvectors

Figure 4.1: All eigenvectors before and after cueing

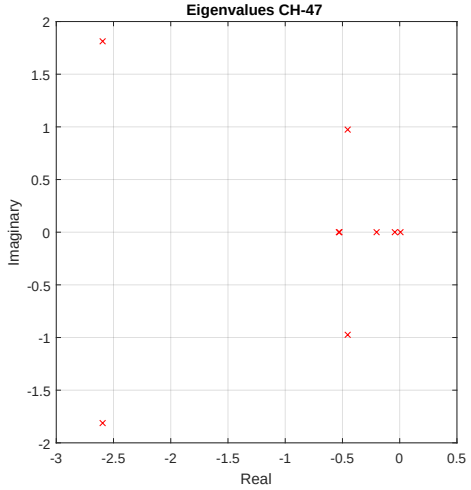

Figure 4.2: Eigenvalues of the CH-47 Chinook

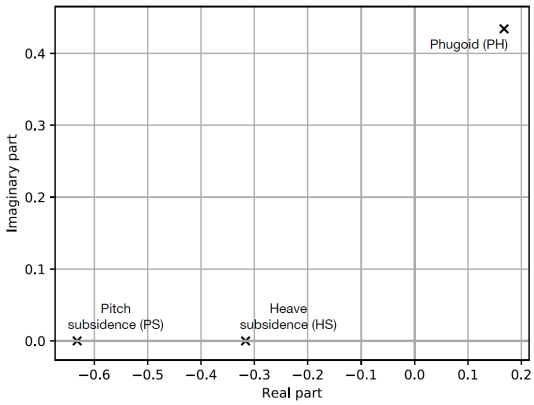

Figure 4.3: Eigenvalues of the AH-64A Apache helicopter[25]

4.2. Comparison with the AH-64 Apache

One of the research questions was to see how sensitive the EMD-based tuning method is to different aircraft types. Therefore the eigenmodes of the Chinook are to be compared to those of different vehicles. A first step of the comparison with the AH-64 Apache will be done in this section, the study will be continued in the final thesis report.

As Miletović et al. analysed the AH-64 Apache attack helicopter with the EMD method, the eigenvalues and eigenvectors of the vehicle are included in [25], however only hover conditions are shown. The eigenvalues are shown in Figure 4.3, which is copied from [25]. The eigenvectors are shown in Figure 4.4. From the figure it can be seen that the Apache has an unstable phugoid motion, which is somewhat comparable to the, albeit much slower, aperiodic pitch motion of the Chinook. The heave subsidence of the Apache does not have an equivalent in the Chinook. The pitch subsidence from the AH-64 also has no clear companion in the CH-47, however the short-period is most comparable with a high frequency and high damping ratio.

From the comparison between the eigenmodes of both vehicles it can be seen that both vehicles behave very differently. This means that it will be interesting to see how a MCA set-up, which is optimised for one vehicle, will perform with a different vehicle.

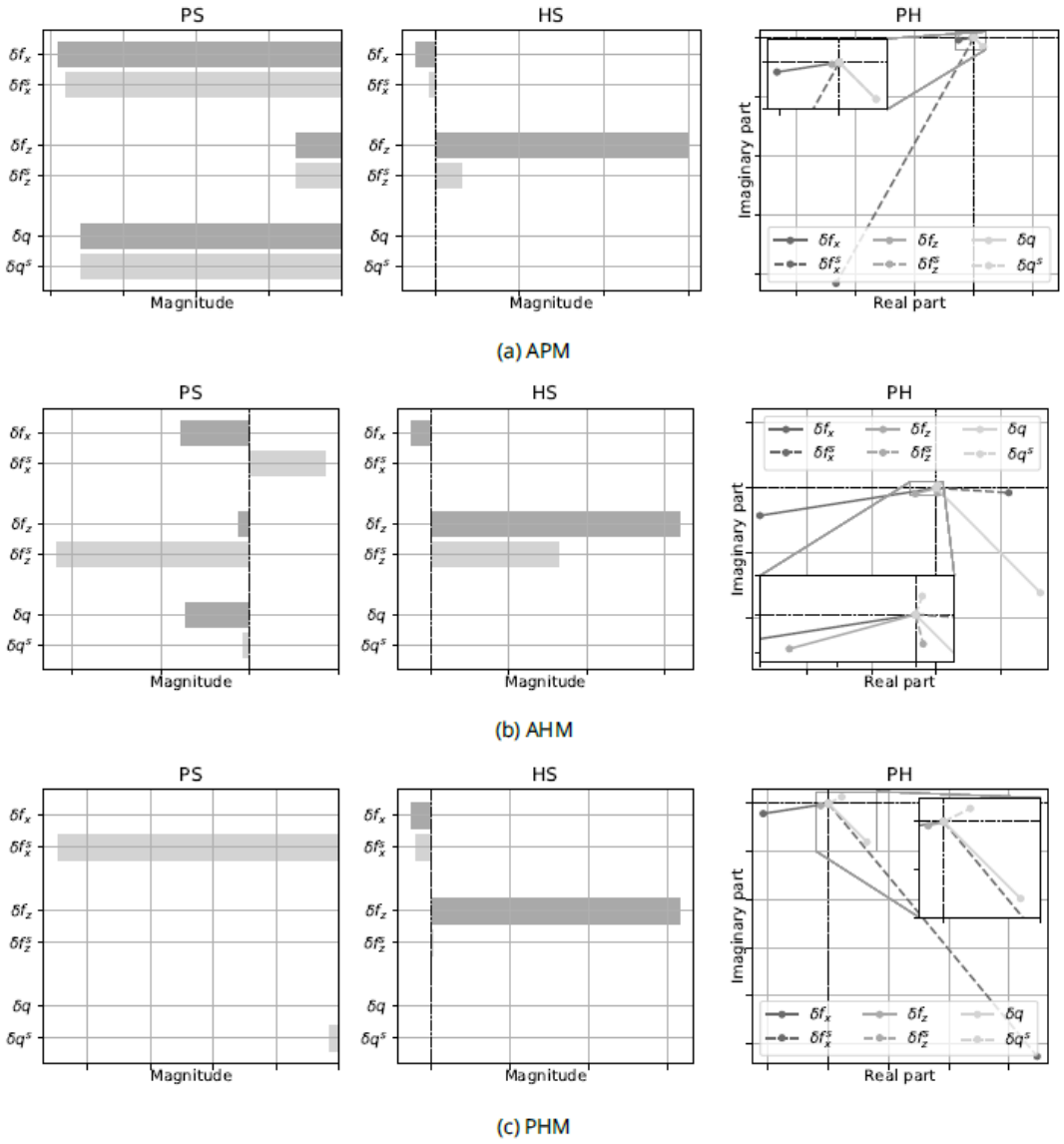

Figure 4.4: Eigenvectors of the AH-64 Apache before and after cueing, from [25]

5

Transient Amplification

Based on the results shown in the previous chapter a few questions rose about the validity and correctness of the model. In this chapter an explanation is given of the phenomena seen in Chapter 4, which mainly lies in the frequency domain. The process of finding this explanation is written in Section B.5.

5.1. Bode's third dimension

To clarify where this seemingly inexplicable magnitude amplification originates, the transfer function of fz_v to fz_s, $H_{fz}(s)$, is taken as an example. It is shown in Equation 5.1, with the settings of Table B.6. In this equation $s = \sigma + j\omega$. It is applied to the first eigenmode of the system: $\lambda_1 = -2.5950 + 1.8123i$.

$$H_{fz}(s) = \frac{s^2}{s^2 + s + 1/4} \tag{5.1}$$

To better understand the characteristics of such a transfer function a widely used tool is the Bode diagram, which is a combination of a magnitude and a phase plot, showing the amplitude attenuation or amplification and phase lead or lag respectively for each input frequency. The Bode plot for this transfer function is shown in Figure B.5, of which the magnitude plot is most important now. To calculate the magnitude of a transfer function as response to a certain input frequency, one substitutes $j\omega$ for s in the transfer function, resulting in the frequency response function (FRF), and subsequently calculates the magnitude: $\|H(j\omega)\|$. Doing this calculation for a series of frequencies one can plot it as shown in Figure B.5. Note that substitution of $j\omega$ for s means that only the *steady state* response (also known as harmonic response) is looked at. However, when doing the same calculations for $s = \sigma + j\omega$, as would be the case for damped dynamics, a different picture emerges.

The magnitude plot can also be generated by calculating $\|H(\sigma + j\omega)\|$, which means that transient signals are included. This is shown in Figure 5.1. It is clearly visible from Figure 5.1a that the gain of the transfer function can indeed raise above 1 under some circumstances. Also, it can attenuate eigenmodes which have a positive real component, or in other words, which are unstable.

In Figure 5.1b the same function is plotted, together with in red accentuated the magnitude at $\sigma = 0$, or $s = j\omega$. This is in fact the very same profile as is shown in Figure B.5. This figure clearly shows how limited insight the Bode actually gives. Also in this figure the intersection of the cylinder with radius $s = \omega_n$ is shown. The $\omega_n = 3.17$ rad/s is equal to the eigenfrequency of the first eigenmode, which in turn is equal to the magnitude of the eigenvector: $\omega_n = \|\lambda_1\|$.

Figure 5.1c presents the profile of the intersection between the cylinder mentioned above and the magnitude surface of H_{fz}, combined with the magnitude ratio of fz_s to fz_v, which is the quotient of the length of the fz vectors of Figure B.4. It is clearly visible that those lines intersect at approximately -2.60, which corresponds with the real part of the eigenvalue.

Lastly Figure 5.1d shows the same 3D magnitude plot, but warped in such a way that the grid is defined by ω_n and ζ, which are the natural frequency and damping ratio respectively. The damping ratio, ζ, is calculated using `zeta = -(cos(angle(D))`, and ω_n is just the magnitude of D: `Wn = abs(D)`. This way of plotting can make more sense from a motion tuning point of view, as it directly shows what the gain of the system will be for a given eigenmode. This plot also includes the lines of $\omega_n = 3.17\,\text{rad/s}$ and $\zeta = 0.82$, the characteristics of this particular eigenmode. The lines intersect each other and the surface at the correct magnitude ratio of 1.31, which strengthens faith that this model is now correct and well understood. For now this effect will be called *transient amplification*, as the transient response is amplified more than what is expected based on the steady state response. This term is already used in the field of, amongst others, semiconductor plasmas and biochemical networks[26–29].

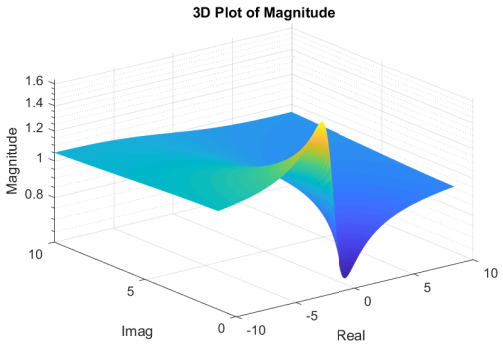

(a) Bode magnitude plot in three dimensions

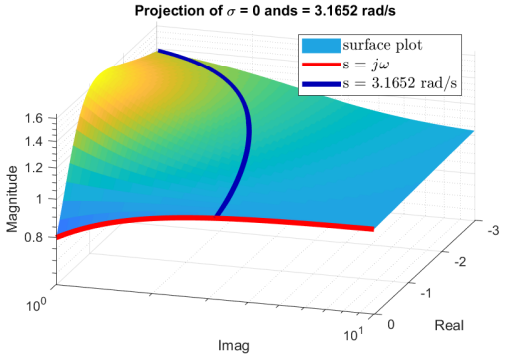

(b) Magnitude plot with projection of Bode plot and profile of eigenfrequency

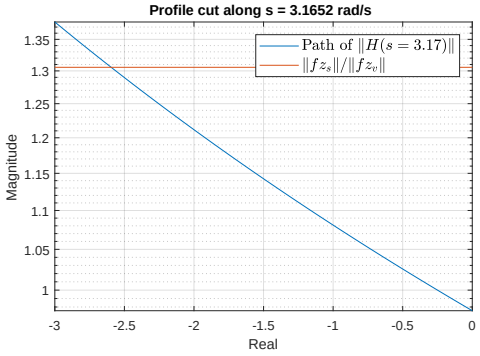

(c) Magnitude at profile cut of eigenfrequency, together with the intersection of the real part of the eigenvalue and the apparent relative gain

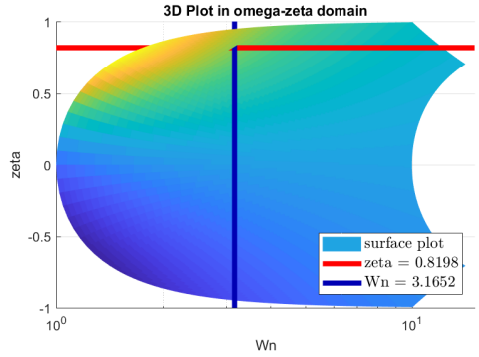

(d) Surface plot in different coordinate system of the eigenvector

Figure 5.1: Bode magnitude plot in 3D for fz_v to fz_s, applied to $\lambda = -2.5950 + 1.8123i$, with a low break frequency

5.2. Effect of break frequency

The effect of amplification of eigenmodes by a high-pass or low-pass filter mainly occurs if the eigenmode frequency happens to lay close to the break frequency of the filter. Also, the damping ratio of the filter should be high. In Figure 5.2 the effect of a higher break frequency of the low-pass filter is shown. The transfer function is $H(s) = s^2/(s^2 + 7s + 49/4)$, where the break frequency of fz is now $\omega_{n_z} = 3.5$. As can be seen from this figure, the closer the break frequency is to the eigenfrequency of the mode, the more distorted the magnitude gets. That is also visible in the eigenvector diagram: Figure 5.3.

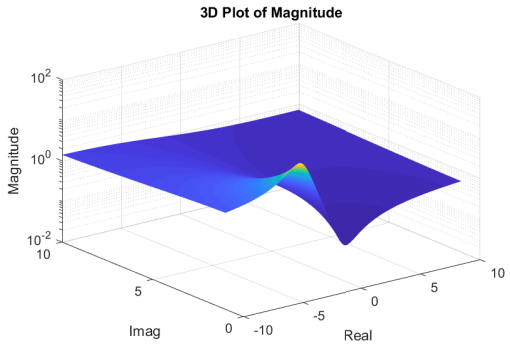

(a) Bode magnitude plot in three dimensions

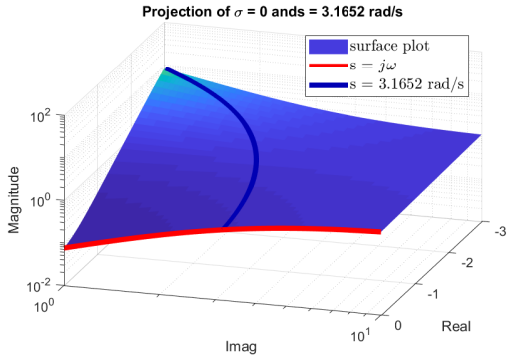

(b) Magnitude plot with projection of Bode plot and profile of eigenfrequency

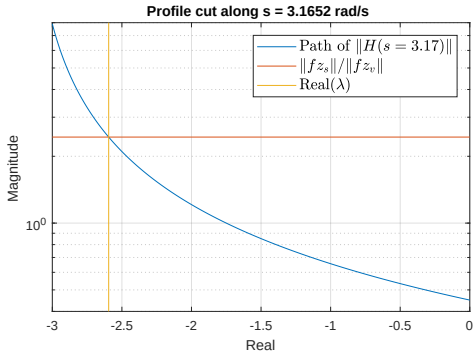

(c) Magnitude at profile cut of eigenfrequency, together with the intersection of the real part of the eigenvalue and the apparent relative gain of the eigenvector

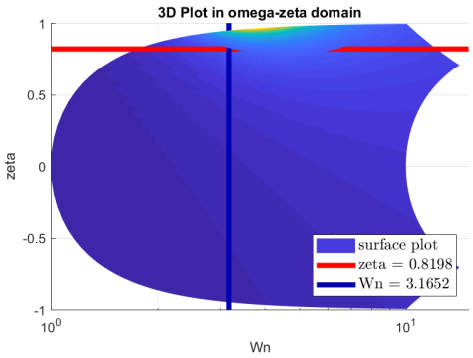

(d) Surface plot in different coordinate system

Figure 5.2: Bode magnitude plot in 3D for fz_v to fz_s, applied to $\lambda = -2.5950 + 1.8123i$, with a high break frequency

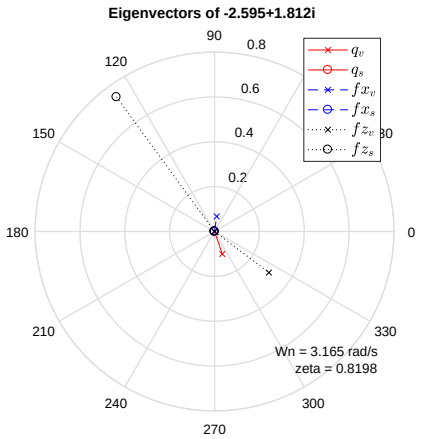

Figure 5.3: Eigenvectors with only heave cueing enabled, with a high break frequency

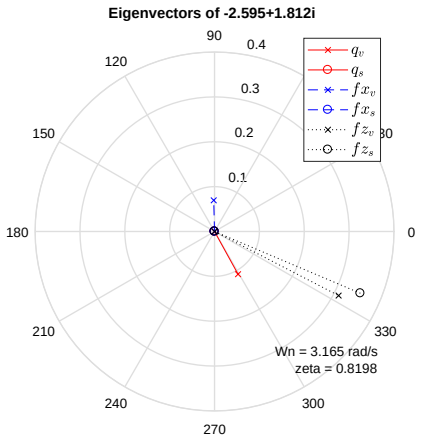

Figure 5.4: Eigenvectors with only heave cueing enabled, with $\zeta_z = 0.5$

5.3. Effect of damping ratio

Analogous to the previous section, the effect of a different damping ratio on the transient could also be interesting to investigate. In Figure 5.5 again the 3D Bode diagrams are shown, but now with a lower damping ratio. All MCA settings are as shown in Table B.6, only with a $\zeta_z = 0.5$. In Figure 5.4 the eigenvector distortion is shown. As can be seen, the area of influence is much smaller, decreasing the chance that the eigenvector appears in the distorted area. In this case it results in a smaller magnitude distortion. However, an eigenfrequency closer to the break frequency of the transfer function would instead have amplified the vector more, as less damping causes increased amplification in situations of resonance.

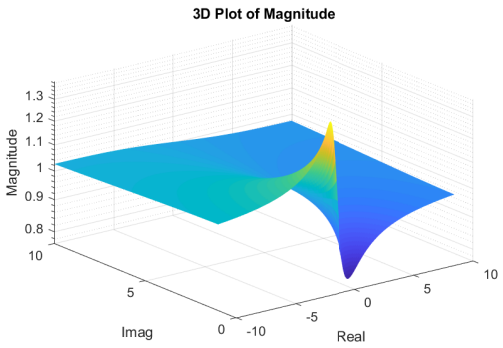

(a) Bode magnitude plot in three dimensions

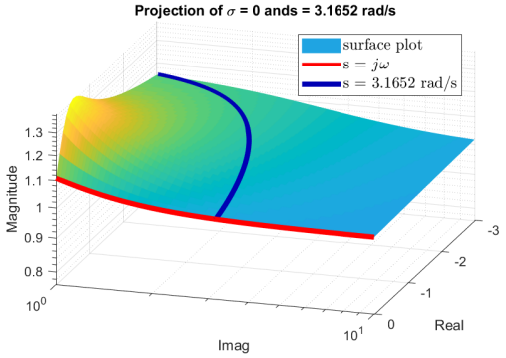

(b) Magnitude plot with projection of Bode plot and profile of eigenfrequency

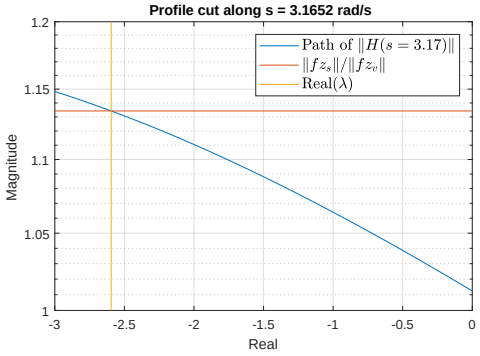

(c) Magnitude at profile cut of eigenfrequency, together with the intersection of the real part of the eigenvalue and the apparent relative gain

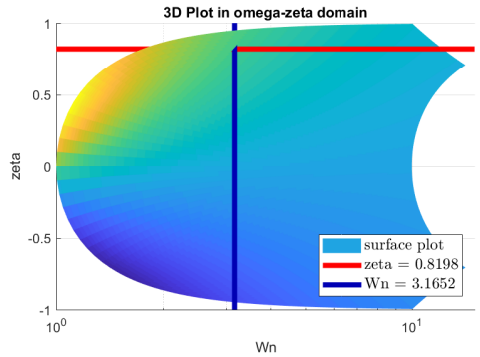

(d) Surface plot in different coordinate system of the eigenvector

Figure 5.5: Bode magnitude plot in 3D for fz_v to fz_s, applied to $\lambda = -2.5950 + 1.8123i$, with $\zeta_z = 0.5$

6

Discussion

Following the preliminary analysis performed in Chapter 4, a few conclusions can be drawn.

First, the CH-47 Chinook is a complex vehicle, mostly due to the AFCS. The full model is very well accepted by pilots, which builds trust that both the flight model and the modelled AFCS are sufficiently similar to the real aircraft.

Based on the eigenvector analysis of the linearised, coupled model, a few questions are raised about the correctness of the linearised part. To answer those questions more research was performed and finally the cause of the distortion was found. This was shown in Chapter 5. It is not fully understood yet what the consequences are of this phenomenon. Maybe some motions are actually amplified by the filter. A short discussion with experts at Desdemona B.V. revealed that usually the gain cannot be raised beyond 0.70, for as otherwise the pilots will complain that motion is too strong. This might be caused by the *transient amplification* effect discussed in Chapter 5, but further analysis will be necessary.

From the questions raised by afore mentioned behaviour, subsequent analysis and the results, it clearly follows that looking at the steady-state frequency response (or Bode plot) of the MCA, like it is done in the OMCT, does not paint the complete picture. The MCA can amplify stable modes, while the MCA is stable as well. This effect was not expected, but it can have serious consequences for what the pilot feels in the simulator.

The shape of the longitudinal eigenmotions of the Apache at hover conditions are known, so in the next stage they can be compared to the eigenmodes of the Chinook, in order to answer research question 3. Knowing about transient amplification, it will be interesting to see how a slightly different mode, in terms of eigenfrequency or damping, will be affected differently by the MCA.

During the analysis it was learned that eigenvectors should be calculated in one go. Doing it in two steps can, and usually will, result in different eigenvectors, as an eigenvector multiplied by any complex value is also an eigenvector. This will muddle the results and make analysis more difficult.

7

Future Work and Methodology

The first steps in answering the research questions have been taken, but the effect of transient amplification needs more attention. For the ease of reading the research questions are repeated below. To answer Question 1 an experiment will be designed with the model of the CH-47 Chinook on the Desdemona simulator[1]. The subquestion of Question 1, "How to compare different MCAs", will need an answer before the experiment takes place. There are different ways of evaluating MCAs, for example the performance of a participant can be a factor, but also the preference could give valuable information. Most likely both measures are captured in the experiment, but how exactly is not decided yet.

Regarding the experiment design, several lessons can be learned from how others have performed experiments. For example, Stoev et al. has performed a very similar study regarding the EMD-method, but applied to a different vehicle[13]. Stoev et al. had good results with doing paired comparisons to evaluate and rate a certain setting of the MCA, as the motion fidelity rating (MFR) scale has some drawbacks that only become more apparent in evaluation of similar-quality MCAs. Similarly, documentation and explanations are available about how to statistically analyse pairwise comparisons[13].

In preparation of the experiment several MCA settings have to be designed. During the design item Question 2 will be answered by comparing the methods of designing a motion cueing solution. Some parameters that are expected to be important are for example the amount of simulator time it takes for a certain method to come up with a solution, the effort and skill required for a method to work and the reproducibility or spread of the results.

For the last question to be answered, a theoretical analysis based on both the eigenmodes of the AH-64 Apache as well as those of the Cessna Citation PH-LAB will be performed, of which the results will be compared to the Chinook.

A more detailed planning can be found in Appendix A.

1. Will an EMD-based MCA be better compared to conventionally tuned MCAs for this type of aircraft?
   (a) How does one compare several MCAs?
2. Will EMD-based tuning be a better method than conventional tuning methods?
   (a) How does one compare and test different tuning methods?
3. How sensitive is the EMD-based tuning method to different aircraft types?
   (a) Will the eigenmodes resulting from this EMD-based MCA be different compared to other types of aircraft?
   (b) Which of the eigenmodes appear in both aircraft?
   (c) Which eigenmodes are important?
   (d) How can one compare eigenmodes and when do they differ enough?

[1] `https://thedesdemona.com/`, accessed on 7 August 2019

8

Conclusions

Following the discussion in Chapter 6, some concluding remarks are given. First, the flight dynamics model of the vehicle, as well as the model of the AFCS, are positively received by active RNLAF CH-47 Chinook pilots. Following the unexpected behaviour of the MCA an explanation is found, which sheds light on the interaction between vehicle model and motion filters, which exposes a potential shortcoming of the OMCT.

In Chapter 3 it is shown that the OMCT is recently implemented. The OMCT attempts to find an objective motion evaluation tool, which helps industry to evaluate motion tuning and science to more easily compare simulator set-ups. However there is still subjectivity involved in the optimisation and cost function definitions which should enable easier comparisons between simulators. Also, the OMCT neglects the interaction between mission, vehicle and motion system, which could attenuate or amplify certain modes. The EMD method aims to alleviate this shortcoming by including the vehicle model in the equation, and evaluate how the MCA deforms the eigenvectors of the simulated vehicle.

The first steps have been taken in analysing the Chinook eigenmotions and comparing it with the Apache's eigenmodes, but more investigation is required. This will be the next step, after which the experiment will be designed and executed.

A

Planning

To finish the study, a few steps still have to be taken, as is described in Chapter 7. In Figure A.1 the detailed planning of those steps can be found. The first step after finishing this report is the verification and validation of the linear model. After that the preparations for the experiment will continue, with the experiment planned in the first week of November. Based on the time it took to write this report, a major part is devoted to writing the final report.

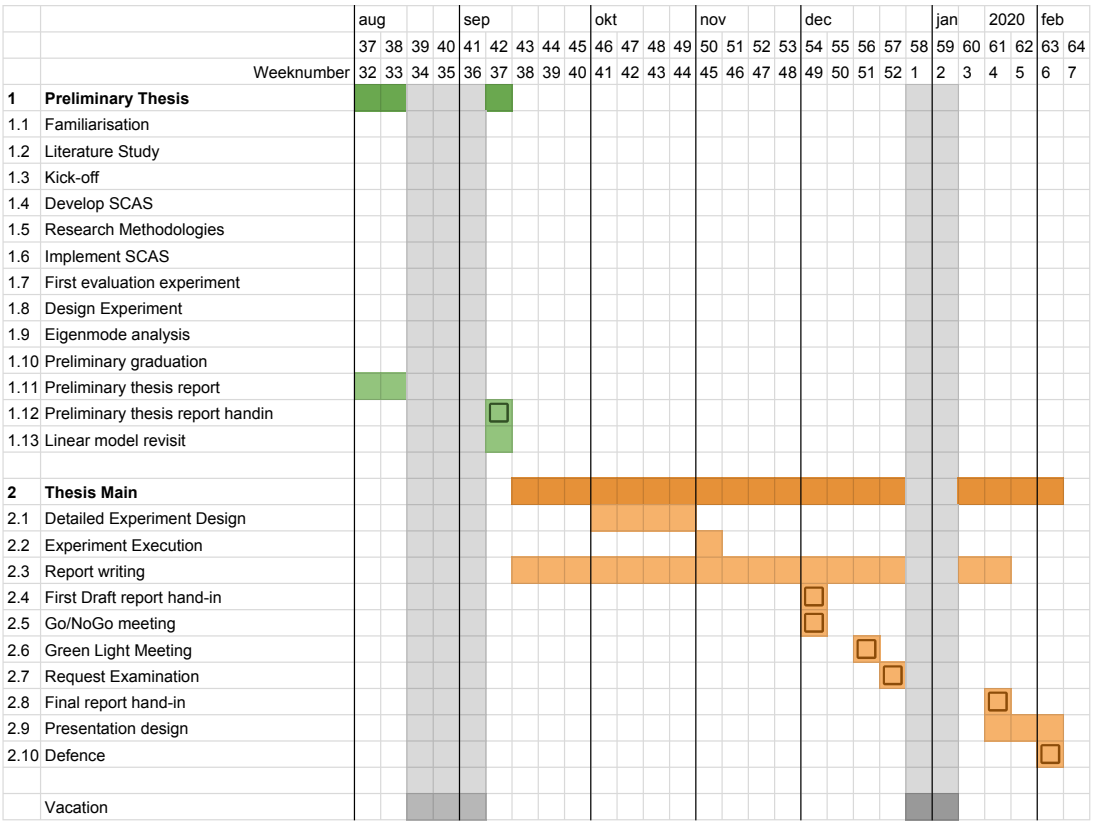

Figure A.1: Gantt chart of the planning for the upcoming months

B

Model Parameters

Table B.1: List of all linearised stability derivatives at four different trim points.

	0	20	80	160
Xu	−0.0206	−0.0093	−0.0058	−0.0471
Xv	0.0005	0.0017	0.0007	0.0020
Xw	0.0242	0.0287	0.0390	0.0861
Xp	0.0528	0.0688	0.0939	0.1412
Xq	−0.1525	−0.1712	−0.1386	−0.6024
Xr	−0.1313	−0.1023	−0.0320	−0.0101
Yu	−0.0014	−0.0003	0.0011	0.0016
Yv	−0.0176	−0.0342	−0.0862	−0.1719
Yw	0.0033	0.0027	0.0042	0.0130
Yp	0.0288	−0.0471	−0.2065	0.0824
Yq	0.0287	−0.0183	0.0893	0.1779
Yr	0.0050	0.0015	−0.0149	0.0216
Zu	0.0243	−0.2018	0.0651	0.0065
Zv	0.0039	0.0043	0.0029	0.0022
Zw	−0.3459	−0.4994	−0.9053	−1.0930
Zp	−0.0269	−0.0152	0.0016	0.0641
Zq	0.0742	0.9294	0.5025	0.4368
Zr	0.0143	−0.0493	−0.1523	−0.3748
Lu	−0.0028	−0.0032	−0.0000	0.0012
Lv	−0.0272	−0.0224	−0.0098	−0.0141
Lw	0.0034	0.0016	0.0056	0.0011
Lp	−0.5249	−0.5879	−0.6939	−0.3614
Lq	0.0884	−0.0612	−0.0225	0.1316
Lr	−0.0293	−0.0320	−0.0589	−0.0551
Mu	−0.0020	−0.0054	−0.0144	−0.0080
Mv	−0.0018	0.0010	0.0054	0.0160
Mw	0.0046	0.0177	0.0292	0.0368
Mp	−0.0248	0.0287	0.2377	0.5614
Mq	−0.7389	−0.9628	−1.7051	−1.9072
Mr	0.0425	0.0390	0.0414	0.1257
Nu	0.0051	0.0025	−0.0001	0.0001
Nv	−0.0023	0.0042	0.0228	0.0471
Nw	0.0016	0.0048	0.0033	0.0025
Np	−0.0404	−0.0521	−0.0744	−0.0332
Nq	−0.2514	−0.2430	−0.1758	−0.4395
Nr	−0.0382	−0.0368	−0.0366	−0.0529

Table B.2: List of all linearised control derivatives at four different trim points.

	0	20	80	160
Xu0	0.0206	0.0129	0.0062	0.0092
Xuc	0.0001	0.0001	0.0003	0.0004
Xus	−0.0042	−0.0042	−0.0056	−0.0064
Xu0t	0.0005	0.0007	0.0010	−0.0001
Yu0	0.0020	0.0017	0.0016	0.0053
Yuc	0.0353	0.0352	0.0348	0.0369
Yus	−0.0004	−0.0007	−0.0002	0.0000
Yu0t	0.0019	0.0024	0.0031	0.0037
Zu0	−0.2784	−0.2669	−0.3627	−0.4740
Zuc	−0.0000	−0.0000	−0.0000	0.0004
Zus	−0.0010	−0.0007	−0.0001	−0.0008
Zu0t	0.0000	0.0000	0.0001	−0.0000
Lu0	−0.0022	−0.0019	−0.0008	−0.0020
Luc	0.0621	0.0621	0.0618	0.0635
Lus	−0.0004	−0.0013	−0.0024	−0.0018
Lu0t	0.0045	0.0049	0.0055	0.0064
Mu0	0.0038	0.0055	0.0119	0.0159
Muc	−0.0000	−0.0000	−0.0001	−0.0001
Mus	−0.0222	−0.0212	−0.0287	−0.0377
Mu0t	−0.0003	−0.0003	−0.0004	−0.0001
Nu0	−0.0000	0.0006	0.0020	0.0043
Nuc	0.0056	0.0054	0.0052	0.0058
Nus	−0.0031	−0.0028	−0.0018	−0.0048
Nu0t	−0.0122	−0.0121	−0.0119	−0.0125

Table B.3: Trimmed states

	0	20	80	160
pos_x	0	0	0	0
pos_y	0	0	0	0
pos_z	0	0	0	0
vel_u	−0.0000	10.2748	41.1505	81.9099
vel_v	−0.0000	−0.0034	−0.0042	0.0953
vel_w	−0.0000	0.5382	0.6477	−8.1170
ang_phi	−0.0069	−0.0063	−0.0065	−0.0117
ang_tht	0.0713	0.0523	0.0157	−0.0988
ang_psi	0	0	0	0
angv_p	−0.0000	0.0000	−0.0000	0.0000
angv_q	0.0000	−0.0000	−0.0000	0.0000
angv_r	−0.0000	−0.0000	−0.0000	−0.0000

B.1. State-Space systems

In Equation B.1 the matrices of the model state-space system are shown, together with its input, states and output vector definitions shown in Equation B.2.

$$
\begin{aligned}
A &= \begin{bmatrix} -0.0206 & 0.0242 & -9.7851 & -0.1525 \\ 0.0243 & -0.3459 & -0.6986 & 0.0742 \\ 0 & 0 & 0 & 1 \\ -0.0020 & 0.0046 & 0 & -0.7389 \end{bmatrix} \\
B &= \begin{bmatrix} 0.0206 & -0.0042 \\ -0.2784 & -0.0010 \\ 0 & 0 \\ 0.0038 & -0.0222 \end{bmatrix} \\
C &= \begin{bmatrix} 1 & 0 & 0 & 0 \\ 0 & 1 & 0 & 0 \\ 0 & 0 & 1 & 0 \\ 0 & 0 & 0 & 1 \\ -0.0206 & 0.0242 & 0 & -0.1525 \\ 0.0243 & -0.3459 & 0 & 0.0742 \\ -0.0020 & 0.0046 & 0 & -0.7389 \end{bmatrix} \\
D &= \begin{bmatrix} 0 & 0 \\ 0 & 0 \\ 0 & 0 \\ 0 & 0 \\ 0.0206 & -0.0042 \\ -0.2784 & -0.0010 \\ 0.0038 & -0.0222 \end{bmatrix}
\end{aligned}
\tag{B.1}
$$

$$
\vec{x} = \begin{bmatrix} u \\ w \\ \theta \\ q \end{bmatrix}, \quad \vec{u} = \begin{bmatrix} \theta_0 \\ \theta_{1C} \end{bmatrix}, \quad \vec{y} = \begin{bmatrix} u \\ w \\ \theta \\ q \\ F_x \\ F_z \\ \dot{q} \end{bmatrix} \tag{B.2}
$$

$$
\begin{aligned}
A &= \begin{bmatrix} -0.7615 & -0.1758 & 0.1876 & 0.7013 & 0.4282 \\ -0.2780 & -0.3037 & 0.4835 & -0.2608 & 0.2879 \\ 0.0790 & 0.4294 & -0.7198 & 0.3767 & -0.4611 \\ 1.7612 & 1.0362 & -1.3272 & -1.2460 & -1.8407 \\ 0.4469 & 0.2958 & -0.4106 & -0.0832 & -1.0965 \end{bmatrix} \\
B &= \begin{bmatrix} 1.9361 & 0.0062 & 0 & -2.2609 & 0 & -0.0138 \\ -0.9272 & 0.1102 & 0 & -1.8287 & 0 & -0.0141 \\ 1.8526 & -0.3031 & 0 & 2.2957 & 0 & -0.0165 \\ -2.1196 & -1.3016 & 0 & 3.9184 & 0 & -0.0070 \\ -0.0373 & -3.2319 & 0 & 1.8208 & 0 & -0.0019 \end{bmatrix} \\
C &= \begin{bmatrix} 0 & 0 & 0 & 0 & 0 \\ -1.5298 & -4.5455 & 7.8662 & -4.4441 & -6.8187 \end{bmatrix} \\
D &= \begin{bmatrix} 0 & 0 & 0 & 0 & 0 & 0 \\ 10.3000 & 0 & 6.2000 & 0 & 0 & 0 \end{bmatrix}
\end{aligned}
\tag{B.3}
$$

B.2. OMCT frequencies

Table B.4: OMCT translational test frequencies, adapted from [18]

Signal number	Frequency rad/s	Frequency Hz	Amplitude m/s^2
1	0.1000	0.015 92	1
2	0.1585	0.025 22	1
3	0.2512	0.039 98	1
4	0.3981	0.063 36	1
5	0.6310	0.1004	1
6	1.000	0.1592	1
7	1.585	0.2522	1
8	2.512	0.3998	1
9	3.981	0.6336	1
10	6.310	1.004	1
11	10.00	1.592	1
12	15.85	2.522	1

Table B.5: OMCT rotational test frequencies, adapted from [18]

Signal number	Frequency rad/s	Frequency Hz	Amplitude °	Angular rate °/s	Angular acceleration $°/s^2$
1	0.1000	0.015 92	6.000	0.6000	0.060 00
2	0.1585	0.025 22	6.000	0.9509	0.1507
3	0.2512	0.039 98	3.981	1.000	0.2512
4	0.3981	0.063 36	2.512	1.000	0.3981
5	0.6310	0.1004	1.585	1.000	0.6310
6	1.000	0.1592	1.000	1.000	1.000
7	1.585	0.2522	0.6310	1.000	1.585
8	2.512	0.3998	0.3981	1.000	2.512
9	3.981	0.6336	0.2512	1.000	3.981
10	6.310	1.004	0.1585	1.000	6.310
11	10.00	1.592	0.1000	1.000	10.00
12	15.85	2.522	0.039 81	0.6310	10.00

B.3. Matlab code

```
bypass = ss(eye(2),...
'InputName',{'coll' 'long'},...
'OutputName',{'coll' 'cycl_l'});

bypass_connect = parallel(ss_scas, bypass, 'name');
oloop = series(bypass_connect, model.ss, 'name');
oloop.OutputName = {'u' 'w' 'tht' 'q' 'fx' 'fz' 'qdot'};

FeedbackChannels = {'tht' 'q'};
K = ss(eye(2),'InputName',FeedbackChannels,...
'OutputName',FeedbackChannels);
cloop = feedback(oloop,K,'name',+1);

ch47 = struct();
ch47.ss = cloop;
ch47.ss_red = minreal(cloop);

%% filter output states only
FilterChannels = {'q' 'fx' 'fz'};
K = ss(eye(3),'InputName',FilterChannels,...
'OutputName',FilterChannels);

ch47.ss_filt = minreal(series(ch47.ss, K, 'name'));
[ch47.V, ch47.D] = eig(ch47.ss_filt.A, 'vector');
ch47.V_rec = ch47.ss_filt.C * ch47.V;
```

Figure B.1: Matlab code showing how connecting the blocks looks like in the code

```
[ch47.V2, ch47.D2] = eig(ch47.ss_init.A, 'vector');
[y0_r, t0_r, ~] = initial(ch47.ss_init, real(ch47.V2(:,2)),t_run);
[y, t, ~] = lsim(mca.ss_combine, y0_r, t0_r);

[total.V3, total.D3] = eig(total.ss_reordered.A, 'vector');
[y3_r, t3_r, ~] = initial(total.ss_reordered,...
real(total.V3(17,15)/ch47.V2(4,2)*total.V3(:,15)),...
t_run);
```

Figure B.2: Matlab code showing the two methods of simulating the initial value problem

B.4. CWA diagram and state-space

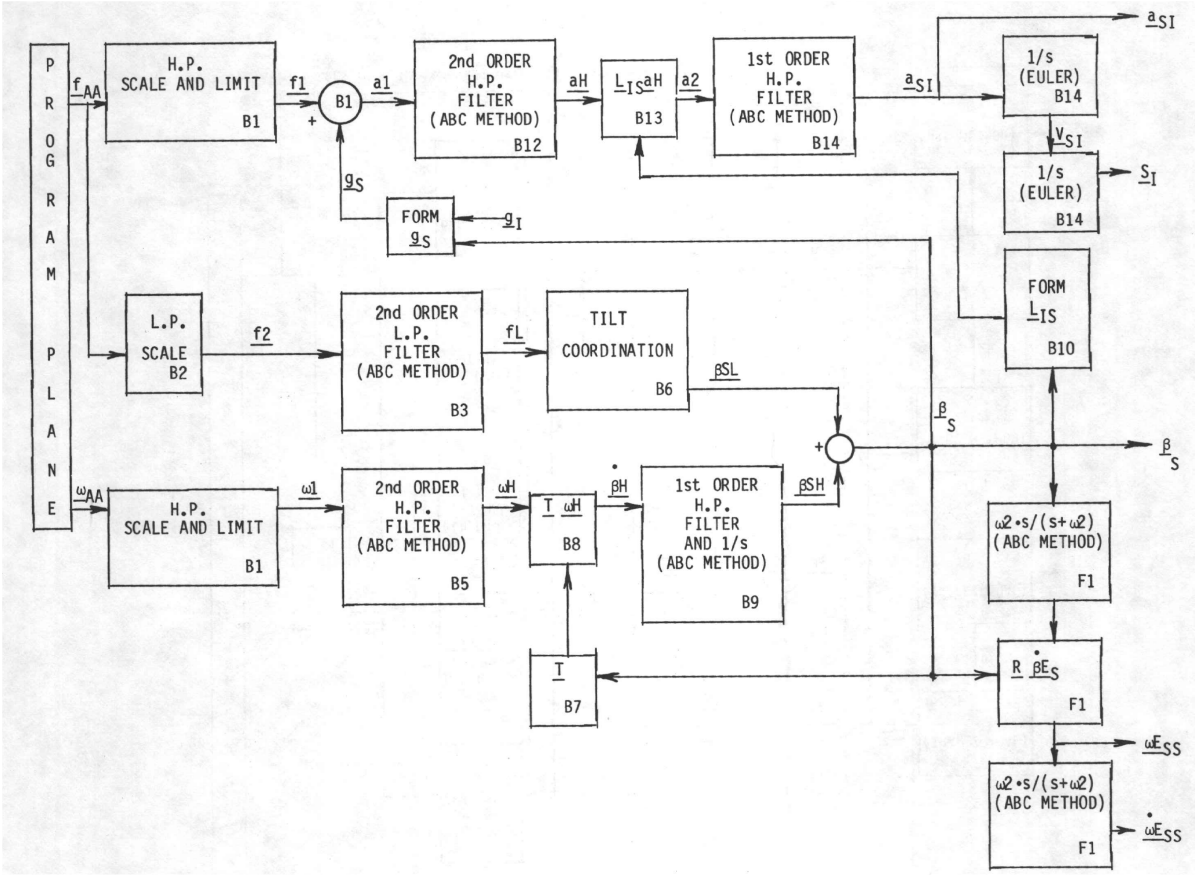

Figure B.3: Diagram of the CWA, from [11]

$$
A = \begin{bmatrix}
0 & 1 & 0 & 0 & 0 & 0 & 0 & 0 & 0 & 0 & 0 & 0 \\
0 & 0 & 1 & 0 & 0 & 0 & 0 & 0 & 0 & 0 & 0 & 0 \\
0 & -0.64 & -1.60 & 0 & 0 & 0 & 0 & 0 & 0 & 0 & -9.81 & 0 \\
0 & 0 & 0 & 0 & 1 & 0 & 0 & 0 & 0 & 0 & 0 & 0 \\
0 & 0 & 0 & 0 & 0 & 1 & 0 & 0 & 0 & 0 & 0 & 0 \\
0 & 0 & 0 & -48.05 & -246.40 & -31.20 & 0 & 0 & 0 & 0 & 0 & 0 \\
0 & 0 & 0 & 0 & 0 & 0 & 0 & 1 & 0 & 0 & 0 & 0 \\
0 & 0 & 0 & 0 & 0 & 0 & -0.64 & -1.60 & 0 & 0 & 0 & 0 \\
0 & 0 & 0 & 0 & 0 & 0 & 0 & 0 & 0 & 1 & 0 & 0 \\
0 & 0 & 0 & 0 & 0 & 0 & 0 & 0 & -6.25 & -5 & 0 & 0 \\
0 & 0 & 0 & 0 & 0 & 0 & 0 & 0 & 0 & 0 & 0 & 1 \\
0 & 0 & 0 & 0 & 0 & 0 & -0.64 & -1.60 & -6.25 & -5 & 0 & 0
\end{bmatrix}
$$

$$
B = \begin{bmatrix}
0 & 0 & 0 \\
0 & 0 & 0 \\
0.70 & 0 & 0 \\
0 & 0 & 0 \\
0 & 0 & 0 \\
0 & 0.50 & 0 \\
0 & 0 & 0 \\
0 & 0 & 0.70 \\
0 & 0 & 0 \\
0.45 & 0 & 0 \\
0 & 0 & 0 \\
0.45 & 0 & 0.70
\end{bmatrix}
$$

$$
C = \begin{bmatrix}
0 & 0 & 0 & 0 & 0 & 0 & 0 & 0 & 0 & 0 & 0 & 1 \\
0 & -0.64 & -1.60 & 0 & 0 & 0 & 0 & 0 & 0 & 0 & 0 & 0 \\
0 & 0 & 0 & -48.05 & -246.40 & -31.20 & 0 & 0 & 0 & 0 & 0 & 0
\end{bmatrix}
$$

$$
D = \begin{bmatrix}
0 & 0 & 0 \\
0.70 & 0 & 0 \\
0 & 0.50 & 0
\end{bmatrix}
\tag{B.4}
$$

$$
\vec{u} = \begin{bmatrix} \dot{q_v} \\ fx_v \\ fz_v \end{bmatrix}, \quad \vec{y} = \begin{bmatrix} q_s \\ fx_s \\ fz_s \end{bmatrix}
\tag{B.5}
$$

B.5. Problem solving

This section describes how, following the questions raised in Chapter 4, subsequent scrutiny lead to the explanations given in Chapter 5. The question which is to be answered is: are the eigenvectors, as shown in Figure 4.1, correct? Because, based on the settings of the MCA different results were expected.

A first cause can be a badly tuned MCA. This MCA is not tuned at all, the parameters are taken from [13], so a certain, relatively large, distortion can be expected. However, the parameters do have an engineering basis, and looking at the amount of distortion, it becomes improbable that this is the only cause of the differences. It also cannot explain why uncoupled modes, mostly fz, amplify as well.

A second option is that there is still a programming error in the model. The preliminary results shown do not strengthen the confidence in the model. A thorough inspection of the model is done. It is assumed that the AFCS is accurate, as all pilots which flew the model are happy with its behaviour. Errors can be present in the linearisation of the AFCS or the linearised flight model. Also the interconnection of the subsystems can be faulty. Assuming there is a mistake in the code, the next steps were taken.

One of the first questions to answer was: at which point in the series of calculations does it go wrong? To answer that, each block from Figure 2.1 is separately checked for errors, by investigating the output of each block to a certain input. Often-used inputs are the impulse and step input. The impulse response clearly shows the eigenmodes of a system, which is especially useful for reviewing the linearised vehicle model. The step input on the other hand is particularly useful for checking the MCA, because the MCA is designed to return the simulator to the starting position after a step input on horizontal or vertical force. In this step no issues surfaced, however, it did become clear that the apparent gain changed between the vehicle model and the motion cueing algorithm (MCA).

In the next step attention shifted to the interconnection between blocks. Matlab's method of connecting by `'name'` was used, which did undergo inspection. It is widely used throughout the simulation, but no issues were found.

Also the method of plotting the eigenvectors was looked at, which did reveal a problem. The eigenvectors are calculated using the Matlab function `eig(A)`[1], both for the system matrices of the vehicle model as well as for the combined model of vehicle and MCA. However, applying the same function to two matrices which have the same eigenvalues can yield different eigenvectors. This is caused by the fact that an eigenvector, multiplied by any (complex) number, is also an eigenvector of that matrix. Comparison between Figure B.4 and Figure 4.1a shows this phenomenon, as only changing parameters of the MCA changes the direction of all eigenvectors. This property makes it difficult to compare eigenvectors of a mode before and after cueing, but it can be solved by calculating the eigenvectors in one go. To achieve this, the signals of the vehicle model (before cueing) have to be included in the output of the MCA, without being affected by it. That is done by a simple unity gain system, bypassing the MCA. In this way the eigenvectors are calculated in one go, resulting in easier comparison between them.

After a thorough inspection of the code and analysis of intermediate results, confidence in the model increased. However, it still remained a question why the eigenvector after cueing, in some cases, was larger than the same eigenvector before cueing. To get better insight, the issue is isolated as much as possible. It also appeared in the heave motion channel, which is supposed to be very linear and uncoupled. So the gain of all other channels was set to 0, which, as expected, removed all motion except heave from the output. It is shown in Figure B.4 how the eigenvector plot looks like with only the heave channel enabled and it clearly shows how the magnitude of fz_s is larger than the magnitude of fz_v. The ratio of the length of these vectors is 1.31. The settings for this MCA are shown in Table B.6.

The Bode plot of the heave channel was checked and is shown in Figure B.5, but it did show the same gain as was set for the MCA. So the Bode diagram shows e.g. a gain of 1, but the magnitude of the eigenvector was still amplified. Then I. Miletović was contacted if this phenomenon was encountered before, who pointed at the third dimension of transfer functions[2]. This did explain the difference between expected and actual gain, and is further detailed in Chapter 5.

[1] `https://nl.mathworks.com/help/matlab/ref/eig.html`, accessed on 17 September 2019
[2] `https://pdfserv.maximintegrated.com/en/an/AN733.pdf`, accessed on 17 September 2019

Table B.6: Settings of the CWA used

K_x	ω_{n_x}	ω_{b_x}	$\omega_{n_{lp_x}}$	ζ_x	K_z	ω_{n_z}	ω_{b_z}	ζ_z	K_q	ω_{n_q}	ζ_q
0	0.0	0	0	0	1.0	0.5	0.0	1.0	0	0.8	1

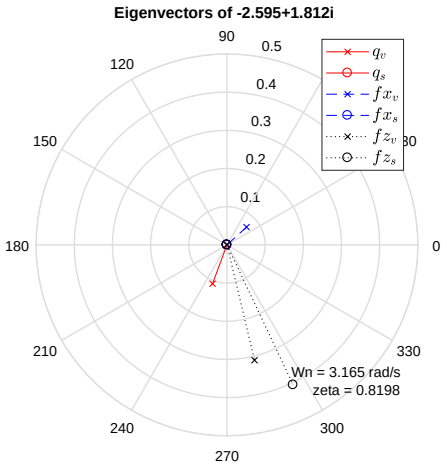

Figure B.4: Eigenvectors with only heave cueing enabled

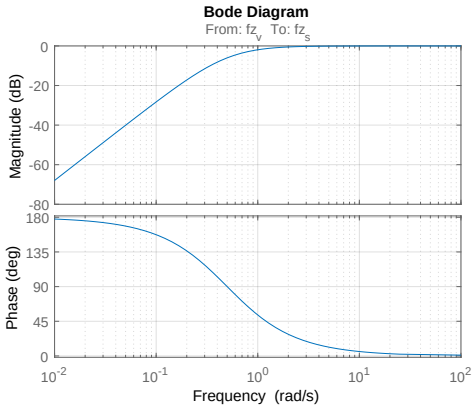

Figure B.5: Bode diagram of the heave channel, showing the characteristics corresponding to the settings from Table B.6

B.6. Timetraces

In the process of checking the connected sub-systems, the time traces were analysed. This is done to review if the response of the MCA was as expected. It is done in two different ways. In the first form the first eigenmode of the vehicle was excited by initialising the vehicle model with the eigenvector corresponding to that eigenvalue. This gives the response of the vehicle, which was subsequently used as input for a simulation of the simulator's motion. This method is an intuitive approach, as generally the output of the vehicle model is used as input of the simulator. The results of this method are shown in the upper figure of Figure B.6.

The second method is to initialise the complete model (vehicle model and MCA) in one go with the eigenmode. Again this is done by initialising the model with the eigenvector corresponding to the same eigenvalue used previously. The output of this system is approach is shown in the bottom part of Figure B.6.

As can be seen in the figure both graphs do not look identical. There are a few issues which makes comparison difficult. First of all, initially both systems were a minimal realisation. This makes it very difficult to initialise them with an eigenvector, as it has no real meaning. The eigenvector can be returned to a physically meaningful state by pre-multiplying it with the C-matrix, but then its shape means that it cannot be used as initial state vector of the system. So the full system is used for this analysis.

The next problem however is that any (complex) value times the eigenvector is also an eigenvector. This means that both systems can be initialised in the same mode, but not in the same state of the mode. This makes comparison difficult. To solve this issue, a state is searched for which appears in both systems, then the eigenvector element corresponding to that state is set equal to each other by rotating and scaling it: `total.V3(17,15)/ch47.V2(4,2)`. Then the eigenvector is multiplied by this value, such that the states which appear in both systems are aligned: `real(total.V3(17,15)/ch47.V2(4,2) * total.V3(:,15))`. The result is that the vehicle mode does compare well in both simulations, as can be seen by comparing the blue lines in both plots of Figure B.6.

The last obstacle is that when setting the initial value of the complete system, the simulator is initialised at a state not equal to zero. This means that the simulator is not only acting on the eigenmotion of the vehicle, but also on its own motion. It is still a question if this behaviour is desired or not.

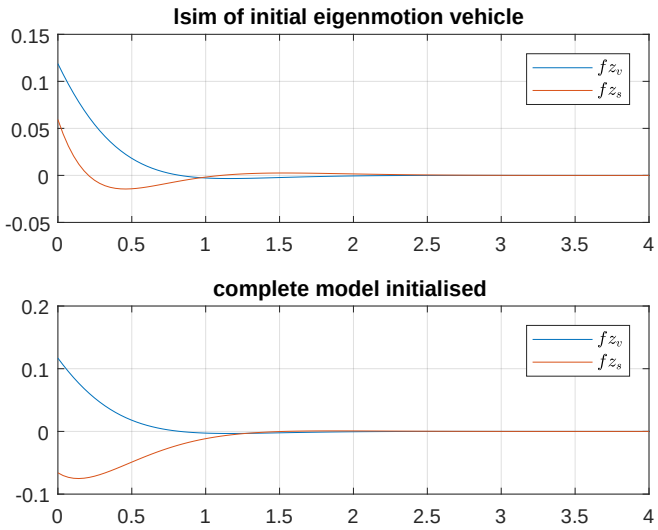

Figure B.6: Comparison of the time traces of the vertical specific force

Bibliography

[1] J. B. Sinacori, *The Determination of Some Requirements for a Helicopter Research Simulation Facility*, tech. rep. NASA-CR-152066 (Systems Technology Inc., Sept. 1977).

[2] I. Miletović, M. D. Pavel, O. Stroosma, et al., "Motion cueing fidelity in helicopter flight simulation: a new perspective", To be published, PhD thesis (TU Delft, 2019) Chap. Appendix A.

[3] G. D. Padfield, *Helicopter Flight Dynamics*, 2nd ed. (Wiley India Pvt Ltd, 2011).

[4] A. D. Marco, E. Duke, and J. Berndt, "A General Solution to the Aircraft Trim Problem", in AIAA Modeling and Simulation Technologies Conference and Exhibit (Aug. 2007), 10.2514/6.2007-6703.

[5] K. Ferguson, D. Anderson, D. Thomson, et al., "Comparing the Flight Dynamics Characteristics of Tandem and Conventional Helicopters for the Purposes of Automatic Control", in (Sept. 2015).

[6] M. D. Pavel, in *Automatic Flight Control Systems*, edited by T. Lombaerts (IntechOpen, Rijeka, 2012) Chap. 6, 10.5772/30512.

[7] A. J. Ostroff, D. R. Downing, and W. J. Rood, *A Technique Using a Nonlinear Helicopter Model for Determining Trims and Derivatives*, tech. rep. (NASA Langley Research Center, Hampton, VA, United States, May 1976).

[8] United States Army Warfighting Center, *CH-47D Advanced Flight Control System (AFCS)* (2006).

[9] J. J. Adams, H. P. Bergeron, and G. J. Hurt, *The effects of motion cues and motion scaling on one-and two-axis compensatory control tasks*, tech. rep. (NASA Langley Research Center, Jan. 1971).

[10] R. Hosman, "Thresholds of motion perception measured in a flight simulator.", in Twelfth Annual Conference on Manual Control, Vol. NASA TMX-73 (May 1976).

[11] L. D. Reid and M. A. Nahon, *Flight Simulation Motion-Base Drive Algorithms. Part 1: Developing and Testing the Equations*, tech. rep. UTIAS 296 (University of Toronto, Institute for Aerospace Studies, Dec. 1985).

[12] G. L. Zacharias, *Motion cue models for pilot-vehicle analysis*, tech. rep. (Bolt Beranek and Newman Inc., May 1978).

[13] S. Stoev, O. Stroosma, M. M. van Paassen, I. Miletovic, and M. Mulder, "Eigenmode Distortion Analysis for Motion Cueing Evaluation in Fixed-Wing Aircraft Simulators", in AIAA Scitech 2019 Forum (Jan. 2019), 10.2514/6.2019-0179.

[14] O. Stroosma, M. M. van Paassen, M. Mulder, R. J. A. W. Hosman, and S. K. Advani, "Applying the Objective Motion Cueing Test to a Classical Washout Algorithm", in AIAA Modeling and Simulation Technologies (MST) Conference (Aug. 2013), 10.2514/6.2013-4834.

[15] J. A. Schroeder, *Helicopter Flight Simulation Motion Platform Requirements*, tech. rep. NASA-TP-1999-208766 (National Aeronautics and Space Administration, July 1999).

[16] S. K. Advani and R. J. A. W. Hosman, "Revising Civil Simulator Standards – An Opportunity for Technological Pull", in AIAA Modeling and Simulation Technologies Conference and Exhibit, AIAA-2006-6248 (Aug. 2006), 10.2514/6.2006-6248.

[17] S. Advani, R. Hosman, and M. Potter, "Objective Motion Fidelity Qualification in Flight Training Simulators", in AIAA Modeling and Simulation Technologies Conference and Exhibit (Aug. 2007), 10.2514/6.2007-6802.

[18] Anonymous, *Manual of Criteria for the Qualification of Flight Simulation Training Devices - Volume 1 - Aeroplanes*, ICAO Doc 9625 (International Civil Aviation Organization, 2009).

[19] R. J. A. W. Hosman, S. K. Advani, and J. Takats, "Status of the ICAO Objective Motion Cueing Test", in Autumn Flight Simulation Conference: Flight Simulation Research - New Frontiers (Royal Aeronautical Society, Nov. 2012).

[20] P. M. T. Zaal, J. A. Schroeder, and W. W. Y. Chung, "Objective Motion Cueing Criteria Investigation Based on Three Flight Tasks", in Flight Simulation Conference - Challenges in Flight Simulations (Royal Aeronautical Society, June 2015).

[21] R. Hosman and S. Advani, "Design and Evaluation of the Objective Motion Cueing Test and Criterion", The Aeronautical Journal **120**, 873 (2016) 10.1017/aer.2016.35.

[22] K. De Ridder and M. Roza, "Automatic optimization of motion drive algorithms using OMCT", in AIAA Modeling and Simulation Technologies Conference (Jan. 2015), p. 1139, 10.2514/6.2015-1139.

[23] M. Jones, "Optimizing the Fitness of Motion Cueing for Rotorcraft Flight Simulation", in Proceedings of the AHS 72nd Annual Forum (May 2016).

[24] W. Dalmeijer, I. Miletovic, O. Stroosma, and M. D. Pavel, "Extending the Objective Motion Cueing Test to Measure Rotorcraft Simulator Motion Characteristics", English, in 73rd Annual AHS International Forum and Technology Display (May 2017), pp. 1876–1891.

[25] I. Miletović, M. Pavel, O. Stroosma, et al., "Eigenmode Distortion as a Novel Criterion for Motion Cueing Fidelity in Rotorcraft Flight Simulation", in 44th European Rotorcraft Forum: Delft, The Netherlands (Sept. 2018).

[26] J. Dixon, A. Lindemann, and J. H. McCoy, "Transient amplification limits noise suppression in biochemical networks", Physical Review E **93** (2016) 10.1103/physreve.93.012415.

[27] S. Dubey, A. Paliwal, and S. Ghosh, "Transient amplification characteristics of frequency modulated wave in semiconductor plasmas", Chinese Journal of Physics (2019) 10.1016/j.cjph.2019.08.010.

[28] S. van Loon, B. Hunnekens, W. Heemels, N. van de Wouw, and H. Nijmeijer, "Transient performance improvement of linear systems using a split-path nonlinear integrator", in 2014 American Control Conference (June 2014), 10.1109/acc.2014.6858934.

[29] K. G. Makris, L. Ge, and H. E. Türeci, "Anomalous Transient Amplification of Waves in Non-normal Photonic Media", Physical Review X **4** (2014) 10.1103/physrevx.4.041044.